DEPARTMENT OF MECHANICAL ENGINEERING
COLLEGE OF ENGINEERING AND TECHNOLOGY
OLD DOMINION UNIVERSITY
NORFOLK, VA 23529

NUMERICAL INVESTIGATION OF HYDROGEN AND KEROSENE COMBUSTION IN SUPERSONIC AIR STREAMS

By
A. A. Taha, Graduate Research Assistant
S. N. Tiwari, Principal Investigator and
T. O. Mohieldin, Associate Professor

FINAL REPORT
For the period ended June 30, 1999

Prepared for
National Aeronautics and Space Administration
Langley Research Center
Attn.: Dr. Samuel E. Massenberg
Technical Monitor
Office of Education
Mail Stop 400
Hampton, VA 23681

Under
Cooperative Agreement NCC1-232
ODURF No. 163631

July 1999

Final Report

NASA Cooperative Agreement NCC1-232
ODURF No. 163631

Numerical Investigation of Hydrogen and Kerosene Combustion in Supersonic Air Stream

By

A. A. Taha, Graduate Research Assistant
S. N. Tiwari, Principal Investigator and
T. O. Mohieldin, Associate Professor
Department of Mechanical Engineering
Old Dominion University

Submitted by

Old Dominion University
Research Foundation
800 West 46th Street
Norfolk, Virginia 23508

Submitted to

National Aeronautics and Space Administration
Langley Research Center
Hampton, VA 23681-0001

July 1999

FOREWORD

This is a progress report on a research project under, "Institute for Computational and Applied Mechanics (ICAM)," for the period ended June 30, 1999. During this period attention was directed to "Numerical Investigation of Hydrogen and Kerosene Combustion in Supersonic Air Streams". Important results of this study are scheduled to be presented at the 9th AIAA International Space Planes and Hypersonic Systems and Technologies Conference, November 1-4, 1999, Norfolk, VA and the 38th AIAA Aerospace Sciences Meeting and Exhibit, Reno, NV, January 11-13, 2000.

This work was supported, in part, by the Old Dominion University's Institute for Scientific and Educational Technology (ISET) through NASA Langely Research Center, Cooperative Agreement NCC1-232. The cooperative Agreement was monitored by Dr. Samuel E. Massenberg, Director, Office of Education, Mail Stop 400.

NUMERICAL INVESTIGATION OF HYDROGEN AND KEROSENE COMBUSTION IN SUPERSONIC AIR STREAMS

A.A. Taha[1], S.N. Tiwari [2], and T.O. Mohieldin[3]

College of Engineering and Technology

Old Dominion University, Norfolk, VA 23529

ABSTRACT

The effect of mixing schemes on the combusion of both gaseous hydrogen and liquid kerosene is investigated. Injecting pilot gaseous hydrogen parallel to the supersonic incoming air tends to maintain the stabilization of the main liquid kerosene, which is normally injected. Also the maximum kerosene equivalence ratio that can maintain stable flame can be increased by increasing the pilot energy level. The wedge flame holding contributes to an increased kerosene combustion efficiency by the generation of shock-jet interaction.

[1]Graduate Research Assistant, Department of Mechanical Engineering
[2] Eminent Professor/Scholar, Department of Mechanical Engineering
[3]Associate Professor, Mechanical Engineering Technology Dept.

TABLE OF CONTENTS

LIST OF TABLES

LIST OF FIGURES

1. INTRODUCTION

The scramjet engine is expected to be the most effective propulsion system, but there are severe conditions for ignition such as low pressure, low temperature, and high airflow speed due to the supersonic incoming air. [1♣] Considerable fundamental research has been conducted in response to the increased interest in the development of scramjet propulsion systems. Many experimental and numerical studies of various aspects of fuel injection in the combustor are discussed in. [2]

The development of hypersonic airbreathing plane capable of horizontal takeoff and landing and acceleration to low earth orbit has attracted significant interest in the aerospace community for some time. It has a significant weight advantage over presently used rocket propulsion systems by eliminating the need to carry onboard oxygen tanks. One of the major challenges in developing such a plane is the design of a suitable propulsion system. Current airbreathing engine designs, which utilize subsonic internal flow velocities, such as turbojet or even RAMJET engines, would be inappropriate because of the extreme conditions seen in hypersonic flight. Temperature recovery from the hypersonic free stream would be in the order of 2000 K or more, leading to engine materials difficulties and loss of usable energy due to dissociation of air molecules. The induced drag on the vehicle due to strong shocks at the engine inlets is a strong function of the flight Mach number so that it rapidly becomes impractical to use subsonic engines at high speeds. A supersonic combustion RAMJET or SCRAMJET has long been considered to be a feasible engine concept for hypersonic vehicles. [3] Figure 1.1 shows a schematic of a SCRAMJET engine concept where the aircraft underbody and engine designs are integrated together.

♣The superscript numbers indicate references.

The shock waves formed by the vehicle forebody and the engine inlets serves as the engine compressor section while the engine exhaust and vehicle afterbody serve as the expansion nozzle to generate thrust from the gases burned in the combustor. The surface geometry would be chosen so that supersonic flow would be maintained throughout the internal passages of the engine avoiding large recovery of temperature and pressure from the free stream air. [4]

Figure 1.2 shows the Airframe-Integrated supersonic combustion ramjet (scramjet) along with a partial cross-section through a typical modular engine. The sidewalls of the inlet continue the compression process, which began on the vehicle forebody. The instream struts complete the compression process and also provide locations for global distribution of fuel. The particular concept depicted here shows a combination of perpendicular and parallel fuel injection, which would typically take place behind a rearward-facing step and at the base of the strut, respectively.[5]

How these fuel-injection modes are used to control heat release is shown in Fig. 1.3. At lower speeds (below Mach 5, and to some extent Mach 5-7), too much heat release too early in the combustor will result in thermal choking and inlet unstart. Parallel fuel injection, which will be shown to have a slower-mixing process, is therefore used extensively to stretch out the combustion zone. Above Mach 7, thermal choking is much less likely to occur, and the faster-mixing perpendicular injection process is utilized to get faster combustion and higher performance. In order to quantify this mixing-controlled combustion philosophy, a considerable amount of research has been done on perpendicular and parallel mixing. Figures 1.4 and 1.5 show mixing efficiency as a function of relative combustor length for each injection mode. The bands represent differences caused by details of the injection layout such as close or wide sparing of fuel injection holes, injector shape, etc. Although the curves for perpendicular and parallel

injection are fairly similar, they produce quite different overall results due to the fact that the non-dimensionalizing parameter, χ_l, is much larger for parallel injection. The mixing length χ_l is also very sensitive to equivalence ratio (Fig. 1.6). This plot shows that the distance required for complete mixing maximizes at an equivalence ratio of unity. This is qualitatively intuitive, since the case where each fuel molecule must find its oxidizing molecule would clearly be more difficult than a case where there is an abundance of either fuel or oxidizer. The magnitudes, however, are very significant. Decreasing the combustor equivalence ratio to 0.8, or increasing it to 1.2, can cut the mixing length (and combustor length) by 30 percent or more!

It should be noted that the data in Figs. 1.4-1.6 are based on many measurements in real supersonic mixing experiments. They are, however, primarily mixing data obtained in cold-flow mixing situations. The impact of combustion is shown in Fig. 1.7, which shows the cold-flow mixing trend (cross-hatched), measured mixing efficiency (open symbols), and measured combustion efficiency (closed symbols) in various configurations. The abscissa is the ratio of combustor length to strut gap, where strut gap is the physical dimension between struts as depicted in Figs. 1.2 and 1.3. Note that combustion efficiency is consistently below mixing efficiency; this indicates chemical kinetics-related or other combustion-chemistry phenomena, which are potentially quite important. These issues are often related to flow-field details at the very local level.

1.1 Injection Modes and Mixing

The thermodynamic conditions at the test section entrance of the Scramjet engine are representative for the lower end of the hypersonic flight regime. For these vehicles it is anticipated that the fuel be used to cool components of the vehicle and of the engine and, thus,

enter the test section at high temperatures (even a supercritical conditions), resulting in fast evaporization and mixing upon injection. The low range of hypersonic flight regime is, therefore, of particular interest, since the level of heating of the fuel will be relatively low, and thus longer residence time will be required for the fuel to achieve complete combustion within the engine combustor. The mixing-combustion coupling at these conditions is of great interest. [6]

It is understood that there exists a strong interaction between mixing and combustion, even in the limiting cases when one or the other becomes rate controlling. Due to this coupling, observations from mixing in non-reacting flows are hard to extend directly to reacting flows. Furthermore, in many practical situations, the Damkohler number, defined as the ratio between the characteristic fluid residence time in the reaction zone and the chemical reaction time scale, is O(1). In such cases, the flowfield may become either mixing or kinetic limited in localized regions; however, in general, combustion takes place in thick, highly turbulent burning regions. The mean and time varying parameters responsible for mixing are affected by heat release, which, in turn, affect the chemical kinetics; thus, mixing and combustion become closely coupled. [7]

Different methods of liquid fuel injection have been investigated. Parallel flow mix through the growth of the shear layer generated at the interface of the different components. It is observed that compressibility plays a major rule in reducing the growth of the shear layer, thus requiring longer fluid residence time to insure good mixing in practical devices. As the compressibility increases, the spreading rate of the shear layer was observed to drop to about ¼ of the compressible shear layer growth for the same velocity and density ratios of the two mixing constituents. The convective Mach number (defined as a measure of the speed of the turbulent structures in the shear layer relative to the free stream) increases the stability of the large-scale

turbulent structures which are responsible for the turbulent shear layer growth. This is of particular significance in high-speed flows, where parallel injection is the preferred mode due to the lower total pressure relative to the other fuel injection and mixing options. An increase in the stability of the large vortical structures in the shear layers due to compressibility is observed even in situation where the turbulence is intentionally intensified. Growth of the shear layer was forced by a pulsating shock impinging on the shear layer in parallel compressible flows in high speed (i.e., Mach 3 and 5, respectively) as a destabilizing mechanism leading to the growth of the shear layer and accelerated mixing. Only a negligible effect was obtained both in the near and far field. However, when a shock of the same strength impinged on the boundary layer of the two flows prior to their coalescence, an increase in the shear layer growth (14 to 26 percent) was experienced. Thus an increase in the turbulence in the boundary layer upstream of the mixing station increased, causing an increase of as much as 26 percent in the shear layer growth. This indicated the significant role played by the small-scale turbulence in the mixing process. Introduction of axial vorticity was shown to improve mixing, which was also attributed to the small-scale turbulence effect on the growth of the shear layer and on the enhancement of turbulence in the shear layer. Mixing at a molecular level is, in particular, important in combustion applications when stoichiometric mixing is a prerequisite to initiate chemical reactions. [6]

The effect of small-scale turbulence on the mixing process in high-speed flows requires more detailed investigation. In particular, mixing at a molecular level, which indicates the ability to initiate chemical reactions, is of a great interest. Concentration distribution is not sufficient to provide this information. Although it is recognized that a reacting flowfield is substantially

modified once exothermic reactions take place, mixing of non-reacting flows needs further investigation to provide further insight of the characteristics of the micro-mixing processes. [6]

Studying the flow field behavior of the transverse injection of the fuel is one of the recent demanding research trends in the combustion field of the scramjet engine. This technique is used to increase the fuel-air mixing in order to achieve the required heat release pattern with the short combustion residence time associated with the high Mach number condition. [2]

Transverse or inclined injection introduces different mixing mechanism. At a macro-scale, axial vorticity is produced at the edges and above the jet as the main flow surrounds the jet in an axial and transverse direction. These vortices break the plume and entrain the injectant into the core flow. The level of mixing obtained by this strong momentum exchange is traditionally quantified by the degree of penetration and concentration decay of the jet injected into the main flow, usually air. [6] Studies performed by Mays et al. [8] and Wood et al. [9] addressed the effect of small-scale turbulence on transverse injection and mixing. It was suggested that the onset and divergence of an instability in the jet is ultimately responsible for the plume fracture. This instability propagates upstream and produces additional turbulence in the core flow. Even in supersonic flows, an upstream interaction exists, as the instability at the jet boundary induces oscillations of the bow shock generated in front of the jet via the separated region in front of the jet. In turn, these shock oscillations contribute to increase the vorticity in the flow. [6]

When heat release effects are included, significant modifications of the turbulent structures occur. It has been indicated that the heat released from chemical reactions both generate and suppress turbulence. It is shown that the turbulent dilation and viscous dissipation in flames reduce small-scale turbulence, while the shear gradient effects, mainly of pressure and density generate new large-scale structures. [6]

Figure 1.8 shows a schematic of the region surrounding a single perpendicular injector. Because the mainstream flow is supersonic, there is a bow shock off of the underexpanded fuel jet and internal wave structure associated with the jet expansion. The boundary layer ahead of the jet separates, and there is a recirculation zone downstream of the injector as well. The details of these local zones are quite important to the ignition, flameholding, and combustion processes and therefore important to real combustor design. [5]

Mohieldin and Tiwari [10] studied numerically the advantage of using the tandem injection on the regular single step tangential injection regarding the mixing aspect in the flow field. Matsuo and Mizomoto [1] studied the flow structure of supersonic flow of Mach 2.5 past a backward-facing step with perpendicular sonic injection from the bottom wall. They examined the effect of both the step height and dynamic pressure ratio of the jet flow to the main flow using the perfect gas condition in two-dimensional space. The effect of H_2-transverse injection on the characteristics of the flow field was investigated numerically by Berman et al. [11] using both adiabatic and constant temperature wall boundary conditions.

Schetz et al. [12] presented a comprehensive review of the mixing of transverse jets and wall jets in supersonic flow. While the stream wise injection has the advantage of adding to the thrust component of the engine, many of the approaches utilized to improve the wall injection have been used successfully to enhance the fuel-air mixing. [2]

Using the rearward-facing step in the supersonic combustors and injecting the fuel perpendicular or at least inclined on the main air flow have the advantage of holding the flame because of the existence of the separated and recirculating regions in the flow field as depicted in Fig. 1.8. This can help solving, in part, the complication of holding the flame in supersonic engines due to the fact that the flow in such engines is not premixed which means that if bluff

bodies are to be used as flame holders they have to be large. This is highly undesirable in supersonic combustors due to very high drag. Therefore, this problem of flame holding could be solved using the rearward-facing steps in the combustors and/or the perpendicular fuel injection. This issue emphasizes the importance of flow field details around the fuel injectors. [5]

An important feature of the normal injection flow field is the gross penetration of the jet into the flow. Baranovsky and Schetz [13] introduced the injection angle as a separate parameter in the correlation, which was set to evaluate the penetration of liquid jets. It was found that the upstream injection (injection angle is greater than 90^{o} with respect to the incoming air flow direction) can be used as a method to increase penetration and residence time of a liquid fuel into a scramjet combustion chamber. It was also found that the maximum penetration takes place at injection angle (θ) =135 degrees.

1.2 Ramp Injection and Mixing

Enhanced fuel/air mixing schemes are required in SCRAMJET engine designs because of the short residence time (on the order of ms) of the gases in the supersonic flowfield of the combustion chamber. Uniform and rapid mixing allows for shorter combustor lengths, higher combustion efficiencies and better engine stability. Various mixing enhancement schemes have been proposed including contoured injection orifices, flowfield and shock oscillations, baroclinic vortex generation, and wall-mounted vortex generators. [4]

Figure 1.9 shows schematic representations of the swept and unswept ramp fuel injector configurations investigated in the study of Donohue. [4] The injector is located on one wall at the inlet of the combustor test section. Fuel is injected from the base of the ramp in the downstream direction, normally with some component upward to increase the penetration of the fuel into the

freestream air. The ramp sidewalls can be swept back to improve the mixing performance of the ramp. A single injector is used for the studies performed by Donohue [4] although normally an array of injectors would be used on several walls and possibly on struts crossing the flowfield in order to fuel the entire cross section of incoming air. The single ramp geometry used can be thought of as one element of an array with symmetry conditions at the top and side walls. More complex injection configurations incorporating transverse injection for better penetration, steps or blunt bodies for flame holding, and wall expansion or compressions would probably be used in conjunction with the ramp injectors in a final design to allow for design optimization at a variety of operating conditions.

A diagram of the important flowfield features in the ramp injector flowfields is shown in Fig. 1.10. The ramp deflects the supersonic free stream, compressing the air along its top surface and generating a shock wave, which reflects off the opposite wall of the wind tunnel. The higher pressure air on top of the ramp spills over into the relatively lower pressure region to the sides of the ramp generating a pair of counter-rotating streamwise vortices. Fuel injected from the base region of the ramp is mixed into the freestream air by the ramp-generated vortices, which are convected downstream along the sides of the fuel jet. The side walls of the swept ramp are angled back to expand the flow at the sides of the ramp, decreasing the pressure in this region and increasing the strength of the vortices formed. The ramp base area provides a subsonic, high temperature region in the flowfield important for flame holding in the reacting case.

There are a number of studies specifically related to the 3-D mixing flowfield of ramp injectors. Hartfield et al. [14] presented measurements of injectant mole fraction in the flowfield of a swept ramp with air injection using the same technique used by Donohue. [4] The results illustrated the strong effect that ramp generated vortices have on the mixing process. Waitz et

al.[15] presented both numerical simulations and experimental measurements of total pressure and fuel concentration for helium injection behind an unswept ramp which added the effect of baroclinic vortex generation when a low density fuel is used. Riggins et al. [16] presented numerical simulations of the mixing flowfields of both swept and unswept ramps with hydrogen injection into high temperature air and went on to calculate the reacting flowfield as well using the SPARK code. These results showed increased penetration and spreading of the jet plume in the reaction case. Daso and Gross [17] computed the flowfield behind swept and unswept ramps with air injection using the USA code and illustrated how side sweep of the ramp significantly increased the mixing downstream. A numerical study designed to investigate the relative importance of ramp generated vortices vs. baroclinic vorticity on supersonic mixing behind swept ramps was performed by Donohue et al. [18]

1.3 Autoignition

McClinton [19] showed that combination of the step-base and the perpendicular injection downstream of the step was effective in enhancing the ignition ability. Huber et al. [20] suggested possible autoignition source in the supersonic combustors and proposed a simple model to predict ignition limits in typical combustors. These candidates are, the base region behind steps and struts, recirculation regions upstream of the fuel jets injected perpendicular to the airflow, and the stagnant region behind the bow shocks upstream of the fuel jets.

Tomioka et al. [21] investigated the flow field at pre-ignition phase in a supersonic combustor with perpendicular injections behind a backward-facing step to understand the mechanism of the ignition enhancement observed in the ignition tests with the same combustor. It was concluded that the interaction of the separation region upstream of the fuel jet and the two-

dimensional step base-recirculating region, namely the merging of these two regions, caused enlargement of the ignition region and the enhancement of the ignition ability. Ignition parameters were compared for the cases with and without the step. As results, the interacted region in case with the step was found to be more preferable ignition source due to its enlarged size.

1.4 Liquid Hydrocarbon Fuels

1.4.1 The Problem of Cooling in High-Speed Vehicles and The Role of Fuel

As air breathing-engine-propelled vehicle speeds increase, thermal problems multiply because of the effect of stagnation temperature. While total cooling needs increase, the most critical regions are the leading edges and the engines. Although thermal effects can be somewhat accommodated by improved materials and passive cooling, sustained hypersonic flight in the atmosphere requires a substantial heat sink. Compared to a mechanical refrigeration system or a non-combustible coolant, the fuel is the best source of cooling. [22]

In the high Mach number region of the flight envelope (M>4), aerodynamic heating is too great for conventional structural materials to survive without active cooling. The fuel not only must have a good heat-of-combustion but also must provide the necessary heat sink for the cooling system. [23]

Higher aircraft speeds also have a direct impact on the operating environment a jet fuel will encounter. The higher speeds mean higher air stagnation temperatures, which increases the aircraft cooling requirements and prevents the use of air as a coolant. Thus, increasing engine thrust-to-weight ratio and aircraft speed result in large heat loads that must be managed with the main coolant available on the aircraft--the fuel. [24]

The fuel in modern military aircraft is the primary coolant for on-board heat sources. It is used to cool aircraft components such as the engine lubricant oil, hydraulic fluid, environmental control system (ECS), avionics and electrical systems, and at high Mach numbers, the air frame. Figure 1.11 illustrates the heat loads from the different aircraft components. As aircraft and engine technology have advanced from the F-4 to tomorrow's advanced fighter, the heat sink requirements of the fuel have increased significantly. The engine is the main heat source for the aircraft at Mach 3 and below, but the ECS is becoming an increasingly important part of the heat management problem. Fuels used in high-speed aircraft will have to absorb large amounts of excess heat for aircraft thermal management purposes. This will result in the fuels being heated to supercritical conditions. [24]

There are some key technical problems associated with flight in the intermediate Mach 3 to 7 range that still need to be addressed. Nearly all of those technical challenges have to do with the handling of the excess heat that is produced either by the propulsion system itself, or by the aerodynamic heating of the airplane surface. Mechanical systems, electric systems, structural elements, passengers, and crew all require cooling. Preliminary engineering estimates suggest that these cooling tasks cannot be performed using conventional aircraft design approaches. Traditionally, this "thermal management" challenges has been met by using the onboard fuel to absorb excess heat. Fuel is circulated through hot sections of the aircraft, usually back into the tanks, and finally to the engine where it is burned. This "recuperative" approach has the benefit that thermal energy dumped into the fuel is then eventually recovered as additional thrust. [25]

1.4.2 Supercritical Conditions and Their Effects

Definition of supercritical conditions: The critical point of a fluid marks the terminus of the vapor liquid coexistence curve. A fluid is said to be "Supercritical" when its temperature and pressure exceed the temperature and pressure at the critical point. [26]

Effect of supercritical conditions on fuel properties: If the fuel temperature becomes too high, the fuel will chemically decompose to form gums and solids that cause sticking of the fuel control valves and fouling of the fuel nozzles and heat exchanger.

It is clear that the future fuels must operate effectively at higher temperatures otherwise there will be serious limitations to aircraft performance. It is estimated that 900 F is the highest operating temperature that can be expected for an advanced hydrocarbon fuel without thermal decomposition (JP-900). At higher Mach numbers (>5), more cooling is required than can be obtained with JP-900 fuel. Such aircrafts will require an *"endothermic"* fuel, where additional heat is absorbed by an endothermic reaction of the fuel.

For speeds above Mach 8, the heat loads are so large that *"cryogenic"* fuels will be required. The physical and chemical properties of supercritical fluids (SCF) are expected to be dramatically different from gases and liquids. It has been found that reaction rates and mechanisms in supercritical fluids can be quite different from those in subcritical fluids. Physical data for larger hydrocarbons (that might be expected to be part of an advanced fuel) is sparse. [24]

For very high temperature test where cracking -decomposition of the fuel into lighter components, which will be discussed later- has occurred, the formation of light gases may significantly modify the fuel properties. It appears that n-dodecane ($C_{12}H_{26}$) properties are similar to those of JP-5 ($C_{11.9}H_{22.2}$), Jet A ($C_{11.6}H_{22}$), and JP-7 ($C_{12.1}H_{24.4}$) and could be used in heat

transfer calculations. The presence of cracking products can significantly modify the fuel's physical properties. At pressures near (but above) the critical pressure the physical properties (C_p especially) are very sensitive to temperature. [24]

Thermal stability of the fuel: The understanding of the thermal stability of jet fuels at supercritical conditions is almost nonexistent. There is some deposition data for fuels that includes supercritical conditions. As illustrated in Fig. 1.12, typically the deposition in "heat-tube" tests is seen to peak at about 700 °F (a range which includes the critical temperature for typical kerosene fuels), drop off as temperature is increased further, then begins to increase again. The deposition peak is attributed either to a change in mechanism or to changes in fuel properties as the fuel is heated to supercritical temperatures. Most hydrocarbons tested had similar critical temperatures. Recent results at Wright Laboratory indicate that the behavior in Fig. 1.12 is due more to the temperature dependence of chemical reactions than to the critical properties of the fuel. The fact that the supercritical deposition mechanism is unclear is not surprising since the mechanism controlling solids deposition in subcritical fuels is not totally known. [24]

Supercritical fuel injection: It might be expected that the injection and mixing of a supercritical fuel might resemble gas injection more closely than liquid injection. It was reported that compressibility can affect atomization in an analytical model. [27]

An additional complication is that the heat added to the fuel (and thus the fuel's temperature) varies throughout an aircraft's mission. Thus the fuel might be injected as a liquid during the acceleration portion of a flight and as a supercritical fluid during cruise and/or decent. It has been found that two-phase fuel injection can dramatically affect spray behavior. [28]

1.4.3 Endothermic Fuels, The Promising Fuel for Hypersonic Combustion Systems

Definitions and differences between cryogenic and endothermic systems: The *"Cryogenic"* fuels are the fuels that have a negative, less than zero, "Boiling Point". Therefore, in order to use these fuels as liquids, they must be cooled beyond the boiling point and storage environments must satisfy this condition. Examples for the cryogenic fuels and their corresponding boiling point temperature are the liquid hydrogen H_2 (-423 F) and liquid methane CH_4 (-259 F).

The *"endothermic"* fuels are the fuels that extract heat while forming from their initial components. Therefore, the decomposition of these fuels into the initial components requires energy for its accomplishment and by that a quantity of heat can be absorbed from the surrounding environment causing the required thermal loading management of the vehicle. An example for the endothermic fuels is the methylcyclohexane MCH ($C_6H_1CH_3$). The boiling point of MCH is 213 °F which means that it is a liquid in the normal ambient conditions.

Cryogenic fuels; advantages and disadvantages: The cryogenic fuels have high energy contents and thermal tolerance. Figure 1.13 shows that hydrogen has almost three times higher energy per unit mass than other fuels. [29]

The temperature limit of a fuel is a key consideration for its selection as a high speed transport fuel. Figure 1.14 shows that hydrogen has the highest temperature limit over other fuels.[29] On the other hand, Fig. 1.15 indicates that cryogenic fuels have relatively poor energy contents per unit volume which is an undesirable property that is magnified by their storage requirements. [29]

Cryogenic fuels must be viewed with extreme caution because of the severe constraints that they place on the design of the aircraft and because of the high cost of transporting, storing,

and delivering them. Hydrogen or methane handling facilities at just a few U.S. airports would be very costly to install and maintain, and of course these fuels raise serious safety questions. From the military standpoint, cryogenic fuels appear impractical because, again, military operations must not be tendered by a need for costly and exotic infrastructures, and by all means not by an uncertain and vulnerable supply of mobility fuels. Nevertheless, serious consideration is being given to such option and it is possible that successful large-scale applications using hydrogen or methane might eventually be developed. [8] Figure 1.16 shows that cryogenic fuels will require totally new fuel delivery, distribution and storage facilities, as well as extensive gate and terminal modifications. [29] Figure 1.17 shows that there will always be losses for cryogenic liquid during refill and tank to tank transfer processes. [29]

Endothermic fuels; the phenomenon and advantages: An innovative approach based on more conventional types of fuels takes advantage of the fact that some hydrocarbons, when they degrade at high temperatures, do so cleanly, i.e., without forming carbonaceous surface deposits. Instead, they break down to smaller hydrocarbons that are then circulated to the combustor. The chemical breakdown itself absorbs heat, thus providing another useful thermal management process. A number of these "endothermic" fuels are known, and some are under serious study. All of the known endothermic fuel reactions require a catalyst to make them proceed and absorb extra heat at moderate temperatures. Hence, variants such as the catalytic heat exchanger are being considered in future aircraft concepts. While the endothermic fuel technique introduces a new element of complexity into aircraft design (and particularly new maintenance requirements and reliability concerns), it has obvious advantages over the use of cryogenic fuels. [25] There are indications that, free of certain environmental and chemical influences, most hydrocarbons tend to have good high-temperature tolerance. [25]

Cryogenic fuels can contribute only sensible and latent heat, whereas certain hydrocarbon fuels can in addition provide cooling through endothennic reactions. Hydrocarbons can undergo both thermal and catalytic reactions. Theoretically, the total heat-sink capacities for hydrocarbon fuels range from about 50% to 112% of the cooling capacity of hydrogen (on a "%" heat of combustion basis) with laboratory proven capabilities up to about 85 %. [22]

The endothermic fuels have the following technical, commercial, and safety advantages;

- Continued availability
- Relatively inexpensive
- Condensed phase under standard temperature and pressure (STP)
- Higher latent heat of vaporization
- Safe handling and storage
- High energy content per unit volume
- No ignition limitations under subsonic combustion conditions
- Non-cryogenic; ** insulation not required ** vapor recovery not required
- Conventional Army/Commercial (A/C) fuel system
- A/C turn-around time not governed by fuel
- Conventional fuel handling/logistics; ** off-site production
- Launch side hardening easier
- Available enabling technologies
- Potentially smaller vehicles

The Cooling capacity of normal and endothermic hydrocarbon fuels: Most hydrocarbons can provide a maximum of only 700-800 Btu/lb enthalpy on being heated from ambient to about 1000 °F. Figure 1.18 shows the heat sink in terms of Btu/lb fuel burned as a

function of Mach number. The indication being that about 2000 Btu/lb will be required at a speed of Mach 10. It is obvious that flight speeds greater than about Mach 5 will require additional cooling capability. This region generally known as the hypersonic region, is where endothermic reactions will have to be utilized in order to employ the higher hydrocarbon fuels successfully. [22]

Types of heat-sink reactions (endothermic reactions):

- Thermal reactions (Non-catalytic reactions)
- Catalytic reactions:
    a) Dehydrogeneration reactions
    b) Dehydrocyclization reactions
    c) Depolymerization reactions [22]

Thermal reactions: The decomposition of hydrocarbons requires energy for its accomplishment, i.e., it is a possible heat-sink reaction. The effect of product distribution for the thermal decomposition of some hydrocarbons is shown in Table 1.1. At higher conversions, the actual reaction is essentially thermally neutral due to increased formation of methane (which is exothermic). [22]

Catalytic reactions: A catalyst may serve either or both of two purposes; to increase the rate of a particular chemical reaction or to cause one of several possible reactions to occur selectively. It is very useful to increase the selectivity of the endothermic reaction. For example, a catalyst that would selectively enhance the rate of certain endothermic cracking or dehydrogeneration reactions of propane to eliminate the formation of methane could increase the heat sink by as much as 300% over the thermal reaction. [22]

♠ **Dehydrogeneration reactions**

The most practical way to do this is to have the reaction go selectively to a product having a resonance-stabilized structure. This not only will produce a more reliable heat sink but also will influence the temperature regime of thermodynamic equilibrium in favor of the desired products.

The ultimate fuel may be a blend of hydrocarbons in order to achieve optimization in such properties of freezing point, volatility, lubricity, heat sink, thermal stability, etc. For example, addition of methyl groups to he basic ring structures can alter these properties, but the more methyl groups that are added the lower is the available heat sink. [22]

♠ **Dehydrocyclization reactions**

In principle, any hydrocarbon structure with sufficient carbon atoms in it could be cyclized to from C_5 or C_6 rings and then dehydrogenated to give a high heat-sink. For example, normal octane can be cyclized to ethylcyclohexane and then dehydrogenated to styrene with a heat sink of about 400 Btu/lb. However, the cyclization step on any catalyst investigated so far is relatively slow and not too selective, which means that the theoretical heat sink cannot be realized. It appears that the most promising utilization of this type of reaction will come in connection with already-formed cyclic structure. [22]

♠ **Depolymerization reactions**

Since the chemical reaction of a polymerization is exothermic, it follows that the reverse reaction of depolymerization is endothermic. This reaction provides a limited heat sink. [22]

Comparison of thermal and catalytic reactions: In general, the catalytic reactions are more favored rather than thermal reactions.

♦ *Concerning the degree of conversion:*

- The heat sink provided by the catalytic reaction is a direct function of the degree of conversion. The greater the degree of conversion, the greater the heat sink.
- The thermal reaction has a maximum heat sink of about 300 Btu's, which occurs at about 60% conversion, and thereafter the heat sink actually decreases because this reaction is not selective and there are competing endothermic and exothermic reactions.

♦ *Concerning the rate of reaction (K):*

- The catalytic reaction has a high intrinsic rate and a low energy of activation and, hence, a high rate of reaction over a broad range of temperature.
- The thermal reaction on the other hand, proceeds very slowly at low temperatures. Although, because of the high energy of activation it responds strongly to the effect of temperature it does not reach comparable rates to the catalytic reaction until about 1200 ^{o}F. This means that the catalytic reaction has a much broader range of temperature over which it can be used successfully for cooling.

♦ Since the rate of reaction is primarily a function of the properties of catalyst, it allows for the possibility of increasing the rate by devising better catalyst. This is not possible of course with thermal reactions. [22]

How can endothermic fuels accommodate the varying heat load? For endothermic fuels, this varying heat load may also be translated to variations in fuel phase. For example, the tow types of endothermic fuel reactions create mixtures of small and large hydrocarbons, these

reaction types are: dehydrogenation such as methylcyclohexane $\Rightarrow$ toluene + H_2, and cracking, such as $C_nH_{2n+2} \Rightarrow$ light gases such as C_2H_4.

These fuel reactions are used to absorb aircraft heat by passing some portion of the fuel through a reaction. Thus, during early portions of a mission, the fuel would probably by-pass the reactor and being injected as a liquid. For high heat load parts of the mission, the fuel might pass entirely through the reactor, emerging as a supercritical fluid. For intermediate heat load parts of a flight, part of the fuel might by-pass the reactor. The fuel to be burned could then consist of part unreacted fuel (liquid) and part hot, reacted fuel (SCF).

The fuel could be injected into the combustor through two separate sets of nozzles (one for liquid and one for SCF), or the fuel could be re-mixed and injected. [24]

Cooling application possibilities: It is possible that turbine engines would be used up to a speed of about Mach 4, a subsonic combustion ramjet at speed up to Mach 7, with a supersonic combustion ramjet being used at speeds above that. [22]

Three different ways of transferring the heat from the engine to the reactor exchanger have been considered. These three ways are illustrated in Fig. 1.19, which represents ramjet engines traveling from right to left; the procedure is described below.

- Direct regeneration cooling between the combustion space and the fuel tubes (containing catalyst) forming the engine.
- Secondary loop design in which a circulating fluid is employed to transfer the heat from the engine to a reactor-exchanger containing the catalyst.
- A system in which some of the inlet air (say 5-10%) is bled through a reactor-exchange system and then employed to cool the walls of the engine by transpiration or film cooling. [22]

A Proposed cooling system: This cooling system design was driven by Mach 5 cruise conditions. Operating conditions for Mach 5 are shown in Fig. 1.20. The maximum pressure is 424 PSIA (2.93 MPA) at the inlet to the cooling panels, and the maximum temperature is 838 °F (448 °C)at the outlet of the cooling panels. The cooling panels are arranged in series with the coolant flowing forward through the airframe nozzle, then downward to cool the turbofan inlet close-off door seals and back through the ramjet. The 77 lbm/s (35 kg/s) flow splits after the last cooling panel outlet with 40 lbm/s (18 kg/s) flowing through the heat exchanger/reactor and the rest flowing to the pre-heater. The flow is re-mixed at the inlet to the expansion tank. The pump requires 143 HP at 242 PSIA (1.67 MPA) and 80% efficiency. A separate power unit using LOX and MCH drive these pumps. The use of cryogenic liquids in large quantities is not allowed on aircraft carriers; however, small amounts of LOX are used for pilot breathing at high altitudes. It is estimated that the quantity of LOX required for the APU would be comparable to that required for the pilot. [23]

Syltherm 800 has a high coefficient of thermal expansion, making an expansion tank necessary. Between room temperature and 838 °F, Syltherm expands 91% in volume. According to the manufacturer, this tank should be designed to be 1/4 full of coolant when cold and 3/4 full when hot. [5] The remaining volume is filled with a nitrogen gas blanket. The tank is located at the lowest pressure point in the system, and the constant flow of coolant liquid through the tank ensures that vapors will be isolated in the tank. The physical arrangement of the components is shown in the scale inboard profile in Fig. 1.21. [23]

A unique feature of this cooling system is that it is self-compensating, i.e., an increase in heat load will lead to an increase in the temperature of the coolant entering the heat rejection devices. The increase in temperature will lead to an increase in the efficiency of the heat

exchanger/reactor, increasing the temperature drop in the coolant. Similarly the preheater will also transfer more heat to the fuel. The effect of the increase in heat load on the temperature of the coolant will have been diminished and a new equilibrium will be established. In this off-design case, the coolant and catalyst may be degraded, but the system will operate until the fuel temperature reaches 925 °F (496 °C); this is the limiting condition for both the catalyst and coolant. Syltherm can operate for five days at a temperature of 932 °F (500 °C), but the pressure would have to be increased to avoid boiling. Note that the heat capacity of the coolant is so great that a 15% increase in heat load will only cause an increase of 6 °F (3.3 °C) in the coolant. [23]

1.5 Piloted Energy for Liquid Hydrocarbon Combustion

Liquid hydrocarbons are attractive candidates for the low range of the hypersonic flght regime due to their high volumetric energy content and the relative simplicity of the operational logistics. Although the energy/mass density of liquid hydrocarbon is lower than that of hydrogen, some of the mass increase wuold be recovered by a small and ligher structure of the vehicle. Liquid hydrocarbon fuels require substantial residence time to achieve vaporization and complete exothermic reactions, and such time is unlikly to be available in reasonable-sized supersonic combustors. The chemical kinetics of hydrocarbons are slow in comparison with gaseous fuels, such as hydrogen. For many realistic operating conditions, exothermic reactions cannot be achieved within the available residence time. Use of a pilot flame with dast kinetics (i.e., gaseous hydrogen) can provide locally, at the liquid injection location, the conditions necessary to accelerate the hydrocarbon reactions rates and reduce the Damkohler number, i.e., high temperature and low fluid velocities. For such a system it is necessary to verify: **(a)** the level of

piloted energy required to ingite and maiantain stable comustion of the liquid fuel, and **(b)** the interaction between the pilot flame and the heat sink represented by the injected hydrocarbon. [6]

Bonghi et al.[30] injected liquid toluene at 5H down stream of a step of height H in a Mach 2.5 flow at 300 K and 1000 K using a parallel hydrogen-pilot flame. Toluene ($C_6H_5CH_3$) is on of the components of catalytically cracker methylcyclohexane (MCH), a candidate fuel for supersonic combustion applications. Segal and Young [6] using the same previous configuration injected the toluene from a reservoir at 300 K, and thus, absorbed energy from the surroundings to vaporize and further heat to the local temperature. The large recirculation region formed by hydrogen-pilot combustion extends beyond the liquid injection station, 5H, and thus a substantial amount of the injected liquid reaches the region of stabilization of the pilot flame. When the amount of liquid increases above a certain quantity, it quenches the pilot flame. The amount of liquid fluid that can be injected without inducing quenching was found to be dependent strongly on the equivalence ratio of the pilot flame and, in smaller proportion, on the air stagnation temperature. It was found that as the pilot energy level increases the amount of toluene that can be injected (while maintaining a stable flame) can also be increased. Beyond a certain value, however, the ratio of energy levels decreases again, as more liquid is injected and the amount that reaches the region of stabilization of the pilot flame increases, inducing quenching. This effect is enhanced by the effect of heat release on the structure of the flow field. A larger deposition of heat in the combustion region caused a pressure increase followed by an enlargement of the recirculation region and a reduction in the local velocity, which favors upstream interaction, further facilitating the arrival of liquid in the recirculation region and quenching of the pilot flame. The increase in the stable flame margin with the air stagnation temperature, T_o, was evident.

1.6 Importance of Modeling and Simulation

The supersonic combustion ramjet (scramjet) is expected to be the most effective propulsion system for the Single Stage To Orbit (SSTO) transportation vehicles and hypersonic transportation vehicles of the next Generation. Many studies on scramjet components such as inlet, combustor and nozzle have been carried out to obtain a better understanding of the performances of the individual components. [31-34] However, it is expected that intensive interactions among these components will occur in real engines. For example, a rise in pressure due to combustion causes separation which propagates upstream into the inlet and changes the inlet back pressure, which may result in unstart condition in the inlet. In the case of interactions, the total performance of the engine cannot be evaluated based on the linear combination of the obtained performance of the individual components. Thus, tests of the models of the whole engine are necessary to elucidate the interactions among these components and the overall performance of the whole engine. [35] Testing of the models of whole engine requires rather big and expensive wind-tunnel facilities. Thus, only a limited number of results on whole engine tests have been reported. [36,37]

Multiphase combustion is such a complex phenomenon that it warrants focused research using modeling and numerical simulations. Though physical experiments are the ultimate test to study the performance of combustion/propulsion systems, they are often extremely expensive and complicated, and at times are not even possible. This is due to the hostile environments, complicated interactions, and couplings. On the one hand, these couplings make it impossible to study the effect of one parameter at a time in a physical experiment of this nature. On the other hand, numerical experiments open an avenue for isolating and understanding the influence of different parameters on complex combustion situations. Furthermore, these can serve as means of

evaluating scaling laws, which would be extremely difficult and expensive to determine from physical experiments alone. Modeling also provides a potential design tool for future combustion and propulsion systems. However, this is not a simple or straightforward extension of computational fluid dynamics (CFD) by including a few more terms in the governing equations.[38]

Numerical simulation is time consuming even with ultrafast modern computers. The fuels of choice, e.g., hydrocarbons or metal slurries, will have a large number of kinetic steps and species involved in their combustion. The computational time increases as the square of the number of species, and calls for reduced chemistry based on sound logic. The presence of solid particles, such as soot or unburned fuel droplets, and their transport in the turbulent flow field complicates the situation even further, and requires extremely small grid sizes. Ultimately, the results of these complex numerical simulations should be made available in the form of user-friendly models for the designer.

Strong interaction of the computational combustion community with experimentalists is needed in order to assure meaningful model validations, and to generate more reliable and advanced models to aid in the design of complex combustion/propulsion systems of the future.

Computational fluid dynamics (CFD) simulations have become invaluable in the design process due to the high costs and long turnaround times encountered in experimental programs and due to the inability to reproduce all desired flowfield conditions in present laboratory facilities. Fundamental numerical techniques for the calculation of compressible flowfields have been available for some time, but the computational resources required for making accurate 3-D simulations of complex flowfields have become more generally available for design purposes only relatively recently. This is, for the most part, due to the many dramatic improvements that have occurred in the performance of computer hardware, but is also due to progress in the

development of efficient and accurate numerical techniques and algorithms. Advances in areas such as grid generation, development of higher order schemes and turbulence modeling makes reasonably accurate simulations of extremely complex flowfields now possible. It is important to point out that if CFD codes are to be incorporated into a design process, the need for experimental validation is a necessity, a point that is sometimes under-emphasized. [4]

One of the advantages of CFD simulations over standard experimental data sets is that all flowfield properties are available everywhere in the flowfield so that any desired quantity can be extracted from the CFD results. Both detailed information about particular flowfield features and global information, such as conservation consistency checks and overall performance quantities, can be calculated from the numerical data set. [4]

The design of fuel injection configurations like the ones considered in the scramjet engines rely on the understanding of extremely complex flowfields with features such as: turbulent mixing, combustion reactions, strong three-dimensionality, compressibility effects, boundary layers and flow separations. The ability to study such flowfields experimentally has been limited because of the difficulty in gaining access into the harsh, yet easily perturbed environment of a supersonic flowfield. Understanding the geometrical complexity of such flows has been limited by the fact that most traditional quantitative measurement techniques are pointwise techniques. Theoretical studies in the past have been stalled by the difficulties in dealing with the highly non-linear set of equations that describe the physics of these flowfields. Numerical approaches give reasonable, and often very accurate, solutions to problems such as these that are not solvable analytically. Recently, due to the development nonintrusive laser diagnostics measurement techniques and to advances in the field of computational fluid dynamics, the ability to study such flowfields has been greatly improved. [4]

Recent advances in numerical simulation techniques and theoretical studies offer new descriptions of the physical phenomena in high-speed flows including mixing and combustion interactions and the onset and development of instabilities and voticity, both in non-reacting and chemically reacting flows. Although numerical simulations offer much physical insight and a great level of detail, the experimental validation of both the theoretical models and the numerical algorithms is largely lacking due to difficulties in measuring essential parameters in these flowfields, such as velocity, temperature and pressure characteristics. Furthermore, there are numerous modeling issues, which are largely unresolved and need insight from experimental observation. Existing experimental facilities are, in general, dedicated to study of only a limited range of topics because of extreme conditions of high enthalpy flow, including an overview of the demands of availability of existing facilities. Certain facilities, capable of reproducing high enthalpy conditions, can operate for only short time durations, insufficient to achieve stable thermal conditions. Other existing facilities are, in general, limited in terms of their experimental flexibility. [6]

2. THEORETICAL MODEL AND COMPUTATIONAL PROCEDURE

The present computational study incorporates two cases with close configuration aiming at studying the effect of mixing schemes on the combustion characteristics in supersonic flow fields. In the first case study gaseous hydrogen is used as the main and only fuel in the system. While in the other case study gaseous hydrogen is used as a pilot energy source for the combustion of liquid kerosene. Both cases are treated three-dimensionally and both of them do have a rearward-facing step down stream of the test section entrance. The geometry of the configurations used in this computational study is presented in Figs. 2.1-2.6. The flow configurations are matched with those employed in the experiments of Segal et al. [7] and Owens et al. [39] respectively. Figure 2.1 depicts schematically the configuration of the first case, which shows that the flow in the vicinity of the fuel injection stations is characterized by the supersonic flow of Mach number 2.0 over a rearward-facing step with transverse sonic gaseous H_2 injection downstream of the step. The length of the test section is 21.3 cm and the cross section is 2.54 by 3.8 cm. The step height (H) is 5 mm in the upper wall. Hydrogen is injected normally to the incoming air flow direction from two stations, 3 and 7 step heights downstream of the step. The experimental injection diameters are 1 mm each. For the sake of facilitating the computational procedures and saving CPU time in the present computational study, the circular injection diameters were simplified to be square ones having the same cross section area. Because of the symmetry in the configuration under study, only one half of the physical domain was simulated with the plan of symmetry located at the centerline of the injection slots. Figure 2.2 presents a 3-D scheme for this configuration with the location of the plan of symmetry. Table 2.1 includes the flow conditions used in this case study.

In the second case study a vitiated airstream with 16% O_2 mole fraction is directed to a test section entrance with a square cross section of 2.54 x 2.54 cm^2. The test section, shown in Fig. 2.3, featured a 10-mm-high (H) rearward-facing step as the main flameholding mechanism. The step included a stagnation chamber from which the pilot flame is generated, parallel to the main flow via three, 1-mm-diameter orifices equally spaced in a transverse direction. Liquid kerosene ($C_{12}H_{26}$) is injected normal to the incoming supersonic air flow through a hole of variable diameter of 0.5 and 1.0 mm. Removable, rearward-facing wedges were attached to the test section wall 2.8H downstream of the step with wedge length of 1.7H. The onset of thermal choking is delayed by diverging the test section starting 7H downstream of the step with a 3-deg half angle. Figure 2.4 presents the three injection configurations to be evaluated in this study. Configuration 1 featured a generic rectangular, rearward-facing step. Configuration 2 featured this step with either a 15 or 30-deg wedge installed 2.8H downstream of the step. Configuration 3 featured the rearward-facing step with beveled-edge step which is shown in Fig. 2.4-c. The beveled step has the same height (10 mm) as the rectangular step, but the edges parallel to the main flow are beveled to facilitate vortex-enhanced mixing.

Figures 2.5a-2.5c show schematic of the combustion flowfield for the three configurations. The air flow underwent expansion around the rearward-facing step where gaseous hydrogen is injected parallel to the main flow. When the pressure rise caused by hydrogen combustion was large enough, the expansion wave around the step turned into a compression shock. At five step heights downstream of the step, liquid kerosene is injected normal to the main flow creating a separation shock upstream of the jet. The jet then broke up downstream of the injection site where it vaporized and mixed with the main flow. Inclusion of the wedges generates the shock waves shown in Fig. 2.5-b, and the beveled step included

shedding of the counter rotating vortices as shown in Fig. 2.5-c. Each of these mechanisms interacts in a different way with the fuel jet. In all three-injection configurations, symmetry at the half width-plan exists. Therefore, only one half of the physical domain can be simulated. Figure 2.6 shows the three gaseous-hydrogen-pilot injection holes at the base of the step with the symmetry plan located at the centerline of the middle hole. Table 2.2 includes the flow conditions used in this case study.

The flow field to be analyzed is governed by the Reynolds averaged compressible form of the Navier-Stokes equations. These equations are closed using the two-equation κ-ε turbulence model. The equations are all-similar and can be expressed into the following common form:

$$\frac{\partial}{\partial t}(\rho\phi)+\frac{\partial}{\partial x}(\rho u\phi)+\frac{\partial}{\partial y}(\rho v\phi)=\frac{\partial}{\partial x}\left[\Gamma_\phi\frac{\partial\phi}{\partial x}-\rho\overline{u'\phi'}\right]+\frac{\partial}{\partial y}\left[\Gamma_\phi\frac{\partial\phi}{\partial y}-\rho\overline{v'\phi'}\right]+S_\phi \qquad (2.1)$$

where the corresponding values for the exchange coefficient Γ_Φ and the source or sink term S_Φ for any variable are summarized in Ref. [40]. The Reynolds stresses $\rho\overline{u'\varphi'}$ and $\rho\overline{u'\varphi'}$ are related to mean flow quantities via K-ε turbulence models. The transport equations for this model are available in Ref. [40].

The finite-volume method incorporated with the quadratic upwind interpolation scheme (QUICK) is employed to integrate and interpolate the partial differential equations represented by the common Eq. (2.1). The SIMPLEC, a variant of SIMPLE method developed by Patankar [41] was used to obtain the numerical solution for the discritized equations. The computer program used an Additive-Corrective Multi-Grid procedure to accelerate the convergence of the standard line-by-line solver. In addition to solving the basic transport equations on the original fine-grid level, multi-grid technique solve an equivalent equation set on each coarse grid level,

transferring correction onto the fine grid levels in an effort to achieve global balance and reduce the overall solution error. The use of multi-grid scheme can greatly reduce the number of iterations and CPU time required obtaining a converged solution. The convergence criterion was set so that the normalized residuals are less than 10^{-6} at any grid node and for any φ equation. The full detailed description of the FULENT code flow solver is provided in Appendix A.

For each case study the computations were performed on different grid sizes and the grid nodes were reasonably distributed and arranged to ensure that region of important influence on the flow field are adequately resolved. In general, the axial grid is clustered at the step and the fuel injection stations while the radial grid is concentrated within the jets, in the jets' interaction zones and towards the walls.

For the first case study a grid with a size of 209x34x23 is used. The aspect ratio was evaluated over the whole domain to make sure that the grid is fine enough to capture the flow features.

Work in building the grid and setting up the simulation procedure for the second case study (pilot hydrogen with kerosene combustion case) is under current investigation.

3. BOUNDARY AND INITIAL CONDITIONS

No-slip boundary conditions are used along the combustor walls as well as along the step boundaries for all cases under study. The walls are assumed adiabatic requiring normal derivative of temperature to vanish. Along the supersonic inflow boundaries uniform conditions are used. Along the supersonic outflow boundaries, non-reflective boundary conditions are used where the boundary values are found by linear extrapolation from the interior points.

Initial guessed values for the most important flow parameters such as temperature, velocity components, heat capacity (C_p), and mass fractions are assumed for the solution to start with. This process is a very important step in speeding the solution convergence. The inlet air values of these mentioned flow parameters are used in patching the whole flow field. The regions around the injection ports are patched using the corresponding values at the injection inlets. The patching process is explained in detailed in section 7.5.1 in Appendix A.

4. RESULTS AND DISCUSSION

In this section some of the data obtained while running the first case (sonic gaseous hydrogen normal fuel injection) are presented. A global overview on the plan of work is presented after which the some figures are presented as part of the available results.

This case was first simulated two-dimensionally and big differences between the experimental and numerically obtained wall pressure distribution were observed. Because of the three-dimensional nature of the normal injection it was necessary to guide the work towards the three-dimensional simulation.

Following the step-by-step technique in the simulation approach, the cold flow field is solved first getting a converged solution. Thereafter, this cold flow converged solution is used as an initial solution for the simulation of the combustion flow field. A rough grid of 161x34x23 was used in the beginning and converged solution was satisfied.

The flow field was simulated first without normal fuel injection for just solving the supersonic flow over the rearward-facing step. This converged solution was used to calculate the flow field with normal fuel injection. A converged solution was obtained for such a case.

The effect of grid refinement was tested by using more refined grid around the injection stations and in the far domain. A bigger grid with size of 209x34x23 was used and the cold flow field with fuel injection was simulated. The "Power Law Scheme" was used to descritize the governing equations.

The effect of the descritization scheme was tested by switching on one of the higher order schemes (both the 2^{nd} order and quadratic schemes were used). The higher order schemes required more time to achieve the convergence criterion. Some illustrative results obtained are presented in this section.

Figure 4.1 presents the normalized upper-wall pressure distribution along the combustor length for both "no-injection" and "with injection" cases. The averaged pressure at each axial location was normalized to the combustor entrance conditions. Both results were obtained using the smaller grid size of 161x34x23. It can be concluded that the pressure distribution with fuel flow and no combustion was essentially identical to those with no fuel flow. This conclusion is well matched with the experimental findings reported by Segal et al. [7]

The effect of grid refinement is shown in Fig. 4.2. The normalized upper-wall pressure distribution along the combustor length is plotted for both coarse and fine grids. A noticeable difference is clear especially just downstream of the step and in the far domain. This led us to discuss the effect of the descritization scheme. A higher order descritization scheme (2^{nd} order scheme) is compared to the power law scheme in Fig. 4.3. In this figure the normalized upper-wall static pressure distribution using both schemes are compared with the experimental values. The higher order scheme shows more comforting trend, especially just downstream of the step.

The combustion flow field simulation is now underway using the higher order scheme solution as an initial solution.

5. CONCLUSIONS

Numerical investigation is conducted to study the effect of the different injection schemes on the mixing and thereupon the combustion of both gaseous hydrogen and liquid kerosene as two different alternative fueling systems in the SCRAM jet engine. The normal injection mode presents good potential towards increasing the mixing efficiency of the fuel and the supersonic incoming air. This effect helps in increasing the fuel residence time in the combustor therefore overcoming the difficulties of maintaining stable and efficient combustion in such very high speed flow fields. Injecting gaseous hydrogen parallel to the incoming air flow from the base of the step to form a pilot flame can help in maintaining the kerosene flame stability. It could be found that the maximum kerosene equivalence ratio that can maintain stable flame is mainly a function of the pilot hydrogen equivalence ratio. The flame stability limit can be increased by injecting more pilot hydrogen to some extent. The wedges increased the mixing efficiency by creating stream wise vortical structures.

Work is still underway to complete simulating the different mixing schemes.

REFERENCES

[1] Matsuo, A., and Mizomoto, M., "Flow Structure of Supersonic Flow Past Backward-Facing Step with Perpendicular Injector," AIAA Paper 98-0939, January 1998.

[2] Tishkoff, J.M., Drummond, J.P., Edwards, T., and Nejad, A.S., "Future Direction of Supersonic Combustion Research: Air Force/NASA Workshop on Supersonic Combustion," AIAA Paper 97-1017, January 1997.

[3] Ferri, A., "Review of Problems in Application of Supersonic Combustion," Journal of the Royal Aeronautical Society, Vol. 68, No. 45, 1964, pp. 575-597.

[4] Donohue, J.M., "Experimental and Numerical Study of Ramp Inectors for Supersonic Fuel/Air Mixing," Ph.D. Dissertation, Department of Mechanical and Aerospace Engineering, University of Virginia, January 1995.

[5] Hussaini, M.Y., Kumar, A., and Voigt, R.G. (eds.), "Major Research Topics in Combustion," Springer-Verlag, New York, Inc., 1992.

[6] Segal, C., and Young, C.D., "Development of an Experimental flexible Facility for Mixing-Combustion Interaction in Supersonic Flow," Journal of Energy Resources, Vol. 118, June 1996, pp. 152-158.

[7] Segal, C., Krauss, R.H., Whitehurst, R.B., and McDaniel, J.C., "Mixing and Chemical Kinetics Interaction in a Mach 2 Reacting Flow," Journal of Propulsion and Power, Vol. 11, No. 2, Mar.-Apr. 1995, pp.305-314.

[8] Mays, R.B., Thomas, R.H., and Schetz, J.A., "Low Angle Injection Into a Supersonic Flow," AIAA Paper 89-2461, July 1989.

[9] Wood, C.W., Thomas, R.H., and Schetz, J.A., "Effect of Oscillating Shock Impingement on the Mixing of a Gaseous Jet in a Mach 3 Airstream," AIAA Paper 90-1982, July 1990.

[10] Mohieldien, T.O., and Tiwari, S.N, "Effects of Tandem Injection On Compressible Turbulent Shear Layer," AIAA Paper 98-1638, April 1998.

[11] Berman, H.A., Anderson, J.D., and Drummond, J.P., "Supersonic Flow over a Rearward Facing Step with Transverse Non-Reacting Hydrogen Injection," AIAA Journal, Vol. 21, No. 12, December 1983, pp. 1707-1713.

[12] Schetz, J.A., Thomas, R.H., and Billig, F., "Mixing of Transverse Jets and Wall Jets in Supersonic Flow," in Separated Flows and Jets, V.V. Kozlov and A.V. Dovgal (Edits.), Springer-Verlag, Berlin, 1991.

[13] Baranovsky, S.I., and Schetz, J.A., "Effect of Injection Angle on Liquid Injection in Supersonic Flow," AIAA Journal, Vol. 18, No. 6, 1980, pp.625-629.

[14] Hartfield, R.J., Jr., Hollo, S.D., and McDaniel, J.C., "Experimental Investigation of a Supersonic Swept Ramp Injector Using Laser-Induced Iodine Fluorescence," Journal of Propulsion and Power, Vol. 10, No. 1, Jan.-Feb. 1994, pp. 129-135.

[15] Waitz, I.A., Marble, F.E., and Zukoshi, E.E., "An Investigation of a Contoured Wall Injector for Hypervelocity Mixing Augmentation," AIAA Journal, Vol. 31, No. 6, June 1993, pp. 1014-1021.

[16] Riggins, D.W., Mekkes, G.L., McClinton, C.R., and Drummond, J.R., "A Numerical Study of Mixing Enhancement in a Supersonic Combustor," AIAA Paper 90-0203, Jan. 1990.

[17] Daso, E.O., and Gross, B., "Analysis of Supersonic Mixing in High Speed Combustors," Presented at the Joint JANNAF Propulsion Meeting, Nov. 15, 1993.

[18] Donohue, J.M., Haj-Hariri, H., and McDaniel, J.C., "Vorticity Generation Mechanisms in Parallel Injection Schemes for Supersonic Mixing," AIAA Paper 92-3286, July 1992.

[19] McClinton, C.R., "Autoignition of Hydrogen Injected Transverse to Supersonic Airstream," AIAA Paper, 79-1239, June 1979.

[20] Huber, P.W., Schchenxnayder, C.J., and McClinton, R.C., "Criteria for Self-Ignition of Supersonic Hydrogen-Air Mixtures," NASA Technical Paper 1457, 1979.

[21] Tomioka, S., Hiraiwa, T., Mitani, T., Zamma, Y., Shiba, K., and Masuya, G., "Auto Ignition in a Supersonic Combustor with Perpendicular Injection Behind Backward-Facing Step," AIAA Paper 97-2889, July 1997.

[22] Lander, H., and Nixon, A.C., "Endothermic Fuels for Hypersonic Vehicles," Journal of Aircraft, Vol. 8, No. 4, 1970, pp. 200-207.

[23] Petely, D.H., and Jones, S.C., "Thermal management For a Mach 5 Cruise Aircraft Using Endothermic Fuel," Journal of Aircraft, Vol. 29, No. 3, May-June 1992, pp. 384-389.

[24] Edward, T., "USAF Supercritical Hydrocarbon Fuels Interest," AIAA Paper 93-0807, Jan. 1993.

[25] JANNAF Ramjet Subcommittee Workshop, "Fuels For High-Speed Flight Vehicles," CPIA Publications 518(2 Vols.), June 1988, pp.5-10.

[26] Savage, P.E., Gopalan, S., Mizan, T.I., Martino, C. J., and Brock, E.E., "Reactions at Supercritical Conditions: Applications and Fundamentals," AICHE Journal, Vol. 4 1, No. 7, July 1995, pp. 1723-1778.

[27] Zhou, Z.W., and Lin, S.P., "Effects of Compressibility on The Atomization of Liquid Jets," Journal of Propulsion and Power, Vol. 8, No. 4, 1992, pp. 736-740.

[28] Chen, S., and Lefebvre, A.H., "Influence of Ambient Air Pressure on Effervescent Atomization," AIAA Paper 92-0640, Jan. 1992.

[29] JANNAF Ramjet Subcommittee Workshop, "Fuels For High-Speed Flight Vehicles," CPIA Publications 518 (2 Vols.), June 1988, pp. 143-182.

[30] Bonghi, L., Dunlap, M.J., Owens, M.G., Young, C.D., and Segal, C., "Hydrogen Piloted Energy for Supersonic Combustion of Liquid Fuels," AIAA Paper 95-0730, Jan. 1995.

[31] Waltrup, P.J., Dugger, G.L., Billig, F.S., and Orth, R.C. , "Direct-Connect Tests of Hydrogen-Fueled Supersonic combustors," 16th Symposium (Int'l) on Combustion, Combustion Institute, 1976, pp. 1619-1630.

[32] McCilinton, C.R., "Interaction Between Step Fuel Injector on Opposing Walls in a Scramjet Combustor Model," NASA TP-1174, 1978.

[33] Trexler, C.A., and Sanders, S.W., "Design and Performance at a Local Mach Number of 6 of an Inlet for an Integrated Scramjet Concept," NASA TN-D-7944, 1977.

[34] Nivkerson, G.R., "Optimized Scramjet Exhaust Nozzles for Hypersonic Propulsion," AIAA Paper 88-3161, 1988.

[35] Tomioka, S., Hiraiwa, T., Sakuranaka, N, Murakami, A., Sato, K., Matsui, A., "Ignition Strategy in A Model SCRAMJET," AIAA Paper 96-3240, July 1996.

[36] Northam, G.B., and Anderson, G.Y., "Supersonic Combustion Ramjet Research at Langley," AIAA Paper 86-0159,1986.

[37] Billig, F.S., "Supersonic Combustion Ramjet Missile," Journal of Propulsion and Power, Vol. 11, No. 6, 1995, pp. 1139-1146.

[38] Roy, G.D., "Propulsion Combustion: Fuels to Emissions," Taylor & Francis Publishers, 1998.

[39] Owens, M., Segal, C., and Auslender, A.H., "Effect of Mixing Schemes on Kerosene Combustion in a Supersonic Airstream," Journal of Propulsion and Power, Vol. 13, No. 4, July-August 1997, pp. 525-531.

[40] Fluent Version 4.4 User's Guide, Fluent Incorporated, New Hampshire, 1996.

[41] Patankar, S.V., Numerical Heat Transfer and Fluid Flow, McGraw Hill, New York, 1980.

Table 1.1 Thermodynamic heats of reaction

Hydrocarbon	Reaction products	ΔH_R, Btu/lb
Methylcyclohexane	Toluene, H_2	940
	Benzene, H_2, CH_4	710
	Cyclohexene, CH_4	286
	Cracked products	−60[a]
n-Octane	Octene, H_2	491
	Octadiene, H_2	ca 900
	Styrene, H_2	1425
	Ethylbenzene (EB), H_2	957
	Xylene, H_2	915
	Toluene, H_2, CH_4	718
	Benzene, H_2, C_2H_6	804
	Cracked products	258
n-Dodecane	Dodecene	330
	Dodecadiene, H_2	595
	Aromatics, H_2	ca 640
	Cracked products	−110[a]
n-Hexadecane (cetane)	Cracked products	131
Dicyclohexyl	Benzene, H_2	1038
	Toluene, pentane	325
	Cyclohexane (CH)	−94[a]
	Hexane	−322[a]
	MCH, pentane	−231[a]
	Light gas	22
	Diphenyl, H_2	1080
	Phenylcyclohexane, H_2	540
Decalin	Naphthalene, H_2	950
	Tetralin, H_2	670
	CH + olefin	143
	MCH + olefin	143
	DMCH + olefin	143
	DECH	−110[a]
	Benzene + olefin	800
	Toluene + olefin	800
	EB + olefin	800
	DEB	−700
	Alkyl aromatics	−400
Ethylbenzene	Styrene	509
	Toluene, CH_4	−273
	Benzene, C_2H_6	−180
	Benzene, C_2H_4	405
JP-7 (F-71), 1200°F	60% cracked, 50% gas	310[b]

[a] Exothermic.
[b] Experimental.

Table 2.1 Free stream and injection nominal operating conditions for the transverse sonic fuel injection case

$P_s)_{air}$ (atm.)	0.5
$T_{total})_{air}$ (K)	741
Mach No.$)_{air}$	2.0
$^*K)_{air}$	1.4
$^{**}M)_{air}$	28.9
$T_{static})_{fuel}$ (K)	500
$P_{static})_{fuel}$ (atm.)	0.5
Mach No.)fuel	1.0
$^*K)_{fuel}$	1.4

*K is the gas constant.
**M is the molecular weight

Table 2.2 Fee stream and injection nominal operating conditions for the piloted-energy kerosene combustion case

Mach No.$)_{air}$	1.8
P total$)_{air}$ (Pa)	430
$T_{total})_{air}$ (K)	1000
Equivalence Ratio$)_{h2}$	0.02
Equivalence Ratio$)_k$	0.325
$T_{total})_k$ (K)	298 and 420

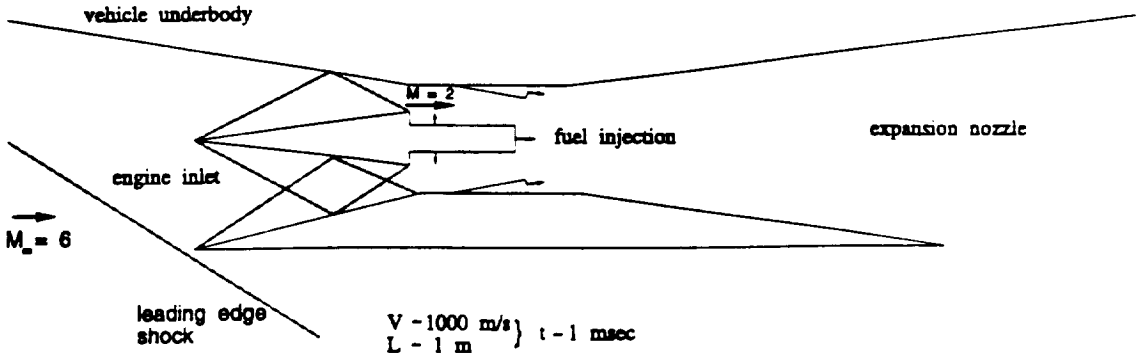

Fig. 1.1 Schematic of a generic scramjet engine configuration.

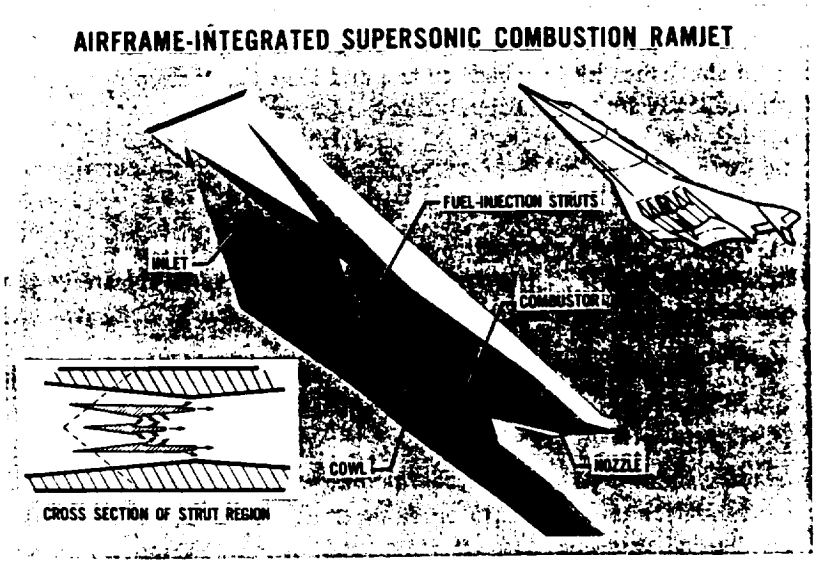

Fig. 1.2 Airframe-Integrated supersonic combustion ramjet (scramjet).

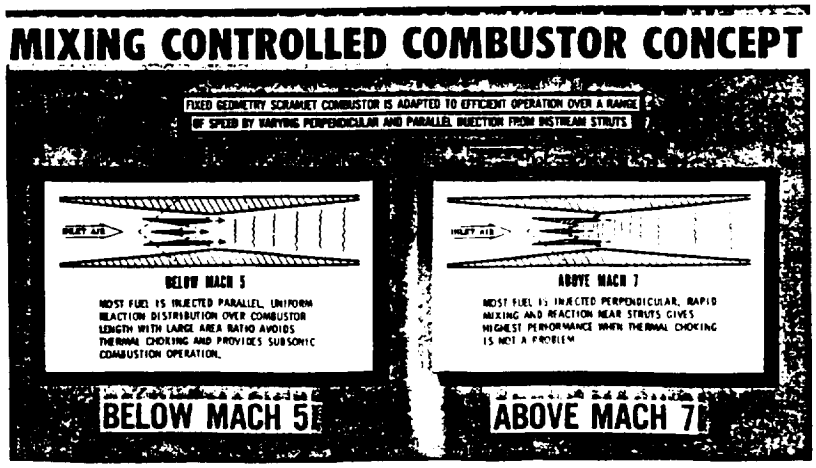

Fig. 1.3 Mixing controlled combustion concept.

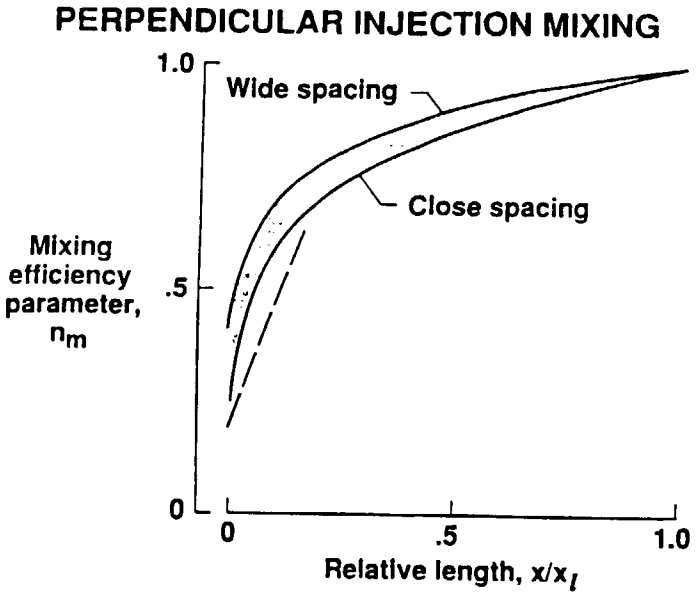

Fig. 1.4 Mixing efficiency as a function of relative combustor length (perpendicular injection mixing).

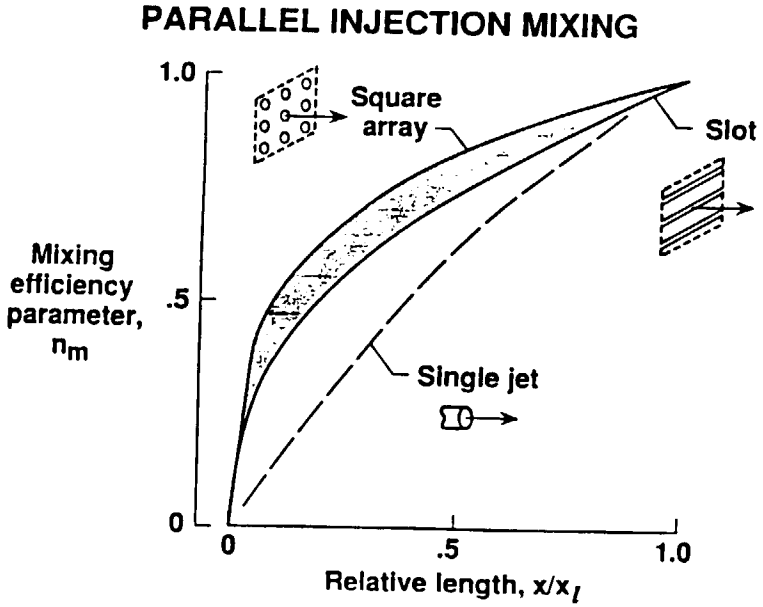

Fig. 1.5 Mixing efficiency as a function of relative combustor length (parallel injection mixing).

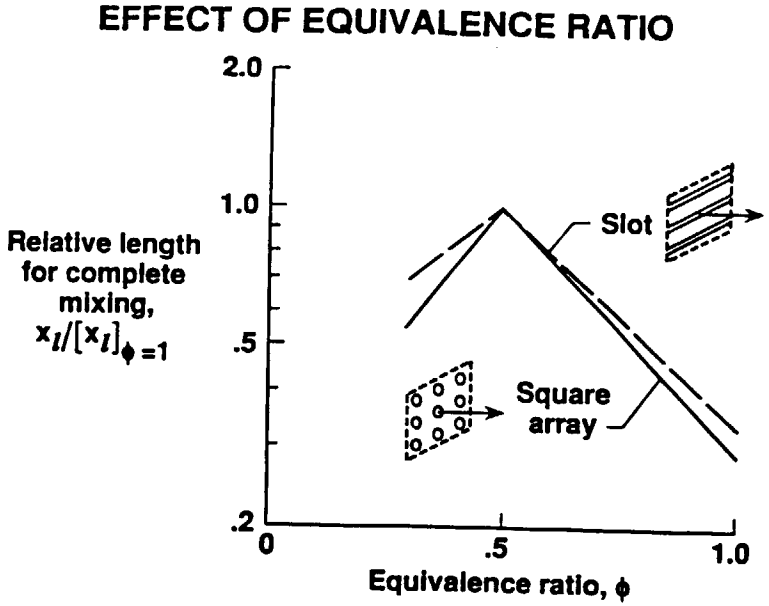

Fig. 1.6 Effect of equivalence ratio.

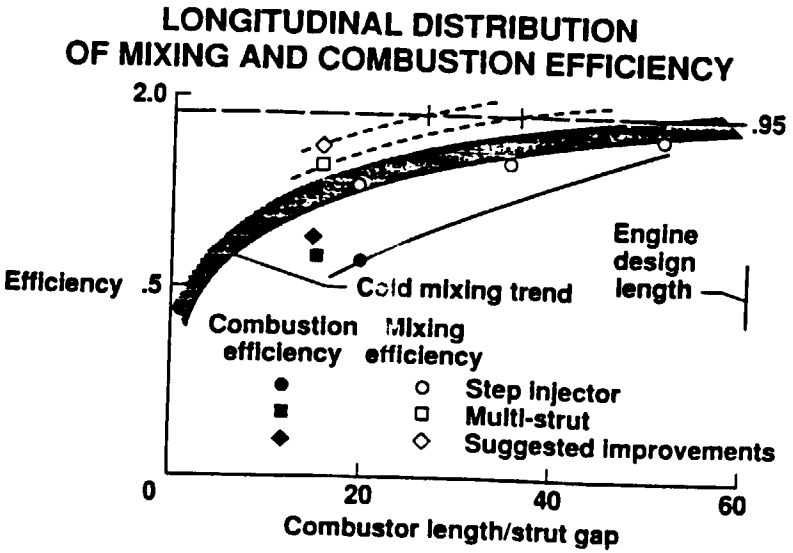

Fig. 1.7 Longitudinal distribution of mixing and combustion efficiency.

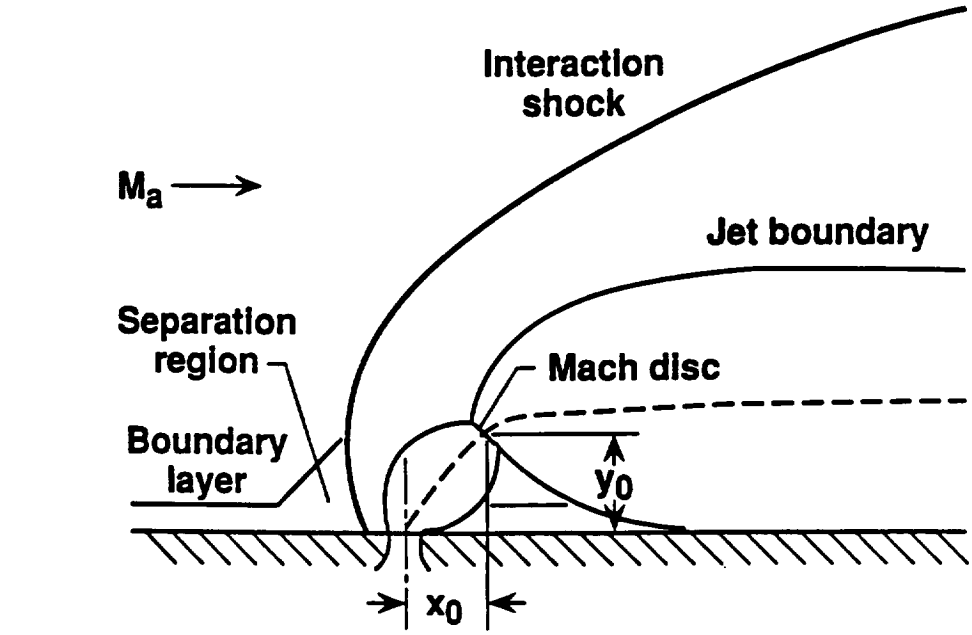

Fig. 1.8 Typical flowfield features of under-expanded jet injected normally into a supersonic free stream.

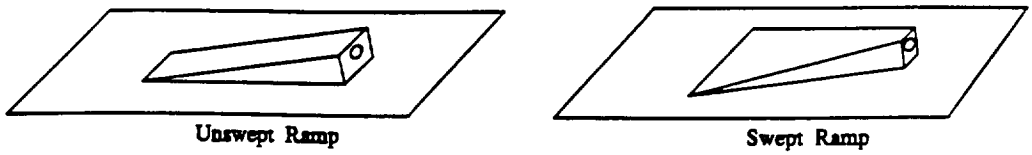

Fig. 1.9 Ramp injector geometries.

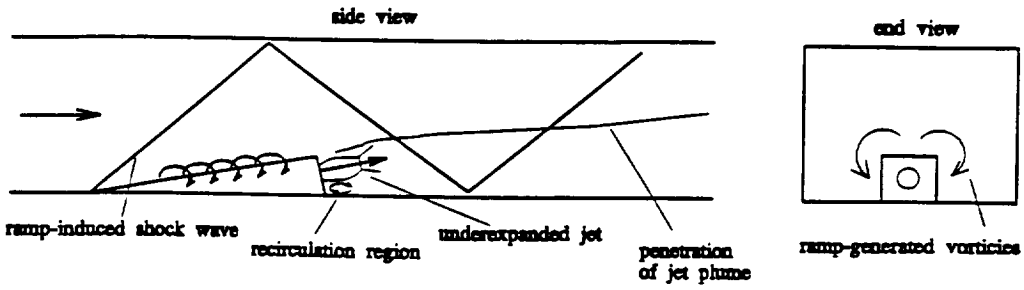

Fig. 1.10 Ramp injector flowfield features

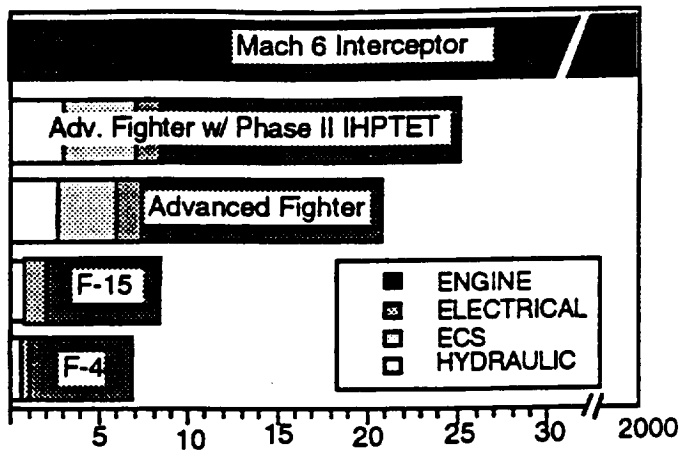

Fig. 1.11 Maximum estimated excess heat loads for various aircraft.

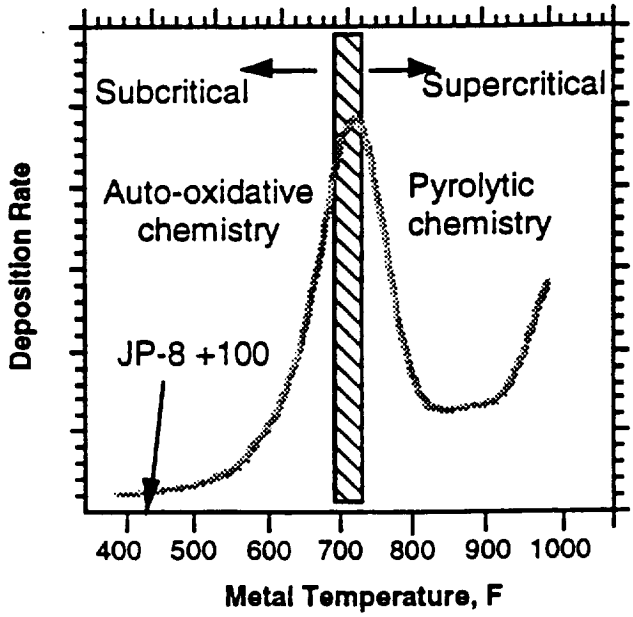

Fig. 1.12 Typical deposition behavior in air-standard jet fuels and model compounds.

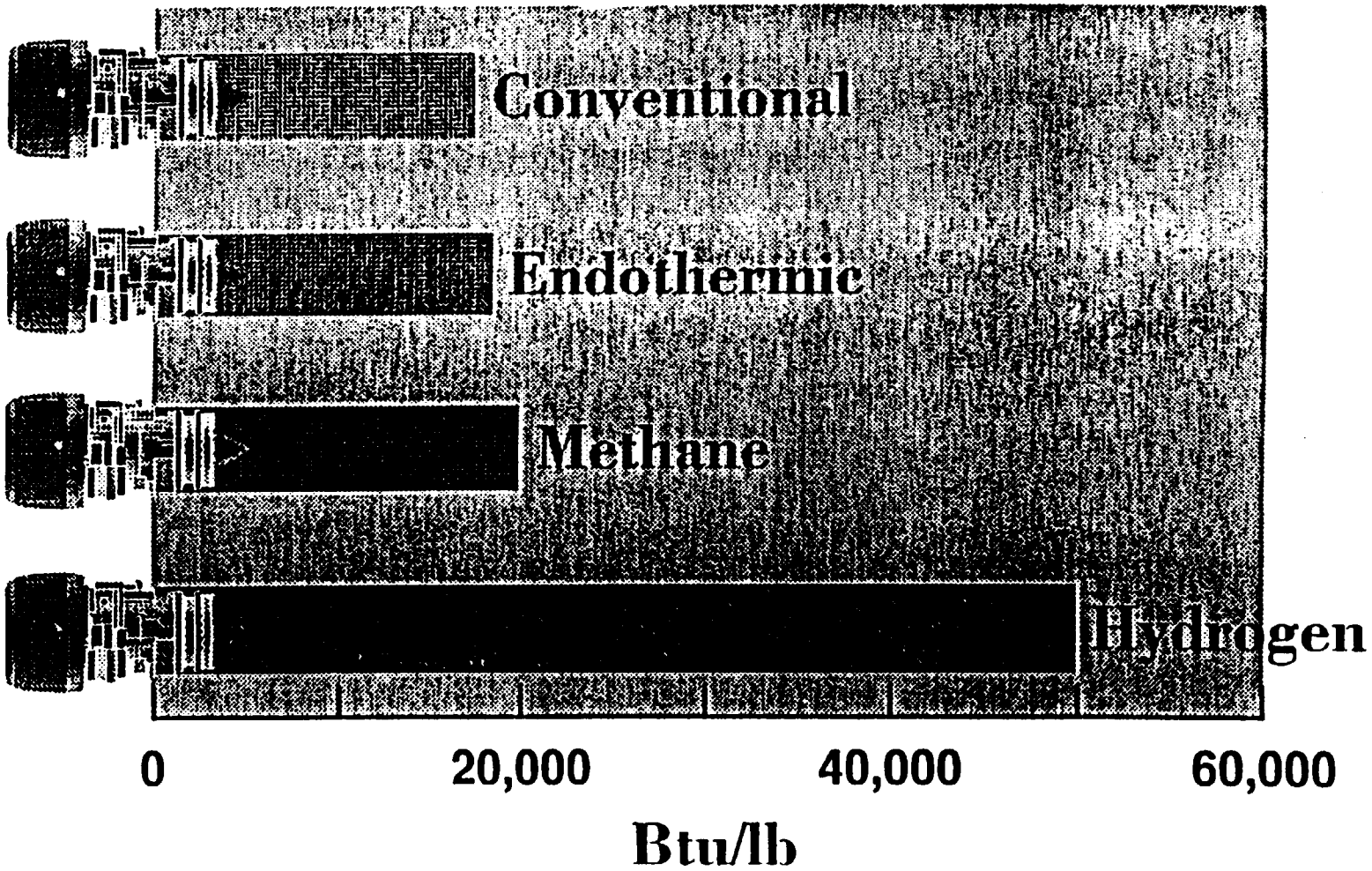

Fig. 1.13 The energy per unit mass for various fuels.

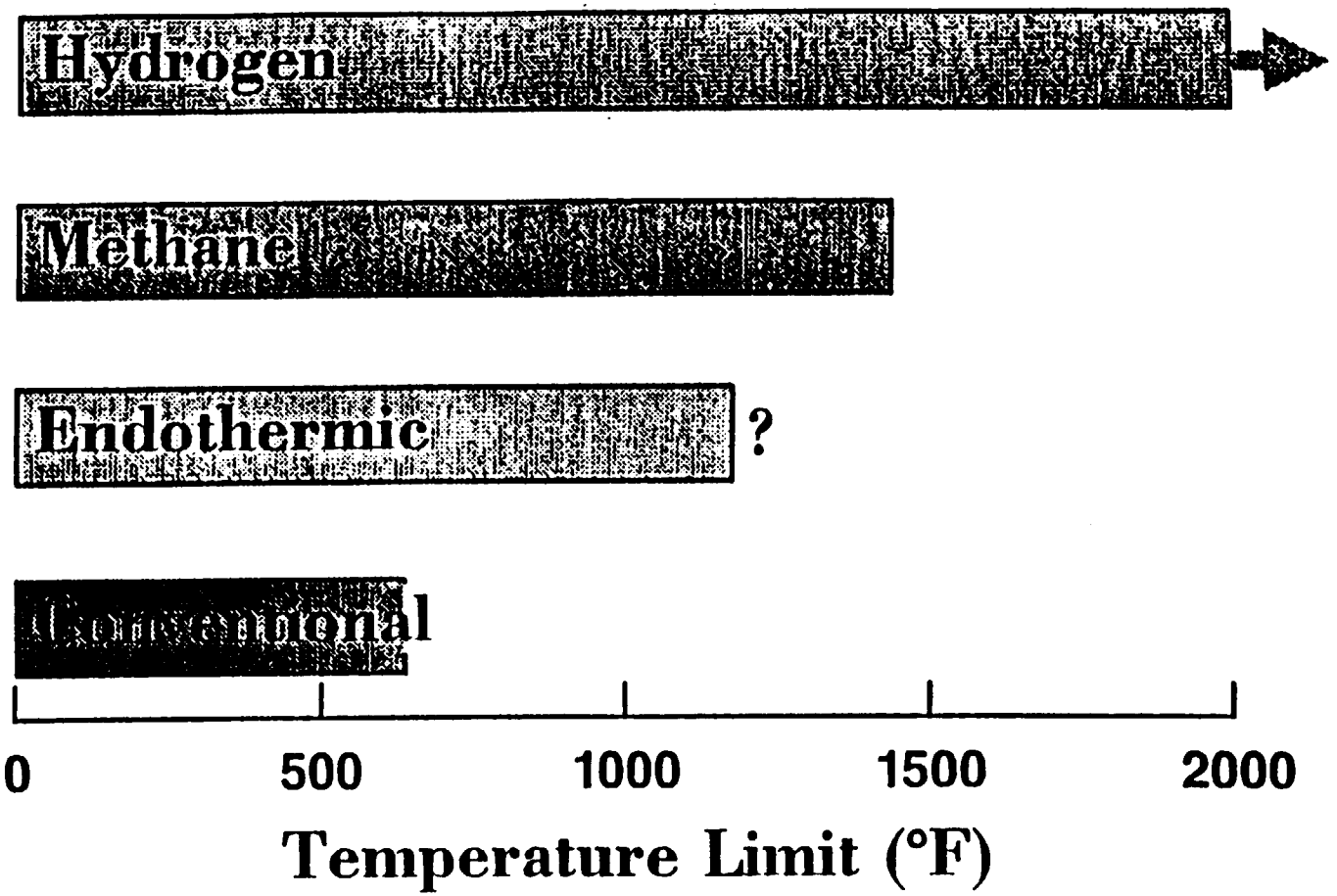

Fig. 1.14 The temperature limit for various fuels.

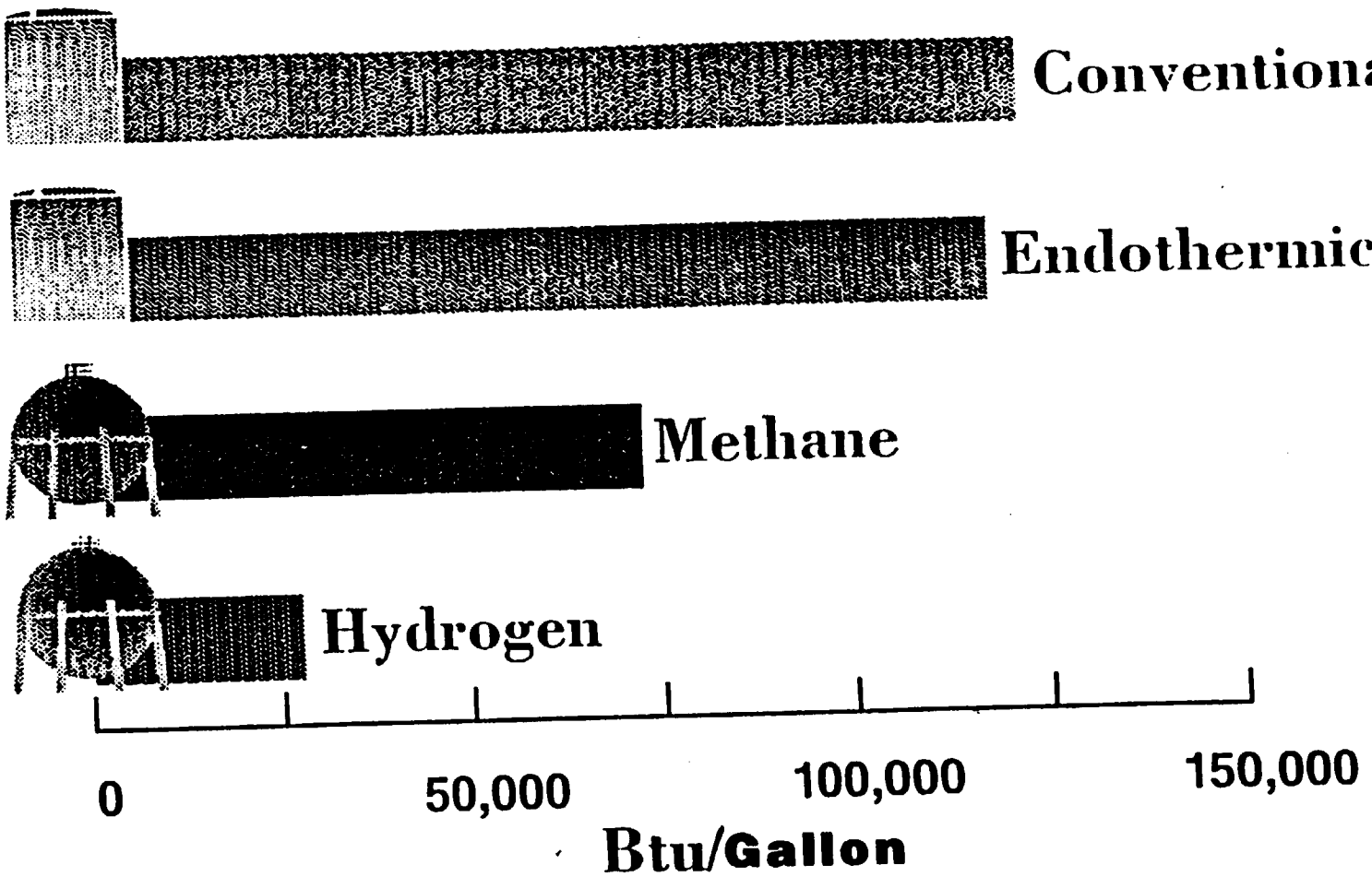

Fig. 1.15 The energy per unit volume for various fuels.

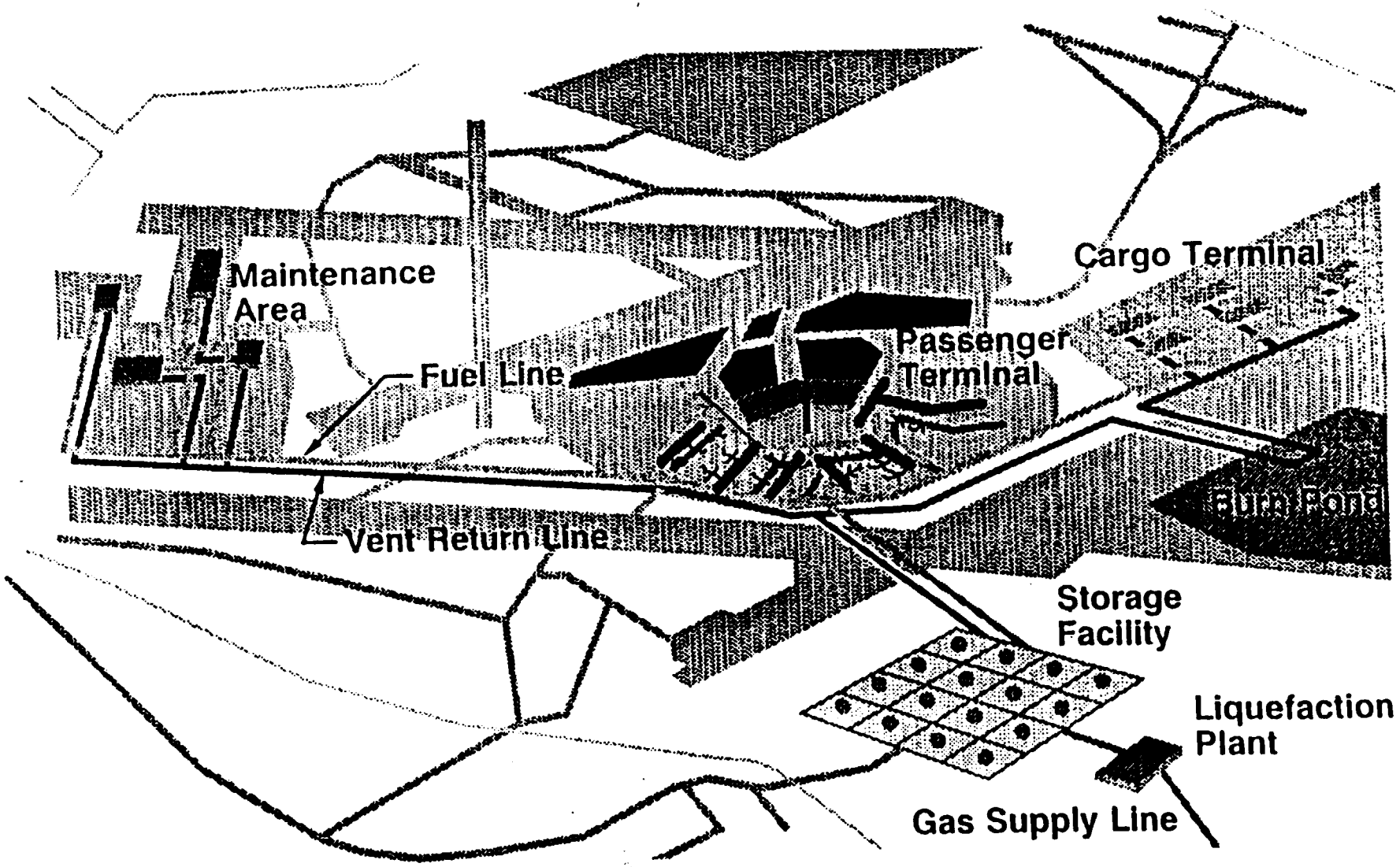

Fig. 1.16 Schematic diagram showing the complex delivry, distribution, and storage processes for cryogenic fuels.

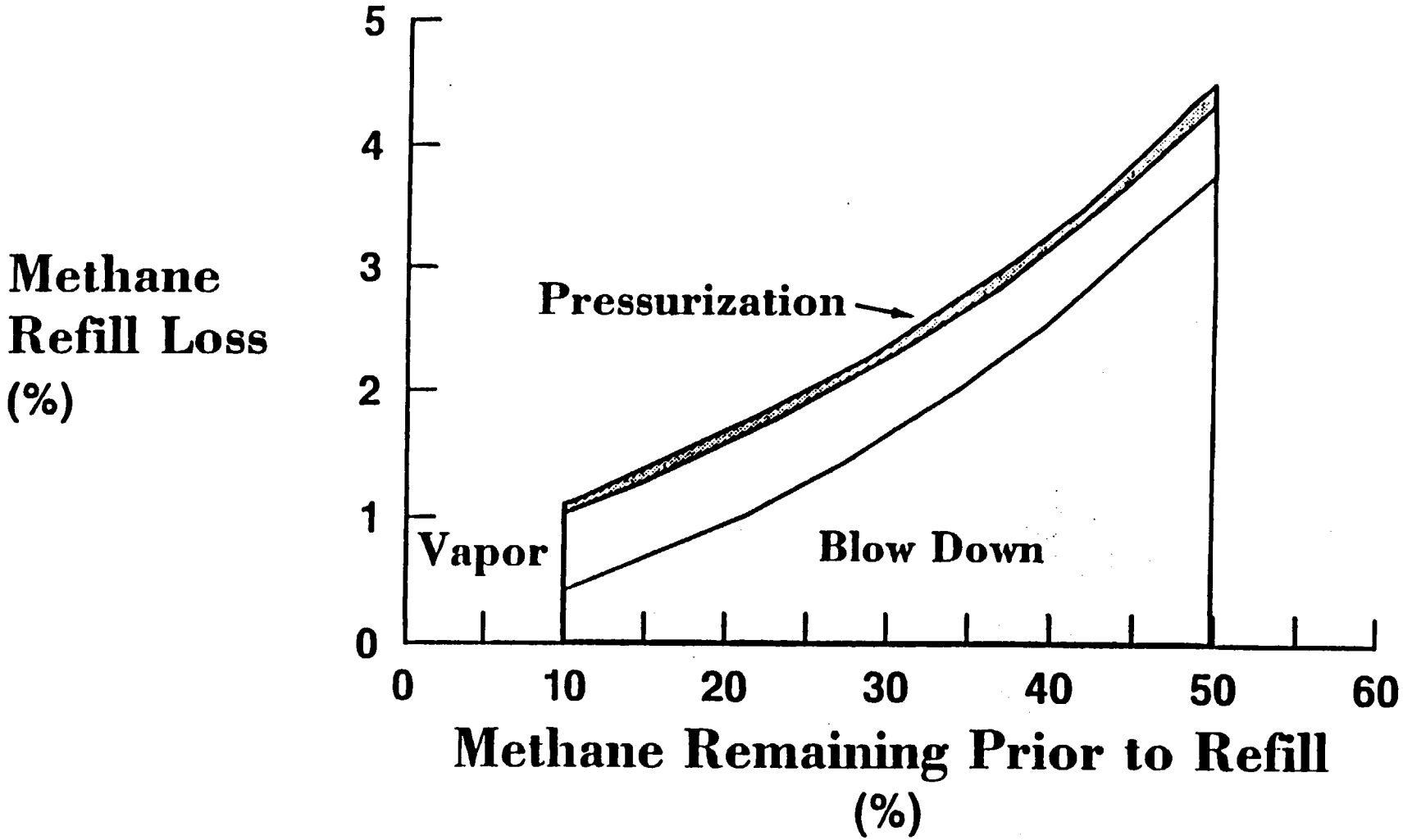

Fig. 1.17 Losses of cryogenic liquid fuels dring refill and tank to tank transfer processes.

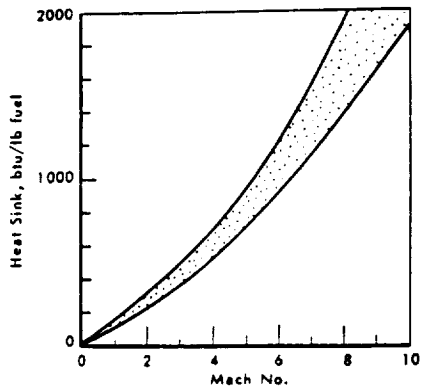

Fig. 1.18 Heat-sink requirement as a function of flight speed.

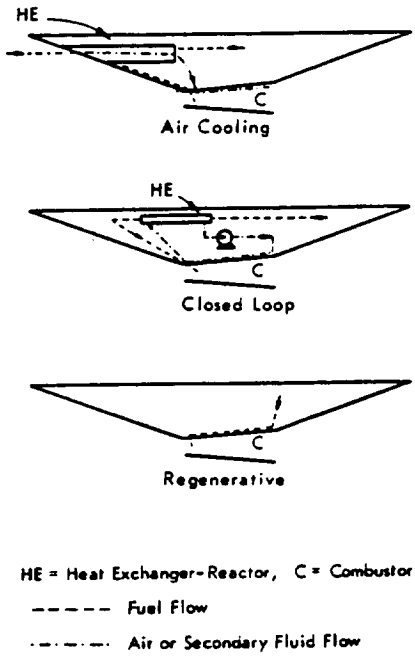

Fig. 1.19 Possible modes of application of cooling for hydrocarbon fuels.

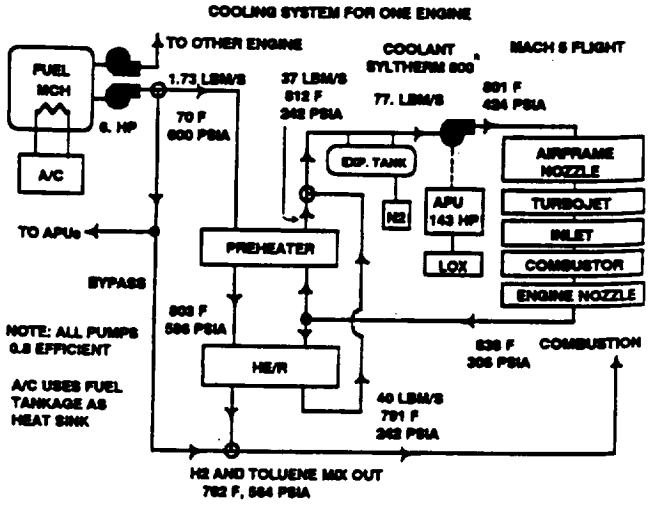

Fig. 1.20 Cooling system schematic for one engine.

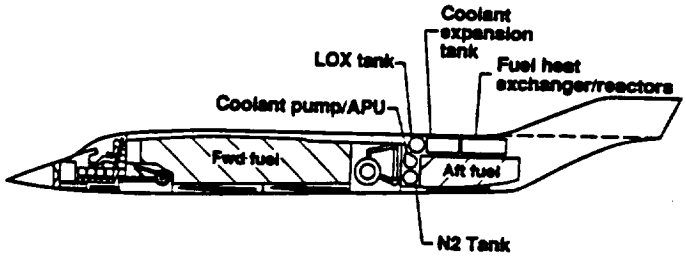

Fig. 1.21 Carrier-based hypersonic aircraft, inboard profile (to scale).

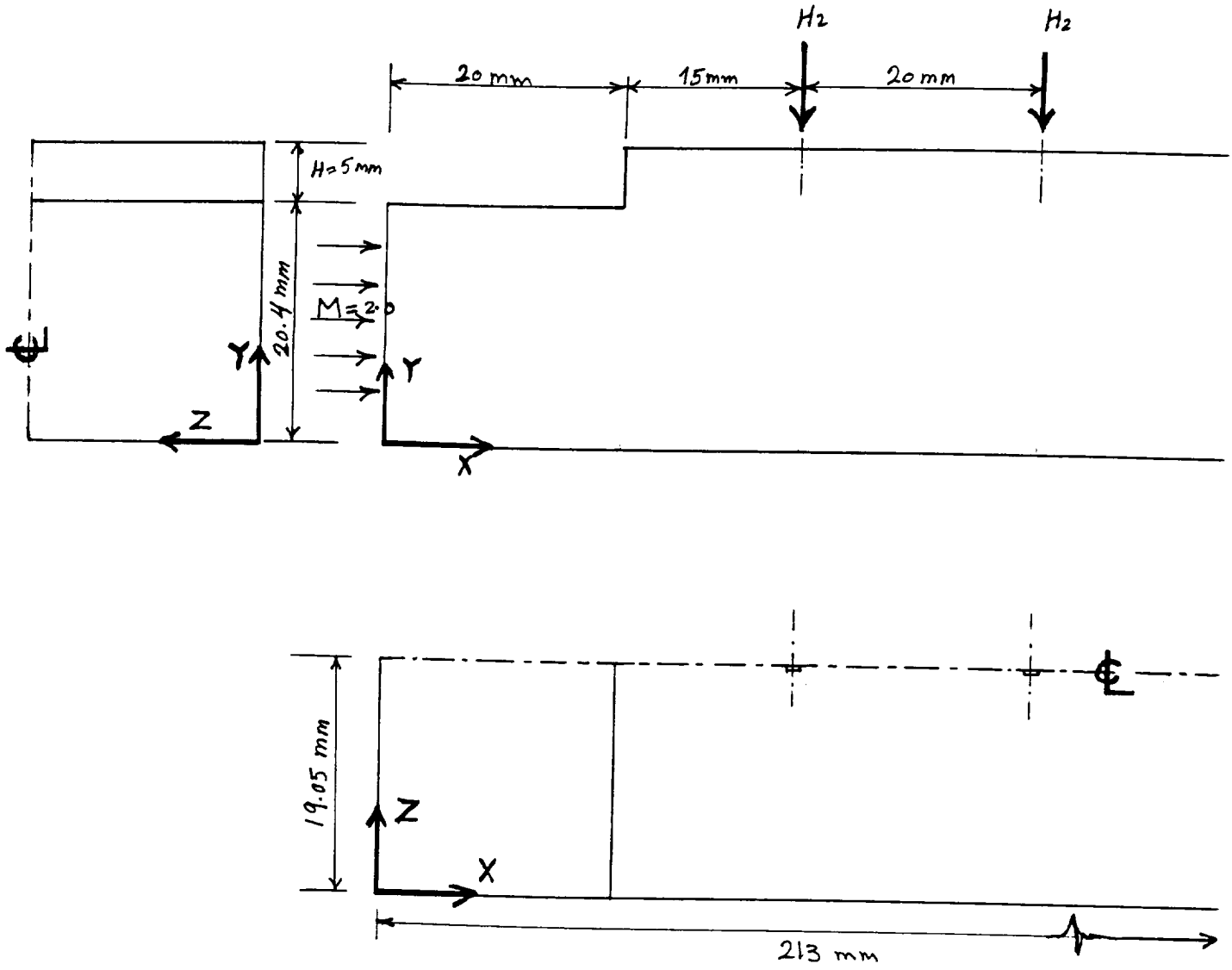

Fig. 2.1 Configuration of the sonic gaseous hydrogen injection case.

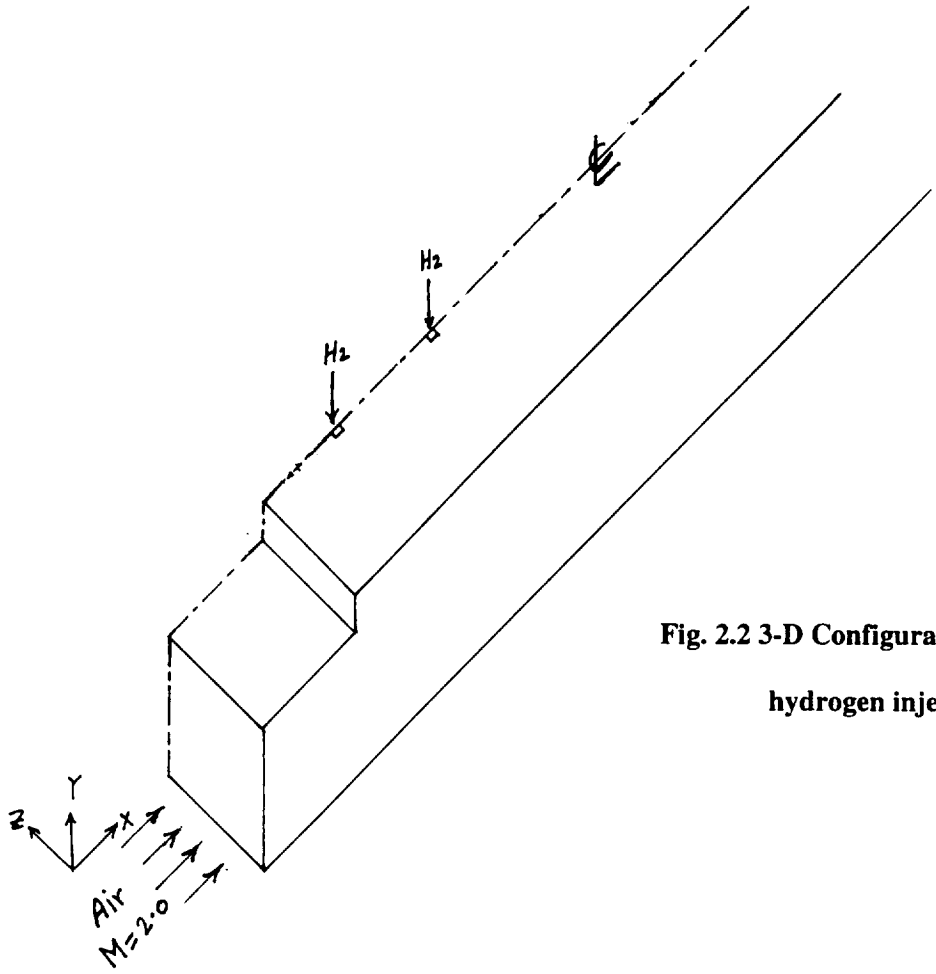

Fig. 2.2 3-D Configuration for the sonic gaseous hydrogen injection case.

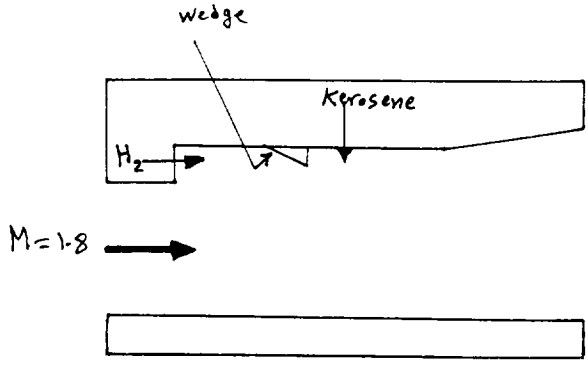

Fig. 2.3 Test section schematic for the kerosene combustion case.

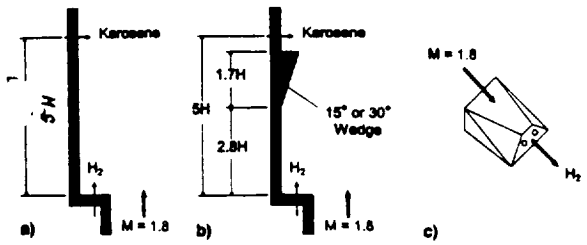

Fig. 2.4 Mixing Schemes used in the piloted-energy kerosene combustion case: a) baseline, b) shock-induced wedges, and c) beveled step for vortex-induced mixing.

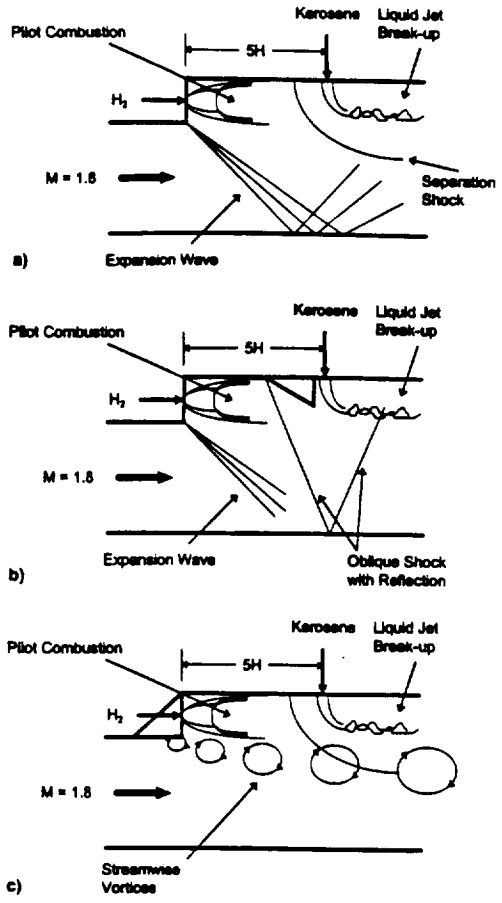

Fig. 2.5 Combustion flowfield schematic: a) baseline, b) baseline with wedge, and c) beveled-step configurations.

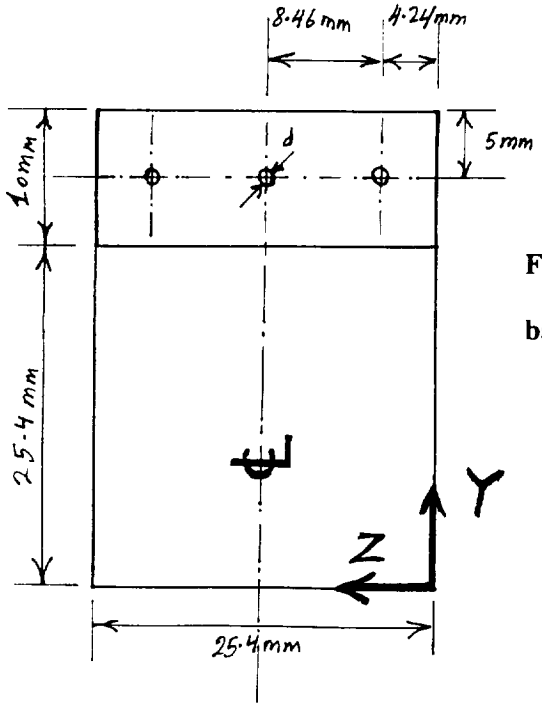

Fig. 2.6 The pilot-hydrogen injection holes built in the step base of the piloted-energy kerosene combustion case.

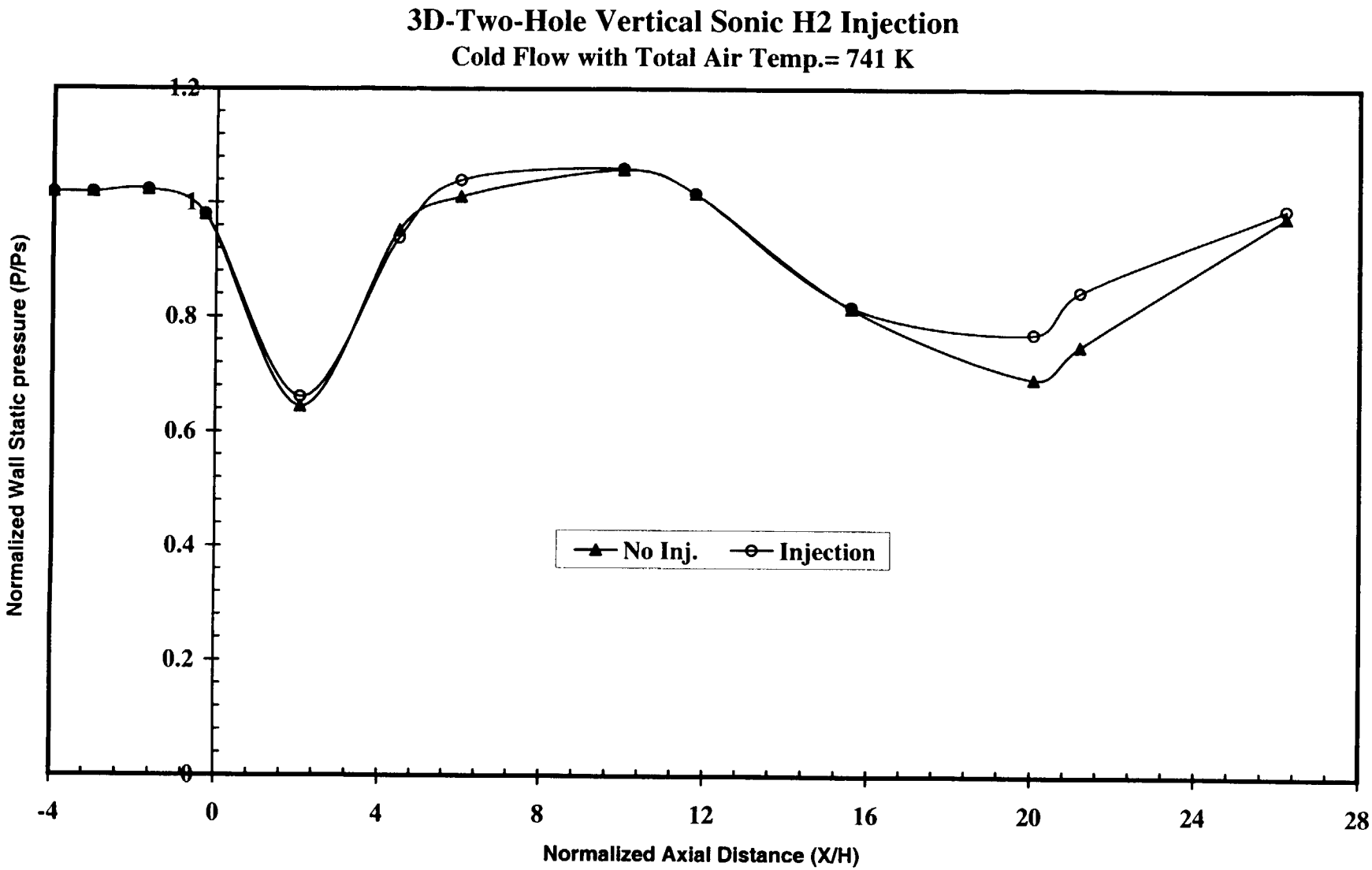

Fig. 4.1 Effect of injection on the flowfield of sonic gaseous hydrogen injection case.

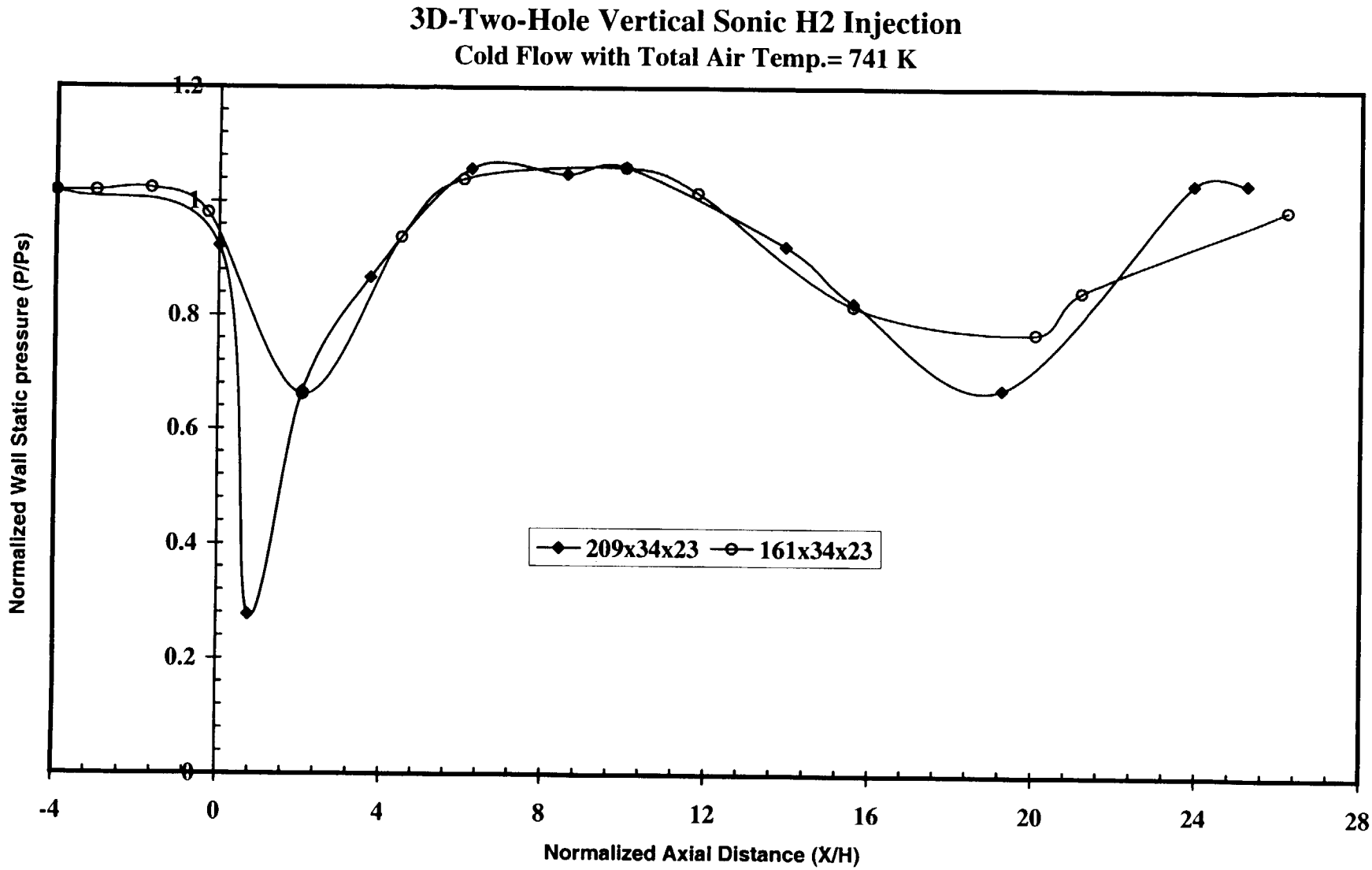

Fig. 4.2 Effect of grid refinement on the flowfield of sonic gaseous hydrogen injection case.

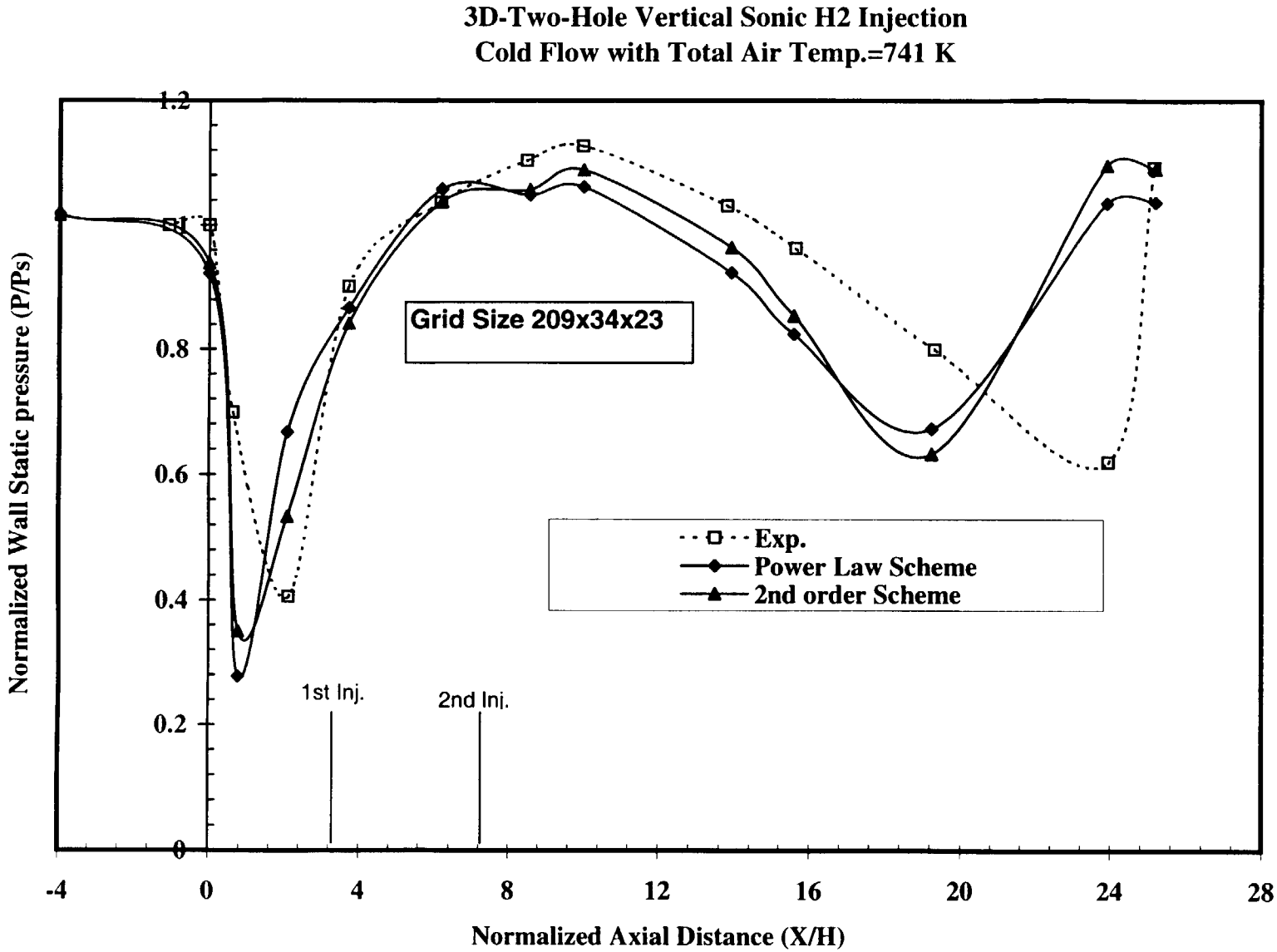

Fig. 4.3 Effect of descritization scheme on the flowfield of sonic gaseous hydrogen injection case.

APPENDIX A

(Attached pages 1-67)

CFD "FLUENT" CODE

1. INTRODUCTION

FLUENT is a general purpose computer program for modeling fluid flow, heat transfer, and chemical reaction. Using FLUENT you can quickly analyze complex flow problems even if you do not have prior expertise in computational fluid dynamics or computer programming. FLUENT enables you to apply computer simulation methods to analyze and solve your practical design problems.

FLUENT incorporates up-to-date modeling techniques and a wide range of physical models for simulating numerous types of fluid flow problems. These are accessible to you through an interactive graphical user interface for problem definition, computation, and graphical postprocessing. When required, FLUENT can also be customized to your specific modeling needs and/or interfaced to your in-house CAD system.

Other CFD Programs from Fluent Inc.: In addition to FLUENT, Fluent Inc. provides other CFD programs: NEKTON, FLUENT/UNS, and RAMPANT. NEKTON is a finite element based program that uses the spectral-element method to solve fluid flow and heat transfer in complex and/or deforming geometries including non-Newtonian and free surface phenomena. NEKTON is ideally suited for prediction of materials processing and coating flows. FLUENT/UNS and RAMPANT are state-of-the-art computer programs for modeling fluid flow and heat transfer in complex geometries. FLUENT/UNS and RAMPANT provide complete mesh flexibility, solving your flow problems with unstructured meshes that can be generated about complex geometries with relative ease. Supported mesh types include 2D triangular/quadrilateral, 3D tetrahedral/hexahedral/pyramid/wedge, and mixed (hybrid) meshes. FLUENT/UNS and RAMPANT also allow you to refine or coarsen your grid based on the flow solution. RAMPANT utilizes a finite volume method tuned for highly compressible flows and FLUENT/ UNS utilizes a pressure-based finite volume method for incompressible and mildly compressible flows. FLUENT and FLUENT/UNS are targeted at similar applications, they differ only in mesh type (FLUENT accepts structured quad/hex meshes whereas FLUENT/UNS accepts meshes of all types, structured or unstructured) and range of physical models available.

1.1 Basic Program Capabilities

FLUENT can model a wide range of physical phenomena, including:

- 2D/3D geometries in Cartesian, cylindrical or general curvilinear coordinates
- steady state or transient flow
- incompressible or compressible flow
- laminar or turbulent flow, using a suite of turbulence models provided
- coupled conduction/convection heat transfer (including both free and forced convection)
- radiation heat transfer

- Mixing of chemical species, including optional multicomponent diffusion models
- reaction of chemical species using either finite rate, equilibrium, or "mixed is burned" chemistry models
- surface reactions, including chemical vapor deposition (CVD)
- NO_x formation and soot formation in combustion systems
- multiphase flows in which two or more continuous phases are present
- free surface flows with complex surface shapes
- solidification/melting of liquids, with free surface effects and continuous casting models
- deforming geometries using moving mesh models (e.g., valve closing)
- sliding/rotating geometries using sliding mesh models (e.g., rotor/stator interactions)
- temperature and composition dependent fluid/material properties
- laminar flow of non-Newtonian fluids
- flow through porous media, including thermal effects of the solid media
- one-dimensional fan/heat-exchanger performance models
- dispersed second phase of particles/bubbles/droplets, including

    - Lagrangian trajectory calculations with stochastic tracking to account for the effects of turbulence,
    - inert heating or cooling of the dispersed phase,
    - evaporation of the liquid droplets into the continuous phase,
    - coal particle devolatilization and char burnout,
    - heterogeneous surface reactions
    - coupled mass, momentum, and heat transfer between the dispersed and continuous phases

The size and scope of your problem (in terms of the number of computational nodes and the number of chemical species and/or reactions) is limited only by your available computer memory.

Applications: The physical models listed above enable you to apply FLUENT to a wide range of applications, such as:

- chemical and process engineering component design
- combustion design and engineering, including gaseous combustion, liquid fuel combustion, and coal combustion
- aerodynamic design
- electronics cooling, manufacture, and design
- power generation
- heat transfer operations
- materials processing
- chemical vapor deposition (CVD)
- spray drying or cooling

- gas cleaning or particle classification
- architectural design (internal and external air flow)
- fire research (open fires, fires in buildings)
- manifold design
- particulate deposition or fouling
- pollution control
- turbomachinery component design

Solution Technique: FLUENT models this wide range of phenomena by solving the conservation equations for mass, momentum, energy, and chemical species using a control volume based finite difference method. The governing equations are discretized on a curvilinear grid to enable computations in complex/irregular geometries. A nonstaggered system is used for storage of discrete velocities and pressures. Interpolation is accomplished via a first-order, Power-Law scheme or optionally via higher order upwind schemes. The equations are solved using SIMPLE-like algorithms with an iterative line-by-line matrix solver and multigrid acceleration.

Boundary Conditions: You can define the unique conditions that describe your problem via a wide variety of boundary conditions, including:

- flow inlets defined via velocity
- flow inlets and/or exits defined via pressure
- flow exits defined via extrapolated/fully-developed outlet conditions
- stationary or moving/rotating walls
- slip (frictionless) or non-slip walls
- isothermal walls or walls with a specified heat flux or external heat transfer condition
- conducting solids
- periodic (fully-developed flow) boundaries
- symmetry boundaries
- cyclic boundaries

1.2 Program Structure

FLUENT is part of the Fluent Suite, which includes the following products:

- FLUENT, RAMPANT, FLUENT/UNS, and NEKTON, the solvers.
- prePDF, the preprocessor for modeling PDF combustion.
- GeoMesh and preBFC, the preprocessors for geometry modeling, block-structured mesh generation, unstructured triangularsurface mesh generation, and 2D unstructured triangular mesh generation.
- TGrid, the 2D triangular and 3D tetrahedral mesh generator.
  grid filters for CAD/CAE packages such as I-DEAS surface and volume grid generators.

Figure A.1 shows the organizational structure of these components. (TGrid does not appear in the diagram because it does not create grids for use in FLUENT.)

preBFC and GeoMesh are used to define the geometry and create a structured grid. preBFC is intended for relatively simple 3D geometries, whereas GeoMesh has considerably more geometry modeling and mesh generation capabilities.

Quadrilateral and hexahedral grids created with GeoMesh can be saved in FLUENT format and read directly into FLUENT. Quadrilateral and hexahedral grids created with preBFC are automatically written in FLUENT format and can be read directly into FLUENT. Grid generation utilities for simple Cartesian and cylindrical-polar meshes are also available within FLUENT.

In addition, volume grids generated in ICEMCFD, I-DEAS, PATRAN, ANSYS, and GRIDGEN can be imported into FLUENT.

Once a grid has been read into FLUENT, all remaining operations are performed within the solver. These include setting boundary conditions, defining fluid properties, executing the solution, refining the grid, and viewing and postprocessing the results.

2. GETTING STARTED WITH FLUENT

FLUENT features a graphical user interface (GUI). Most operations, including file reading/writing, problem setup, calculation, and postprocessing, can be accomplished via the GUI. The menu-driven text interface is also available for these and additional operations. In this chapter, the use of the GUI and the text interface is demonstrated by setting up and solving a sample problem.

2.1 Overview of Using FLUENT

FLUENT and Preprocessors: FLUENT is designed to run as a stand-alone program, or in conjunction with GeoMesh or preBFC. Geometries that can be modeled with Cartesian or cylindrical coordinates in either 2D or 3D may be set up and solved using FLUENT alone. For other analyses in which body-fitted coordinates are required, GeoMesh or preBFC can be used to set up the geometry and grid.

Planning Your CFD Analysis: When you are planning to solve a problem using FLUENT, you should first give consideration to the following issues:

- Definition of the Modeling Goals:
  What specific results are required from the CFD model and how will they be used?
  What degree of accuracy is required from the model?
- Choice of the Computational Model:
  How will you isolate a piece of the complete physical system to be modeled? Where will the computational domain begin and end? What boundary conditions

will be used at the boundaries of the model? Can the problem be modeled in two-dimensions or is a three-dimensional model required?

- Design of the Grid:
  Will your model use a Cartesian grid or a Body-Fitted Coordinate (BFC) grid? What grid topology will work best in Body-Fitted Coordinates? What degree of accuracy will be required in each region of the domain? Where are the flow details that will require a refined grid?

- Choice of Physical Models:
  Is the flow laminar or turbulent? Which turbulence model should be applied? Is the flow steady or unsteady? Is heat transfer important? Will buoyancy effects be significant? Will you treat the fluid as compressible or incompressible? Are there other physical models that should be applied?

- Determination of the Solution Procedure:
  Can the problem be solved simply using the default solution parameters in FLUENT? Can convergence be accelerated via a more judicious solution procedure? Perhaps the problem involves "highly coupled" physics, in which the governing equations have a high degree of interdependency. Will you need a step-wise solution procedure to obtain a stable solution? How long will the problem take to converge on your computer?

Careful consideration of these issues before beginning your CFD analysis will contribute significantly to the success of your modeling effort.

Problem-Solving Steps: Once you have determined the important features of the problem you want to solve, the basic procedural steps you will follow are those shown below. Steps that are optional are noted as such.

1. Create or import the model geometry and grid
2. Choose the basic equations to be solved (e.g., enthalpy, species, turbulence transport)
3. Identify additional models needed (fans, porous media, special boundary conditions, species transport or chemical reaction, etc.)
4. Specify the boundary conditions
5. Specify the fluid properties
6. Set up a dispersed phase (optional)
7. Adjust the solution control parameters (optional)
8. Calculate a solution (fluid phase and/or dispersed phase)
9. Examine the results
10. Save the results
11. Consider revisions to the numerical or physical model

3. GEOMETRY SETUP/GRID GENERATION

3.1 Overview of Geometry and Grid Definition Options

FLUENT employs what could be termed a grid-based geometry, in which the geometry of your model is determined by control volumes defined by the grid. You can choose to use either of the following:

- Curvilinear body-fitted coordinates (BFC) in which the grid lines are determined by a coordinate system that conforms to the geometric boundary of your model.
- Cartesian or cylindrical coordinates in which the grid lines are aligned with the cartesian (x, y, z) or cylindrical (r, θ, z) coordinates and may not conform to oblique or curved boundaries of your physical geometry.

In addition, you can choose one of several techniques to create the grid, using preBFC, GeoMesh, or FLUENT, or importing the grid from an external CAD package. These grid generation choices are discussed in more detail in this section.

Body-Fitted Coordinates vs. Cartesian or Cylindrical Coordinates: Figure A.2 depicts a problem that has been defined first with body-fitted coordinates and then with Cartesian coordinates. The approximation of the geometry via Cartesian or cylindrical coordinates is evident in the second example. Generally, you will choose to use body-fitted coordinates if your physical geometry is not approximated well by a simple Cartesian or cylindrical coordinate system and you are concerned with an accurate description of the flow and/or heat and mass transfer at the physical boundaries. Sometimes, however, you may choose the simplicity of a Cartesian or cylindrical coordinate system, even if the physical boundaries of the problem must be approximated by a "stair-step" pattern in the grid. Figure A.3 illustrates one such "stair-stepped" model in which the accuracy of the predicted flow field is unlikely to be severely impacted by the approximation of the curved boundary. This is often true when the flow field is dominated by internal shear layers and jet mixing as in the example shown. However, when the wall boundary layers are of great importance to the overall flow pattern, an accurate body-fitted description of the boundary is important, as illustrated in the diverging duct example shown in Fig. A.4.

Preprocessor or FLUENT? If you choose to use body-fitted coordinates (BFC), you must define your problem geometry and the computational grid using preBFC or GeoMesh. If you choose to use Cartesian or cylindrical coordinates, you can define the problem geometry and grid in preBFC or you can perform the grid generation directly in FLUENT. Figure A.5 illustrates these alternate setup options.

3.2 Geometry/Grid Requirements and Considerations

3.2.1 Geometry/Grid Requirements in FLUENT

FLUENT imposes several geometry setup and grid construction requirements that you should be aware of before beginning your problem setup:

- Axisymmetric geometries must be defined such that the axis of rotation is the X-axis of the Cartesian coordinates used to define the geometry (Fig. A.6).

- Three-dimensional geometries that are rotationally cyclic must be defined such that the axis of rotation is the Z-axis of the Cartesian coordinates used to define the geometry (Fig. A.7) when the Cartesian velocity formulation is used. The axis of rotation should be defined as the X-axis when the cylindrical velocity formulation is used.

- Physical boundaries that are to be modeled as cyclic boundaries must be located at the grid planes I = 1 and I = NI where NI is the maximum I index in your grid. (See Figs. A.7 and A.8). Cyclic boundaries cannot be located on planes of constant J or K. For rotationally cyclic geometries, J should be the radial direction and K should be the axial direction.

- Interior regions (e.g., regions of dead or wall cells that are surrounded by live cells on more than one edge) should, ideally, be at least two control volumes wide and must be at least one control volume wide in each coordinate direction. This restriction exists due to the logic used in FLUENT to store quantities associated with the wall surface. An interior wall region that is only one cell thick may be used but will not provide sufficient storage for correct reporting of surface quantities (pressures, heat fluxes, etc.) associated with the two live cell interfaces on either side of it. Furthermore, there are two cases in which an interior wall region that is only one cell thick should not be used because it can adversely affect the calculation:

  - The combination of one-cell-thick walls and a cut link for any variable should not be used.
  - One-cell-thick walls cannot be used with the VOF model.

Care should be taken to observe these constraints when defining your problem geometry and computational grid.

3.2.2 Choosing a Good Grid

Accuracy and Stability: The grid is a discrete representation of the continuous field phenomena that you are modeling and the accuracy and numerical stability of your FLUENT simulations depend on your choice of grid. In other words, the density and distribution of the grid lines determines the accuracy with which your FLUENT model represents the actual physical phenomena.

Differencing Schemes: In FLUENT, the control volume method, sometimes referred to as the finite volume method, is used to discretize the transport equations. In the discrete form of the equations, values of the dependent variables appear at control volume boundary locations (cell faces). These values have to be expressed in terms of the values at the nodes of neighboring cells in order to obtain algebraic equations. This task is accomplished via an interpolation practice, also called a "differencing scheme". The choice of differencing scheme not only affects the accuracy of the solution but also the stability of the numerical method.

The use of an interpolation assumption introduces a discretization error, which decreases as the grid spacing is reduced. In practice, it is necessary to obtain sufficiently accurate solutions by employing grids that are not excessively fine. One measure of the discretization error of a scheme is the so-called truncation error of a Taylor series approximation to the derivatives in the governing differential equations. Truncation error occurs due to the approximate nature of the finite difference representation and can be reduced by increasing the order of the interpolation method. You should note, however, that for a given grid, higher order schemes (i.e., those with smaller truncation errors) do not necessarily lead to smaller solution errors. The discretization error is also related to how well the interpolation assumption represents the real physical phenomena. For example, for a one-dimensional situation, in which diffusion plays a dominant role in the conservation equation, a linear profile for the dependent variable is expected. However, if both convection and diffusion are present, but convection plays a dominant role, a linear profile introduces large errors since an exponential profile is expected.

Numerical Diffusion: In addition, a dominant source of errors in multi-dimensional situations is the so-called false diffusion or numerical diffusion. The term false diffusion is used because its effect on a flow field is analogous to that of increasing the real diffusion coefficient. False diffusion is only noticeable when the real diffusion is small, that is, when the situation is convection-dominated. The phenomenon of false diffusion arises due to one-dimensional interpolation practices being employed in a multi-dimensional situation. Therefore, this source of error occurs when the flow is oblique to the grid lines and when there is a nonzero gradient of the dependent variable in the direction normal to the flow direction.

The ideal differencing scheme, therefore, has the following attributes:

- low truncation error
- low numerical diffusion
- physically meaningful variation

The first and second attributes directly affect the accuracy of the solution. The accuracy can be increased by increasing the number of grid lines.

Differencing Schemes in FLUENT: The default differencing scheme used in FLUENT is the so-called power-law scheme. This scheme is derived from the exact analytical solution to the one-dimensional convection-diffusion equation. The power-law scheme is very stable and gives physically meaningful (bounded) solutions but, in certain situations, is

susceptible to numerical diffusion effects. These effects, as mentioned earlier, are maximum when the flow is aligned at 45 degrees to the grid lines and there are significant gradients in the direction normal to the flow. Higher-order methods which are less susceptible to numerical diffusion, but also less stable compared to the power-law scheme, are also available in FLUENT.

Solutions in which truncation error and/or numerical diffusion are significant are termed grid-dependent. If the grid is refined until the solution no longer varies with additional grid refinement, you have achieved a grid-independent solution. When you are interested in quantitative accuracy, you should ensure grid independence of the solution in this way.

Resolution of Flow Details: The overall number of grid lines to be used in a FLUENT simulation is usually determined by noting the locations and sizes of expected flow features such as shear layers, separated regions, boundary layers, and mixing zones, and then choosing a sufficient number of grid lines to resolve these important flow details. Typically, inlets and outlets should be defined by a minimum of two or three cells and are best represented via 10 to 12 cells. Where large gradients are expected, as in shear layers or mixing zones, the grid should be fine enough to minimize the change in the flow variables from node to node. Separated regions should include at least 5 or 6 cells across the separation and are best represented with more cells. In general, no flow passage should be represented by fewer than 3 or 4 cells. Figure A.9 illustrates the resolution of the flow using two different grids in a simple driven cavity.

Grid Spacing Near Walls: The spacing between a wall and the adjacent grid line can impact the accuracy of the computed shear stress and heat transfer coefficient at the wall. This is particularly true in laminar flow where the grid adjacent to the wall should obey

$$y_p \sqrt{\frac{u_\infty}{\nu x}} \leq 1 \qquad \text{(A.1)}$$

Where y_p = distance to the wall from the adjacent node
u_∞ = free-stream velocity
ν = kinematic viscosity of the fluid
x = distance along the wall from the starting point of the boundary layer.

Equation (A.1) is based upon the computed boundary layer profile in laminar flow over a flat plate at zero incidence. This criterion ensures that the gradients at the wall (e.g., $\delta u/\delta n$) are adequately approximated by the difference expression (e.g., $(Up - U_{wall})/\Delta n$). The situation is depicted visually in Fig. A.10.

Similar guidelines for the choice of the near-wall grid spacing in laminar flows can be derived based on the analytical solutions for fully-developed flows. For fully-developed

laminar flow in a pipe of radius R, you should choose $\frac{\Delta n}{R} \leq 0.1$ and for fully-developed laminar flow between parallel plates separated by a height H, you should choose $\frac{\Delta n}{H} \leq 0.05$.

These guidelines yield prediction of τ_w, within 10% of the theoretical values for fully developed flows. Placement of the grid lines closer than these guidelines improves the accuracy of your predictions. In developing flows, where the boundary layers are thinner, the near-wall grid spacing should be smaller than that based on these guidelines.

Non-Uniform Grid Spacing: Often the guidelines noted above may give rise to a very large number of computational cells. One way to minimize the number of cells while maintaining a sufficient degree of accuracy in the solution is to use a non-uniform grid. In a non-uniform grid, the grid spacing is reduced in regions where high gradients are expected and increased in regions where the flow is relatively uniform.

Certain guidelines should be followed in the generation of non-uniform grids. Most importantly, the rate of change of grid spacing should be minimized. Normally the spacing between adjacent grid lines should not change by more than 20% or 30% from one grid line to the next. This implies expansion factors between 0.7 and 1.3. This is an accuracy consideration, primarily impacting the accuracy of the diffusion terms in the governing transport equations.

Cell Aspect Ratios: The aspect ratio of the computational cells is an additional issue that arises during the setup of the computational grid. While large aspect ratios may be acceptable in some problems, a general rule of thumb might be to avoid aspect ratios in excess of 5:1. This limit can be acceptably exceeded when the gradients in one direction are very small relative to those in the second direction, such as occurs in a fully developed pipe flow. Conversely, excessive aspect ratios can lead to stability problems, convergence difficulties, and/or the propagation of numerical errors.

Grid Skewness: When you use Cartesian coordinates to define your model, the coordinate system guarantees that the grid lines intersect at 90 degree angles. When you use body-fitted coordinates, the grid lines you generate may not be orthogonal. While some degree of non-orthogonality is allowable, and is accounted for in the solution process, your computational grid should maintain grid intersection angles close to 90 degrees whenever possible. Figure A.11 depicts two examples of grids with excessive skewness (departure from orthogonality). Whenever possible you should limit the skew in your grid to less than 45 degrees.

3.3 Grid Lines, Nodes, Control Volumes, and Cell Types

In order to understand the relationship between the computational grid and geometry, you need to understand the grid definition and cell numbering system used by FLUENT.

Figure A.12 illustrates this nomenclature which is described below. Note that, internally, FLUENT uses a different numbering system. See the user-defined subroutine chapter for details.

Grid Lines and Nodes: Figure A.12 shows solid lines which are grid lines (lines of constant I or lines of constant J). The grid lines intersect at node points, with the intersection of grid lines I and J forming node (1,J).

Control Volumes: The grid lines define the boundaries of control volumes or cells. These control volumes are used when integrating the governing equations and form the basis of your computational model. Each control volume in your FLUENT model has a cell type. The cell type tells FLUENT whether the control volume is filled with fluid, or if the control volume defines a wall, inlet, exit, etc.

Cell Center/Storage Locations: The cell center (1,J) is located at the geometric center of the control volume or cell (I,J). This cell center is the storage location for all dependent variables in FLUENT.

Grid and Cell Numbering: Figure A.12 shows the control volume (1,J) which is located between grid lines 1-1 and I and grid lines J-1 and J. That is, the grid point (I,J) is located at the upper right corner of control volume or cell (I,J). In 3D, grid point (I,J,K) is located at the upper right, front corner of cell (1,J,K).

The relationship between grid numbers and cell numbers is clarified in Figure A.13. Figure A.13a shows a matrix of 6 grid lines in each computational direction, i.e., a 6 x 6 grid. The grid points (1,I) and (6,6) are indicated in the figure. These grid lines define a block of 5 control volumes in each coordinate direction. The cell numbering is noted in Figure A.13b, with the first cell in the lower left corner denoted as cell (2,2) and the last cell in the upper right corner denoted as cell (6,6).

Fictitious Boundary Cells: FLUENT adds an additional ring of cells or control volumes around the perimeter of your computational model. These control volumes are used to define boundary conditions at the edge of the physical domain. Thus, the complete FLUENT description of the example shown in Fig. A.13 becomes that of Fig. A.14, in which there is a matrix of 7 x 7 control volumes. The first cell in the lower left corner is cell (1,1) and the final cell in the upper right corner is cell (7,7). Both of these cells are part of the group of fictitious boundary cells surrounding the matrix of 5 x 5 physical control volumes.

4. BASIC PHYSICAL MODELS FOR FLOW AND HEAT TRANSFER

This chapter describes the basic physical models that FLUENT provides and the input commands that you use to define and use them.

4.1 Selecting Physical Models and Defining the Problem Scope

When you are beginning the setup of a new FLUENT model you must begin by defining the problem scope in terms of the basic physical models that should be applied. FLUENT's default physical models consist of laminar, isothermal, single-component flow. However, you can alter this problem scope, as described in this section, to include the following:

- Cylindrical velocity formulation for 3D problems
- Turbulent flow
- Heat transfer
- Radiation heat transfer
- Periodic flow and heat transfer
- Porous media
- Compressible flow
- Time dependence
- Lumped parameter fan models
- Lumped parameter heat exchanger models
- Chemical species transport and/or reaction
- Phase change
- Multiphase flow
- Swirling and rotating flows
- Rotating reference frames
- Sliding mesh
- Deforming mesh
- Non-Newtonian viscosity

4.2 Turbulence Models

In turbulent flows, the velocity at a point is considered as a sum of the mean (ensemble-averaged) and fluctuating components:

$$u_i = \bar{u}_i + u_i' \tag{A.2}$$

Substituting expressions of this form into the instantaneous momentum equations (and dropping the overbar on the mean velocity, u) yields the ensemble-averaged momentum equations:

$$\frac{\partial}{\partial t}(\rho u_i) + \frac{\partial}{\partial x_j}(\rho u_i u_j) = \frac{\partial}{\partial x_j}\left(\mu\left[\frac{\partial u_i}{\partial x_j} + \frac{\partial uj}{\partial xi}\right] - \left(\frac{2}{3}\mu\frac{\partial u_l}{\partial x_l}\right)\right) - \frac{\partial p}{\partial x_i} + \rho g_i + F_i + \frac{\partial}{\partial x_j}\left(-\overline{\rho u_i' u_j'}\right) \tag{A.3}$$

Equation (A.3) has the same form as the fundamental momentum balance with velocities now representing ensemble-averaged (or mean-flow) values. The effect of turbulence is incorporated through the "Reynolds stresses", $\rho u_i u_j$. FLUENT relates the Reynolds stresses to mean flow quantities via one of three turbulence models:

- The k-ε model
- The RNG k-ε model
- The Reynolds Stress Model (RSM)

4.2.1 Choosing the Appropriate Turbulence Model

The process of selecting a turbulence model for a given turbulent flow problem is greatly facilitated when you have a good understanding of the salient features of the flow in question. Based on this understanding, you should then consider which model would be more suitable. To do so, you must know the capabilities and limitations of the individual models. This section provides you with an overview of the models and general guidelines that will help you choose the correct turbulence model for the flow you want to model.

The standard k-ε model proposed by Jones and Launder has been the workhorse of engineering turbulence models for more than two decades. It falls in the category of "two-equation" turbulence models based on an isotropic eddy-viscosity concept. As such, it is more universal than other low-order turbulence models such as algebraic ("zero-equation") and one-equation models. Robustness, economy, and reasonable accuracy for a wide range of turbulent flows explain its popularity in industrial flow and heat transfer Simulations. It is a semi-empirical model, and the derivation of the model equations, including the various model constants, relies on phenomenological considerations and empiricism.

The Renormalization Group (RNG) k-ε model also belongs to the k-ε family of models. The model equations in their RNG form are similar to those for the standard k-ε model. There are major differences, however, between the RNG and standard k-ε models. The RNG model was derived using a more rigorous statistical technique, and its model constants are derived "analytically".

The Reynolds Stress Model (RSM) is the most elaborate turbulence model that FLUENT provides. Eschewing the isotropic eddy viscosity hypothesis, the RSM closes the Reynolds stresses by solving their transport equations (6 additional equations in 3D, in comparison with k-ε models). As such, the RSM accounts for the history and transport of the Reynolds stresses in a rigorous manner. The effects of streamline curvature, swirl, and rotation are all directly accounted for by the transport equations for the Reynolds stresses.

Major Differences Between the RNG k-ε Model and the Standard k-ε Model:
The RNG k-ε model differs from the standard k-ε model in several important ways:

- While the standard k-ε model is based on the traditional Reynolds-averaging technique, the RNG model is derived by a more rigorous statistical (scale-elimination) technique.
- The RNG model has an additional term in its ε equation which significantly improves the accuracy for rapidly strained flows.
- The effect of swirl on turbulence is included in the RNG model, which enhances the accuracy for swirling flows.
- The RNG theory provides an analytical formula for turbulent Prandtl numbers, while the standard k-ε model uses user-specified, constant values.
- While the standard k-ε model is a high-Reynolds-number model, the RNG theory provides an analytically-derived differential formula for effective viscosity that accounts for low-Reynolds number effects.

All the features listed above make the RNG k-ε model more accurate and reliable for a wide class of flows than the standard k-ε model.

Examples of flows for which use of the RNG k-ε model is particularly beneficial are as follows:

- Separated flows and recirculating flows (e.g., backward- or forward-facing steps, sudden expansions, diffusers, bluff bodies, lift devices at a high incidence)
- Flows in curved geometries and flows that are rapidly strained (e.g., curved ducts, bluff bodies, highly accelerating/decelerating flows, stagnation and detaching flows)
- Time-dependent flows with large-scale organized structures (e.g., vortex shedding, shear-layer instability)
- Heat transfer in low-Prandtl-number fluid flows (e.g., liquid metal flows)
- Low-Reynolds-number or transitional flows (e.g., flows in an otherwise quiescent enclosure where the flow is turbulent in regions of limited extent, but is otherwise laminar)
- Flows with streamwise vortices and secondary flows (e.g., secondary flows in curved ducts and transition ducts, horseshoe vortices around junctions, streamwise vortices behind aerodynamic/hydrodynamic bodies such as ground vehicles, under-water bodies, and airplanes)
- Swirling flows (e.g., swirl combustors, cyclones)

If you expect that the flow you are modeling exhibits any of the features listed above, it is recommended that you use the RNG k-ε model.

RNG k-ε Model vs. the Differential Reynolds Stress Model: Although the RNG model provides substantial improvements over the standard k-ε model as stated above, it should be understood that the RNG model is still based on the isotropic eddy-viscosity concept. Consequently, there is a limit to what the RNG model can offer when the anisotropy of turbulence has a dominant effect on the mean flow. Such cases include

highly swirling flows, flows with strong streamline curvature, stress-driven secondary flows, and evolution of streamwise vortices. Among these, for instance, stress driven secondary flows cannot be predicted by the RNG model. In the RSM, all of these effects are automatically accounted for in the transport equations for the Reynolds stresses. When your simulation requires rigorous modeling of these features, you should consider using the RSM.

Turbulence Modeling in Swirling Flows: If your FLUENT model involves a highly swirling flow, you should use the Reynolds Stress Model or the RNG k-ε model to obtain a more accurate flow prediction. Generally, these models provide better accuracy in modeling devices such as cyclone separators or swirl nozzles in which the Swirl Number, S, approaches or exceeds unity. The Swirl Number can be defined as the ratio of the axial flux of angular momentum to the axial flux of axial momentum:

$$S = \frac{\int r v_\theta v \, dA}{\overline{R} \int u v \, dA} \tag{A.4}$$

Conservation of angular momentum ($r^2\Omega$ = constant) creates a tendency in the fluid toward a free-vortex form as depicted in Fig. A.15. When the angular momentum in the fluid is quite high, this form may not be captured by the k-e model due to the assumption of isotropy used in the calculation of the Reynolds stresses. If your FLUENT model includes highly swirling flow, you should consider applying the Reynolds Stress Model (RSM) or the RNG k-ε model.

Computational Effort: CPU Time and Solution Behavior: Due to the extra terms and functions in the governing equations and a greater degree of nonlinearity, computations with the RNG k-ε model tend to take more CPU time than with the standard model. However, the difference is marginal (10-15% increase compared to the standard k-ε model).

Since diffusion has a stabilizing effect on the numerics, the k-ε model, which usually gives larger turbulent diffusivity, is more stable. The RNG model is more likely to be susceptible to instability. However, you should understand that this is because the RNG model, where appropriate, yields a correct level of turbulent viscosity (which is usually smaller than that computed by the standard k-ε model). The RNG model is more faithful in responding to any physical instabilities such as time-dependent turbulent vortex shedding.

Compared with the k-ε models, the RSM requires additional memory and CPU time due to the increased number of the transport equations for Reynolds stresses. However, efficient programming in FLUENT has reduced the CPU time per iteration significantly. On average, the RSM in FLUENT requires 50-60% more CPU time per iteration compared to the k-ε models. It should be noted, however, that the inter-coupling among the Reynolds stresses and mean flow makes solution convergence relatively slow, and that 15-20% more memory is needed.

Enthalpy Sources Due to Reaction: Sources of enthalpy, S_h, in Equation (A.5) include the source of enthalpy due to chemical reaction:

$$S_{h,reaction} = \sum_j \left[\frac{h_j^o}{M_j} + \int_{T_{ref,j}}^{T} C_{p,j}\, dT \right] R_j \tag{A.9}$$

where h_j^o is the enthalpy of formation of species j' and $R_{j'}$ is the volumetric rate of creation of species j'.

4.4 Compressible Flows

Compressibility effects are encountered in gas flows at high velocity and/or in which there are large pressure variations. When the gas flow velocity approaches or exceeds the speed of sound or when the pressure change in the system ($\Delta p/p$) is large, the variation of the gas density with pressure has a significant impact on the flow velocity, pressure, and temperature. Compressible flows create a unique set of flow physics for which you must be aware of the special input requirements and solution techniques described in this section. Figure A.16 illustrates several examples of compressible flows computed using FLUENT.

When to Use the Compressible Flow Model: Compressible flows can be characterized by the value of the Mach number

$$M = u/c \tag{A.10}$$

where c is the speed of sound in the gas:

$$c = \sqrt{\gamma RT} \tag{A.11}$$

and γ is the ratio of specific heats (C_p/C_v).

When the Mach number is less than one, the flow is termed subsonic. At Mach numbers much less than one (e.g., $M < 0.3$ or so), compressibility effects are negligible and the variation of the gas density with pressure can safely be ignored in your flow modeling. When the Mach number approaches unity, however, compressibility effects become important. The flow will choke at Mach 1.0. When the Mach number exceeds 1.0, the flow is termed supersonic. Supersonic flows may contain shocks and expansion fans which can impact the flow pattern significantly and which require compressibility in your FLUENT model. FLUENT provides a full range of compressible flow modeling capabilities for subsonic, transonic, and supersonic flows.

Special Physics of Compressible Flows: Compressible flows are typically characterized by the total pressure P_o (isentropic stagnation pressure) and total

temperature T_o (isentropic stagnation temperature) of the flow. These quantities can be related to the static pressure and temperature via the following relationships:

$$\frac{p_o}{p_s} = \left[1 + \frac{\gamma - 1}{2} M^2\right]^{\frac{\gamma}{\gamma - 1}} \tag{A.12}$$

$$\frac{T_o}{T_s} = 1 + \frac{\gamma - 1}{2} M^2 \tag{A.13}$$

These unique relationships describe the variation of the static pressure and temperature in the flow as the velocity (Mach number) changes under isentropic (loss-free, constant enthalpy) conditions.

For a given pressure ratio from inlet to exit, for example, Equation (A.12) can be used to estimate the exit Mach number (which would exist in a one-dimensional isentropic flow). For air, Equation (A.12) predicts a choked flow (Mach number of 1.0) at an isentropic pressure ratio, P_s/P_o, of 0.5283. This choked flow condition will be established at the point of minimum flow area (e.g., in the throat of a nozzle). In the subsequent area expansion the flow may either accelerate to a supersonic flow in which the pressure will continue to drop, or the flow may return to subsonic flow conditions, decelerating with a pressure rise. When a supersonic flow is exposed to an imposed pressure increase, a shock will occur, with a sudden pressure rise and deceleration accomplished across the shock.

Basic Equations for Compressible Flows: Compressible flows are described by the standard continuity and momentum equations solved by FLUENT, and you do not need to activate any special physical models (other than the compressible treatment of density as detailed below). The energy equation solved by FLUENT, Equation (A.5), correctly incorporates the coupling between the flow velocity and the static temperature, and should be activated whenever you are solving a compressible flow. In addition, you should activate the optional viscous dissipation terms in Equation (A.5), which become important in high-Mach-number flows.

5. CHEMICAL SPECIES TRANSPORT AND REACTING FLOW

FLUENT models chemical species transport and chemical reactions using the reacting flow models described in this chapter. You can model any number of chemical species and any number of chemical reactions, limited only by the memory available on your computer. This chapter describes the chemical species modeling options in FLUENT, the options that you use to define chemistry, and the computational techniques that can be employed to yield a successful simulation.

Reacting Systems Handled by FLUENT: Chemical reactions in FLUENT may be of the following types:

- Fluid phase reactions that may involve multiple chemical reaction steps, equilibrium chemistry, gaseous combustion, NO, and other pollutant formation, etc.
- Liquid fuel combustion in which fuel vapor is generated via evaporation of liquid droplets and a combustion reaction occurs in the gas phase.
- Surface reactions (e.g. Chemical Vapor Deposition) in which the reaction occurs at a solid (wall) boundary.
- Particulate reactions (e.g. coal combustion) in which reaction occurs by the evolution of a combustible gas and/or at the surface of a solid particle.

This section describes how you can model these reacting systems.

Reaction Modeling Options: FLUENT provides three reaction modeling approaches:

1. Generalized Finite Rate Formulation

This approach is based on the solution of species transport equations for reactants and product concentrations, with the chemical reaction mechanism defined by you. The reaction rates that appear as source terms in the species transport equations are computed from Arrhenius rate expressions or by using the eddy dissipation concept due to Magnussen and Hjertager. Models of this type are suitable for a wide range of applications including combustion simulation.

2. Mixture Fraction/PDF Formulation

In this approach individual species transport equations are not solved. Instead, transport equations for one or two conserved scalars (the mixture fractions) are solved and individual component concentrations are derived from the predicted mixture fraction distribution. This approach has been specifically developed for the simulation of turbulent diffusion flames and similar reaction processes and offers many benefits over the finite rate formulation approach. In the conserved scalar approach, turbulence effects are accounted for with the help of a probability density function or PDF. Reaction mechanisms are not explicitly defined by you, instead the reacting system is treated via either chemical equilibrium calculations or a flame sheet (mixed-is-burned) approach.

3. Premixed Front Tracking Formulation

This model has been specifically developed for combustion systems, or other reacting systems, that are of the purely premixed type. In these problems perfectly mixed reactants and burned products are separated by a "flame front". The so called "G equation" is solved to predict the position of this front. The influence of turbulence can be accounted for by means of a relationship between laminar and turbulent flame speed.

5.1 Modeling Species Transport and Finite Rate Chemistry

FLUENT can model the mixing and transport of chemical species by solving conservation equations describing convection, diffusion, and reaction sources for each component species. This modeling capability and the inputs you provide when using it

are described in this section. Note that you may also want to consider modeling your reacting system using the mixture fraction approach.

5.1.1 Species Transport Equations

When you choose to solve conservation equations for chemical species, FLUENT predicts the local mass fraction of each species, m_i, through the solution of a convection-diffusion equation for the i'th species. This conservation equation takes the following general form:

$$\frac{\partial}{\partial t}(\rho m_i)+\frac{\partial}{\partial x_i}(\rho u_i m_i)=-\frac{\partial}{\partial x_i}J_{i,i}+R_i+S_i \tag{A.14}$$

where R_i, is the mass rate of creation or depletion by chemical reaction and S_i, is the rate of creation by addition from the dispersed phase. An equation of this form will be solved for N-1 species where N is the total number of fluid phase chemical species present in the system.

Mass Diffusion in Laminar Flows: $J_{i,i}$ is the diffusion flux of species i', which arises due to concentration gradients. In the simplest case, this diffusion flux can be written as:

$$J_{i,i}=-\rho D_{i,m}\frac{\partial m_i}{\partial x_i} \tag{A.15}$$

Here $D_{i,m}$ is the diffusion coefficient for species i' in the mixture. Note that for laminar flows a full multi-component diffusion equation may be selected to replace Equation (A.15) and that binary diffusion coefficients may be used to compute the diffusion coefficients in non-dilute mixtures.

Mass Diffusion Due to Thermal Gradients: The diffusion flux, $J_{i,i}$, may optionally be augmented by a thermal diffusion term, $-D_i^T\frac{1}{T}\frac{\partial T}{\partial x_i}$ (also called Soret diffusion).

Mass Diffusion in Turbulent Flows: In turbulent flows, FLUENT computes the mass diffusion in the form:

$$J_{i,i}=-\left(\rho D_{i,m}+\frac{\mu_t}{Sc_t}\right)\frac{\partial m_i}{\partial x_i} \tag{A.16}$$

where S_{ct} is the effective Schmidt number, $\frac{\mu_t}{\rho D_t}$ (with a default setting of 0.7).

Treatment of Species Transport in the Energy Equation: For many multicomponent mixing flows, the transport of enthalpy due to species diffusion

$\left(\nabla.\left[\sum_{k=1}^{n}(h_k)J_k\right]\right)$ can have a significant effect on the enthalpy field and should not be neglected. In particular, when the Lewis number $Le = \frac{\rho D}{k/c_v}$ is far from unity, when the species involved have significantly differing heat capacities, this term cannot be neglected. You should also consider using second order discretization schemes to reduce numerical errors that can be significant in the computation of this term.

5.1.2 The Generalized Finite Rate Formulation for Reaction Modeling

The reaction rates that appear as source terms in Equation (A.14) are computed by FLUENT from Arrhenius rate expressions or by using the eddy dissipation concept due to Magnussen and Hjertager. Models of this type are suitable for a wide range of applications including laminar or turbulent reaction systems, and combustion systems including premixed or diffusion flames. When required, custom reaction rates can also be supplied through the use of user-defined subroutines.

Reaction Rate Calculations: The source of chemical species i' due to reaction, $R_{i'}$, is computed as the sum of the reaction sources over the k reactions that the species may participate in:

$$R_{i'} = \sum_k R_{i',k} \tag{A.17}$$

where $R_{i',k}$ is the rate of creation/destruction of species i' in reaction k. Reaction may occur in the continuous phase between continuous phase species only, or at surfaces resulting in the surface deposition or evolution of a chemical species. The reaction rate, $R_{i',k}$, is controlled either by an Arrhenius kinetic rate expression or by the mixing of the turbulent eddies containing fluctuating species concentrations. You can also enter alternate reaction rates using user subroutines.

The Arrhenius Rate: The Arrhenius reaction rate is computed as:

$$R_{i',k} = -\nu'_{i',k} M_{i'} T^{\beta_k} A_k \prod_{j\ reactants} C_j^{\nu'_{j',k}} \exp(-E_k/RT) \tag{A.18}$$

\where $\nu'_{i',k}$ = molar stoichiometric coefficient for species i' in reaction k (positive values for reactants, negative values for products)

$M_{i'}$ = molecular weight of species i' (kg/kmol)

β_k = temperature exponent (dimensionless)

A_k = pre-exponential factor (consistent units)

C_j = molar concentration of each reactant species j' (kmol/m^3)

$\nu_{j',k}$ = exponent on the concentration of reactant j' in reaction k

E_k = activation energy for the reaction (J/kmol)

You input values for $\nu'_{i',k}$, β_k, A_k, $\nu_{j',k}$, and E_k during the problem definition in FLUENT.

The Eddy Breakup Model: The influence of turbulence on the reaction rate is taken into account by employing the Magnussen and Hjertager model. In this model, the rate of reaction $R_{i,k}$ is given by the smallest (i.e. limiting value) of the two expressions below:

$$R_{i,k} = -\nu'_{i,k} M_i A \rho \frac{\varepsilon}{k} \frac{m_R}{\nu'_{R,k} M_R} \tag{A.19}$$

$$R_{i,k} = -\nu'_{i,k} M_i A B \rho \frac{\varepsilon}{k} \frac{\sum_P m_P}{\sum_P \nu'_{R,k} M_P} \tag{A.20}$$

Where m_p represents the mass fraction of any product species, P
m_R represents the mass fraction of a particular reactant, R
R is the reactant species giving the smallest value of $R_{i,k}$
A is an empirical constant equal to 4.0
B is an empirical constant equal to 0.5

The eddy breakup model relates the rate of reaction to the rate of dissipation of the reactant and product containing eddies. k/ε represents the time scale of the turbulent eddies following the eddy break up model of Spalding. The model is useful for the prediction of premixed and diffusion problems as well as for partially premixed reacting flows.

Turbulent Reacting Flows: In turbulent reacting flows, FLUENT calculates the reaction rates from the Arrhenius expression (Equation (A.18)) and the eddy breakup model (Equations (A.19) and (A.20)). The limiting (slowest) rate is used as the reaction rate and the contribution to the source terms in the species conservation and enthalpy equations are calculated from this reaction rate. Energy released by or required for the chemical reaction is accounted for in the source term of the enthalpy equation as shown in Equation (A.9).

The introduction of the kinetic term into the rate expression for turbulent flows is useful as it can act as a cut-off to the mixing controlled rate when chemistry is very slow. However, in many practical situations, the eddy breakup model describes the limiting rate. This is fortunate as it allows calculations to be made without knowledge of accurate Arrhenius rate data, the latter being hard to obtain for many industrial fuels.

Multi-Step Reactions: For systems involving multi-step reactions, you may need to take special measures if you use the eddy breakup model to compute the reaction rate. Consider, for example, the following sequential reactions:

$$CH_4 + \frac{3}{2} O_2 \rightarrow CO + 2H_2O \tag{A.21}$$

$$CO + \frac{1}{2} O_2 \rightarrow CO_2 \tag{A.22}$$

If the product concentration determines the reaction rate (Equation (A.20)), as is the case for a premixed or partially premixed flame, the reaction rate will be unphysically low because the concentration of $C0_2$ (the final product) is not included in the m_p summation for Reaction (A.21). The rate of breakdown of fuel is thus affected somewhat by the concentration of CO, which is an intermediate product with a small concentration in most practical cases. The resulting reaction rate is, therefore, too low.

To remedy this problem, you should replace Reaction (A.21) with

$$CH_4 + \frac{3}{2}O_2 \rightarrow CO + 0.001CO_2 + 2H_2O \tag{A.23}$$

When you include $C0_2$ as a product in Reaction (A.23), its concentration will be included in the computation of the reaction rate and the resulting rate will be more realistic. Since the stoichiometric coefficient for $C0_2$ in Reaction (A.22) is very small, this method should not have any adverse effect on the overall reacting system.

It should be pointed out that the eddy dissipation model and its constants were originally devised for single-step representations of chemistry. The extension to multiple reaction steps should be made with caution.

Stability and Convergence in Reacting Flows: Obtaining a converged solution in a reacting flow can be difficult for a number of reasons. First, the impact of the chemical reaction on the basic flow pattern may be strong, leading to a model in which there is strong coupling between the mass/momentum balances and the species transport equations. This is especially true in combustion, where the reactions lead to a large heat release and subsequent density changes and large accelerations in the flow. All reacting systems have some degree of coupling, however, when the flow properties depend on the species concentrations. These coupling issues are best addressed by the use of a two-step solution process, as described below, and by the use of underrelaxation and multiple sweeps of the solver.

A second source of convergence trouble in reacting flows is the interdependence of the species equations on the concentrations of the other chemical species in the model. This issue arises because the species conservation equation for one species may be dominated by the reaction source term, which is a function of other chemical species concentrations. Because FLUENT does not simultaneously update all species concentrations, this interdependence can lead to convergence difficulties. This issue implies an increase in the number of iterations required to yield a converged solution to reacting flows. It also implies that simpler reaction systems converge more easily. That is, a one or two reaction system involving 6 or 7 chemical species converges more easily than a system involving 10 species in a complex reaction sequence.

A third convergence issue in reacting flows involves the magnitude of the reaction source term. When your FLUENT model involves very rapid reaction rates (i.e. much more rapid than the rates of convection and diffusion), the matrix solution of the species transport equations becomes numerically difficult. This is because the matrices to be solved are no longer diagonally dominant, but depend instead on large source terms that may drive rapid and unstable variations in the species concentrations. Such systems are termed "stiff" systems and are created when you define models that involve very rapid kinetic rates, especially when these rates describe reversible or competing reactions. Very rapid chemistry may be treated more successfully using the chemical equilibrium calculations available in the mixture fraction/PDF modeling approach.

Two-Step Solution Procedures: Solving a reacting flow as a two-step process can be a practical method for reaching a stable converged solution to your FLUENT model. In this process, you begin by solving the flow equations only, temporarily turning off the species equations. When the basic flow pattern has thus been established using constant properties (constant concentrations), you can enable the species equations.

Cold Flow Simulations: In combustion systems, the two-step calculation procedure described above is conducted by initially solving the "cold-flow", or unreacting flow. This cold-flow solution provides a good starting solution for the calculation of the combusting system. This two-step approach to combustion modeling can be accomplished using the following procedures:

- Set up the problem including all species of interest in the reacting flow, but without the reactions defined.
- Solve an initial solution after first turning off the product species (and, perhaps, enthalpy) equations.
- Add the reaction modeling inputs, including enthalpies of formation.
- Turn on all equations, patch an ignition source (as described below), and resolve the reacting flow.

Ignition in Combustion Simulations: If you introduce fuel to an oxidant, spontaneous ignition does not occur unless the temperature of the mixture exceeds the activation energy threshold required to maintain combustion. This physical issue manifests itself in a FLUENT model as well and you have to supply an ignition source to initiate combustion. This ignition source may be a heated surface that heats the gas mixture above the required threshold level. Often, however, it is the equivalent of a spark: an initial solution state that causes combustion to proceed. This "spark" or "initial solution state" is supplied by you via the PATCH command: the spark is defined by patching a hot temperature into a region of the FLUENT model that contains a sufficient fuel/air mixture for ignition to occur. Often you may need to patch both the temperature and the fuel/oxidant/product concentrations to produce ignition in your model. The initial patch has no impact on the final steady-state solution-no more than the location of a match determines the final flow pattern of the torch that it lights.

6. BOUNDARY CONDITIONS

6.1 Overview of Defining Boundary Conditions in FLUENT

Boundary Condition Options: Boundary conditions provide FLUENT with information on flow/thermal conditions at the boundaries of your physical model. FLUENT provides a wide variety of boundary condition options, including:

- Flow inlets and exits
- Wall boundaries
- Symmetry boundaries
- Periodic boundaries
- Cyclic boundaries

Flow inlets and exits can be defined via pressure and/or velocity specification. Flow exits can alternately be defined in terms of zero normal gradient (or extrapolated) conditions.

Wall boundaries can be stationary or moving (e.g., rotating or sliding), slip or non-slip, smooth or rough. Walls may be treated via a variety of thermal boundary conditions (fixed temperature, fixed heat flux, or fixed external heat transfer conditions). Note that when an energy balance (conduction equation) is computed within wall regions, the thermal treatment of the wall is as a special "conducting wall" region and not as a boundary condition. Despite this, inputs that govern the conduction equation in walls are defined via the boundary condition input procedure and are covered in this chapter.

Symmetry and cyclic boundary conditions provide a means by which the scope of the computational model may be reduced by exploiting the repeating nature of the geometry and flow pattern. Periodic boundaries allow you to model fully developed flows.

Input of Boundary Conditions: Boundary conditions are defined in FLUENT by

- assigning boundary conditions to a particular type of control volume defined as the "cell type"
- assigning boundary condition values to individual control volumes via "patching"
- assigning "fixed" values to individual control volumes

In the first approach, boundary conditions are defined for all cells of a selected cell type. Using this approach, the boundary condition values may be uniform for all cells of the selected cell type, or values may vary via a polynomial function, a piecewise-linear spatial function, or a harmonic function. In the second approach patching-numerical values of boundary conditions are assigned on a cell-by-cell basis, allowing complete flexibility for the input of non-uniform boundary conditions. Patching can also

be used to input velocity boundary conditions via local coordinate systems. Fixing allows you to fix velocity values, for example, at live cells, simulating the effect of a fan or impeller without requiring the input of additional (and unknown) variable information at these cells.

6.2 Flow Inlets and Exits

FLUENT provides three types of boundary cell types for the specification of flow inlets and exits: velocity inlet, pressure inlet, and outlet. This section provides an overview and introduction to flow boundaries.

6.2.1 Inlet and Exit Boundary Conditions for Compressible Flows

Special attention should be paid to the setting of boundary conditions at flow inlets and exits when solving compressible flows. FLUENT provides several possible combinations of compressible flow boundary conditions.

Supersonic Flows with supersonic Inflow and Outflow: When the flow is known to be supersonic at all inlets and Supersonic at the flow exit, you must choose the following inlet/exit boundary conditions:

- Velocity inlet boundaries to define the velocity and static pressure (v, p_s, T_o) at all supersonic inlets (SUPERSONIC INFLOW BOUNDARY)
- Outlet boundary with the command SUPERSONIC OUTFLOW BOUNDARY enabled to define only a single flow exit.

Supersonic Inflow with Subsonic Outflow: When the inlet flow is supersonic but the flow exit is subsonic you can use the following combination:

- Velocity inlet boundaries to define the velocity and static pressure (v, P_s, To) at the flow inlet
- Pressure inlet boundaries to define the exit static pressure (P_s).

III-Posed Supersonic Inflow Conditions: Supersonic flow inlets should not be defined via input of stagnation conditions (P_o, T_o) at pressure inlet boundaries. Figure A.17 illustrates this ill-posed inlet treatment for supersonic flow. Such problem definitions do not uniquely define the static pressure (and mass flow rate) in the fluid.

Multiple Supersonic/Subsonic Flow Inlets: Multiple supersonic flow inlets can be defined via (v, P_s, To) boundary conditions. You can also combine a supersonic flow inlet that has been defined via (v, P_s, To) with a subsonic flow inlet that has been defined via (P_o, T_o) stagnation boundary conditions or via (ρv, T_o) mass flux boundary conditions. Note that only a single supersonic flow exit should be defined.

6.3 Velocity Inlet Boundary Conditions

Velocity inlet boundary conditions are used to define the flow velocity, along with all relevant scalar properties of the flow, at flow inlets. In special instances, inlet cells may be used to define the flow velocity (but not the scalar properties) at flow exits.

6.3.1 Inputs at Velocity Inlet Boundaries

At a flow inlet, velocity magnitudes for all velocity components are defined. In addition, appropriate scalar quantities are requested as input, depending upon the problem scope defined. Thus your inputs may include:

- Cartesian (or, optionally, normal, tangential, cylindrical-polar, or angular) velocity components
- Mass flux (for compressible flows only)
- Turbulence intensity/length scale
- Temperature (total temperature for compressible flow)
- Chemical species mass fractions (or mole fractions)
- Static pressure (supersonic inflow boundaries only)

7. USING THE SOLVER

7.1 Basics of the Overall Solution Algorithm

FLUENT solves the governing partial differential equations for the conservation of mass, momentum, energy and chemical species in a general form which can be written in Cartesian tensor notation as:

$$\frac{\partial}{\partial t}(\rho\phi)+\frac{\partial}{\partial x_i}(\rho u_i\phi)=\frac{\partial}{\partial x_i}\left[\Gamma_\phi\frac{\partial\phi}{\partial x_i}\right]+S_\phi \qquad \text{(A.24)}$$

where ϕ is the conserved quantity and the terms are the convection (LHS), diffusion, and source terms. The equations are reduced to their finite-difference analogs by integration over the computational cells into which the domain is divided. Integration in time is fully implicit.

After integration of equations of the form of Equation (A.24), the resulting algebraic equations can be written in the following common form:

$$\phi_P\sum_i(A_i-S_P)=\sum_i(A_i\phi_i)+S_\phi \qquad \text{(A.25)}$$

where the summation is over the neighboring finite difference cells i = *N*, *S*, E, W, F, B (which stand for North, South, East, West, Front, and Back). The A's are coefficients which contain contributions from the convective and diffusive fluxes and S_C *and* S_p are the components of the linearized source term, $S_\phi = S_c + S_p\phi_p$. A power-law differencing

scheme (or the optional Second Order Upwind or Quadratic Upwind Scheme) is used for interpolation between grid points and to calculate the derivatives of the flow variables. The set of simultaneous algebraic equations is solved by a semi-implicit iterative scheme which starts from arbitrary initial conditions (except at the boundaries) and converges to the correct solution (i.e., that which satisfies the governing equations) after performing a number of iterations.

Each iteration consists of the steps, which are illustrated in Fig. A.18. These steps are outlined below:

1. The u, v, and w momentum equations are each solved in turn using current values for pressure, in order to update the velocity field.

2. Since the velocities obtained in Step I may not satisfy the mass continuity equation locally, a "Poisson-type" equation is derived from the continuity equation and the linearized momentum equations. This "pressure correction" equation is then solved to obtain the necessary corrections to the pressure and velocity fields such that continuity is achieved.

3. The κ and ε equations are solved using the updated velocity field (for turbulent flow only).

4. Any auxiliary equations (e.g., enthalpy, species conservation, or any additional turbulence quantities) are solved using the previously updated values of the other variables.

5. The fluid properties are updated.

6. A check for convergence of the equation set is made.

These steps are continued until the error has decreased to a required value. When interphase coupling is included, the source terms of the appropriate gas flow equations are augmented.

7.2 Residual Reporting

Introduction: The process of obtaining a converged solution is of great importance in FLUENT simulations. So that you can monitor this process, FLUENT provides a running report of the residuals for each equation at each iteration. The residuals are a measure of how closely each finite difference equation is balanced, given the current state of the solution. In this section, a definition of the residuals is given, and the use of commands for displaying un-normalized and/or peak residuals and for plotting residuals during the calculation is described.

Definition of Residuals: At each iteration of its solution algorithm, FLUENT reports a residual for each equation that has been solved. These residuals provide a measure of the degree to which each equation is satisfied throughout the flow field. FLUENT computes residuals for each conservation equation by summing the imbalance in the equation for all cells in the domain. A detailed description of the calculation of the residuals is provided below.

After discretization, the conservation equation in two dimensions for a general variable ϕ_p, can be written as:

$$A_P\phi_P = A_E\phi_E + A_W\phi_W + A_N\phi_N + A_S\phi_S + S_C \tag{A.26}$$

where

$$A_P = A_E + A_W + A_N + A_S - S_P \tag{A.27}$$

The nomenclature for these equations is displayed in Fig. A.19, which shows a typical computational cell surrounding the node P, with neighboring nodes E, W, S and N. The quantity ϕ might be any dependent variable (u velocity, turbulence energy, enthalpy, etc.). The coefficients A_E, A_W, A_N, *and* A_S are the finite difference coefficients which combine convection and diffusion through the control volume surrounding point P. The quantities S_C *and* S_p are components of the linearized source term which incorporate any terms in the equation which do not fall into the convection/diffusion form.

The residual, R, computed by FLUENT, is the imbalance in Equation (A.26), summed over all of the computational points P:

$$R = \sum_{nodes\ P} \left| \left[A_E\phi_E + A_W\phi_W + A_N\phi_N + A_S\phi_S + S_C - A_P\phi_P \right] \right| \tag{A.28}$$

R is the un-normalized residual and always has the SI units kg-(units of ϕ)/sec.

When the residuals are normalized, normalization is by the left hand side of Equation (A.26), again summed over the computational nodes:

$$\overline{R} = \frac{\sum_{nodes\ P} \left| \left[A_E\phi_E + A_W\phi_W + A_N\phi_N + A_S\phi_S + S_C - A_P\phi_P \right] \right|}{\sum_{nodes\ P} \left| \left(A_P\phi_P \right) \right|} \tag{A.29}$$

In the normalized residual expressions for the momentum equations, the denominator term $A_p\phi_p$ is replaced by $A_P\sqrt{u_P^2 + v_P^2 + w_P^2}$

$\overline{R}$ is the normalized residual. FLUENT reports normalized residuals unless you request that un-normalized residuals be displayed.

Definition of Pressure Residual: The preceding equations, Equations (A.28) and (A.29), are the residuals reported by FLUENT for all variables except the pressure. The residual for pressure is actually the imbalance in the continuity (pressure correction) equation:

$$R = \sum_{nodes\ P} \left| (C_W - C_E + C_S - C_N) \right| \tag{A.30}$$

where *Cw, CE, Cs, CN* are the convection of mass (kg/s) through each face of the control volume surrounding point P. Normalization of the pressure residual is accomplished by dividing by the residual (or continuity imbalance) at the second iteration:

$$\overline{R} = \frac{R_{iteration\ N}}{R_{iteration\ 2}} \tag{A.31}$$

Equation (A.31) implies that if the imbalance in continuity at iteration 2 is quite small, the normalized residual will be relatively large. If you make a good initial guess of the flow field, therefore, you can actually cause the normalized pressure residual to be larger than the normalized residual resulting from a poor initial guess. In such cases, you should examine the reduction of the un-normalized residual with iteration, since this value is insensitive to the initial guess.

7.3 Judging Convergence

Introduction: A FLUENT calculation is converged when all governing equations are balanced at each point in the solution domain. This section provides guidance on how to judge the convergence of your solution via residual values and how to monitor the progress towards convergence via residual histories and histories of solution variables.

General Guidelines for Residual Values: The residuals for each flow variable give you a measure of the magnitude of the error in the solution at each iteration. As discussed in the preceding section, these residuals are normalized unless you request that they be un-normalized. Generally, a solution is well converged when the normalized residuals are on the order of 1×10^{-3} An important exception is the enthalpy residual which should be about 1×10^{-6}. (The P-1 radiation residual should also be 1×10^{-6}.)

In addition you may find that the residuals of the species transport equations will need to decrease to 1×10^{-5} to 1×10^{-6} when you are solving problems involving mixing of two species of very different molecular weights (e.g., H_2 and WF_6). If the residuals have decreased to this level, are monotonically decreasing, and the flow field looks unchanged from the solution 50 iterations earlier, then the solution can be called "converged". Sometimes you may not need to generate a completely converged solution, if you can pickup the basic features of the flow field right away. When you are interested in quantitative results, however, complete convergence of the solution is essential.

7.4 Solution of the Continuous Phase Equations

FLUENT uses a control volume based technique to solve the conservation equations for mass, momentum, energy, species, and turbulence quantities described in the preceding sections. This control volume based technique consists of:

- Division of the domain into discrete control volumes using a general curvilinear grid,
- Integration of the governing equations on the individual control volumes to construct the algebraic equations for discrete unknowns (velocities, pressure, scalars)
- Solution of the discretized equations

The discretization of the differential equations, and the techniques used by FLUENT to solve them are described in this section.

7.4.1 The Control Volume Technique

FLUENT uses a control volume based technique to convert the differential conservation equations to algebraic equations which can be solved numerically. This control volume technique consists of integrating the differential equations about each control volume, yielding a finite-difference equation that conserves each quantity on a control-volume basis.

The Non-Staggered Control Volume Storage Scheme: FLUENT defines the discrete control volumes using a non-staggeredgrid storage scheme as illustrated in Fig. A.20. In this scheme, the same control volume is employed for integration of all the conservation equations and all variables (pressure, Cartesian velocity components, Reynolds stress components, and all scalars) are stored at the control volume cell center.

Volume Integration of the Differential Equations: The integration of the differential equations can be illustrated most easily in simple Cartesian coordinates, and is demonstrated below for a one-dimensional equation set. Consider first the one-dimensional differential equations for continuity, momentum, and a scalar quantity ϕ:

$$\frac{\partial}{\partial x}(\rho u)=0 \tag{A.32}$$

$$\frac{\partial}{\partial x}(\rho u)=-\frac{\delta p}{\delta x}+\frac{\delta}{\delta x}\left[\mu\left(\frac{\delta u}{\delta x}\right)\right]+F \tag{A.33}$$

$$\frac{\delta}{\delta x}(\rho u\phi)=\frac{\delta}{\delta x}\Gamma\frac{\delta\phi}{\delta x}+S_{\phi} \tag{A.34}$$

Equations (A.32) through (A.34) can be volume integrated about a control volume employing the Divergence Theorem:

$$\int_{volume\ V} \frac{\delta}{\delta x}(\rho u)dV = \int_{A} \rho u\,.\,dA \tag{A.35}$$

Volume integration of (A.32) on the control volume of Fig. A.21 thus yields:

$$(\rho u A)_e - (\rho u A)_w = 0 \tag{A.36}$$

or:

$$J_e - J_w = 0 \tag{A.37}$$

Integration of the momentum Equation (A.33) yields:

$$(\rho u^2 A)_e - (\rho u^2 A)_w = -(p_e - p_w)A + \left(\mu\left[\frac{u_E - u_P}{\Delta x}\right]A\right)_e - \left(\mu\left[\frac{u_P - u_W}{\Delta x}\right]A\right)_w + F\Delta V \tag{A.38}$$

or:

$$J_e u_e - J_w u_w = -(p_e - p_w)A + \left[\frac{\mu_e}{\Delta x_e}(u_E - u_P) - \frac{\mu_w}{\Delta x_w}(u_P - u_W)\right]A + F\Delta V \tag{A.39}$$

and integration of the scalar equation, (A.34), yields:

$$J_e\phi_e - J_w\phi_w = \left(\Gamma_e \frac{\Phi_E - \Phi_P}{\Delta x_e} - \Gamma_w \frac{\Phi_P - \Phi_W}{\Delta x_w}\right)A + S_\Phi \Delta V \tag{A.40}$$

Note that the equations solved by FLUENT are extensions into three-dimensional curvilinear coordinates of those shown above for one-dimensional Cartesian coordinates.

Closure of that Discrete Equations: the Equations (A.37), (A.39), and (A.40) are algebraic equations can be solved provided that the unknowns (u, p, and ϕ) are interpolated in a manner that relates their values at the control volume faces to the stored values at the control volume centers. The discretization procedures used by FLUENT to perform this interpolation are described in the following section.

7.4.2 Discretization Procedures in FLUENT

Solution of the finite-difference equations presented in the preceding section requires:

- Calculation of the pressure stored at the control volume faces (p_e, p_w.)
- Calculation to determine the face fluxes (J_e, J_w);

- Interpolation to relate the face values of the unknowns (u and ϕ) to the stored values at the control volume centers.

In FLUENT, the face fluxes are obtained such that the face velocities obey an averaged momentum balance and the face pressures are obtained such that the velocities stored at cell centers obey the mass balance. These calculation procedures ensure that the FLUENT formulation avoids oscillatory (or "checkerboard") pressure or velocity fields and that the physical variation of pressure and momentum between cell centers is accurately represented.

The interpolation to determine face values of the unknowns is accomplished via either the Power Law. blended Second Order Upwind/Central Difference, or QUICK interpolation schemes, described below.

The Power Law Scheme: The power law interpolation scheme interpolates the face value of a variable, ϕ, using the exact solution to a one-dimensional convection-diffusion equation. This one-dimensional equation describes the flux of ϕ as:

$$\frac{\delta}{\delta x}(\rho u \phi) = \frac{\delta}{\delta x}\Gamma\frac{\delta \phi}{\delta x} \tag{A.41}$$

where Γ and ρu are constant across the interval δx. Equation (A.41) can be integrated to yield the following solution describing how ϕ varies with x:

$$\frac{\delta(x)-\phi_o}{\phi_L-\phi_o} = \frac{\exp\left(P_e\frac{x}{L}\right)-1}{\exp(P_e)-1} \tag{A.42}$$

where:

$\phi_o = \phi|_{x=0}$ *and* P_e *is the peclet number,*
$\phi_L = \phi|_{x=L}$

$$P_e = \frac{\rho u L}{\Gamma} \tag{A.43}$$

FLUENT uses 7.4-11 in an equivalent "power law" format, as its default interpolation scheme.

The variation of $\phi(x)$ between x = 0 and x = L is depicted in Fig. A.22 for a range of values of the Peclet number. Figure A.22 shows that for large Pe, the value of 0 at x = L/2 is approximately equal to the upstream value. This implies that when the flow is dominated by convection, interpolation can be accomplished by simply letting the face

value of a variable be set equal to its "upwind" or upstream value. When the Pe = 0 (no flow, or pure diffusion), Figure A.22 shows that 0 may be interpolated via a simple linear average between the values at x = 0 and x = *L*. When the Peclet number has an intermediate value, the interpolated value for ϕ at x = L/2 must be derived by applying the "power law" equivalent of Equation (A.42).

Higher Order Interpolation Schemes: As an alternative to the Power-Law Differencing Scheme, FLUENT provides two higher order schemes: QUICK and a blended Second Order Upwind/Central Difference scheme. These schemes compute the face value of an unknown (e.g., ϕ_f) based on the values stored at the two adjacent cell centers (ϕp and ϕ_E) and on a third cell center at an additional upstream point (e.g., ϕ_w). Using the nomenclature depicted in Fig. A.23, the face value can be written in terms of these neighbor values as:

$$\phi_f = \theta\left[\frac{\Delta x_D}{\Delta x_C + \Delta x_D}\phi_C + \frac{\Delta x_C}{\Delta x_C + \Delta x_D}\phi_D\right] + (1-\theta)\left[\frac{\Delta x_U + 2\Delta x_C}{\Delta x_U + \Delta x_C}\phi_C - \frac{\Delta x_C}{\Delta x_U + \Delta x_C}\phi_U\right] \quad \text{(A.44)}$$

where ϕ_f is the face value, ϕ_D is the downstream value, ϕ_C is the center cell value, and ϕ_U is the upstream value. Equation (A.44) computes the face value with second or third order accuracy, depending upon the choice of θ, as shown in Table (A.1). FLUENT chooses θ for the two higher order schemes in a manner which eliminates oscillations or overshoots, as noted below.

Bounding of the Higher Order Schemes: While higher order schemes provide greater accuracy, numerical instabilities can occur unless the interpolation is appropriately bounded. Second-Order Central Difference will yield oscillations at discontinuities, and Second-Order Upwind or QUICK will produce undershoots and overshoots. Linear combinations of the methods can, however, produce a scheme which is both stable and accurate.

Bounding of the Second-Order Scheme: For the Second-Order scheme, such linear combinations are created through variation of the parameter θ in Equation (A.44). In the blended Second-Order Upwind/Central Difference Scheme used by FLUENT, θ is computed as:

$$\theta = \max\left(0, \min\left(\tilde{\phi}_C, 1\right)\right) \quad \text{(A.45)}$$

where

$$\tilde{\phi}_C \equiv \frac{\phi_C - \phi_U}{\phi_D - \phi_U} \quad \text{(A.46)}$$

Bounding of the QUICK Scheme with Limiters: For a uniform grid, Equation 7.4-13 can be rewritten as

$$\phi_f = \phi_C + \frac{1}{4}[(1+k)(\phi_D - \phi_C) + (1-k)(\phi_C - \phi_U)] \tag{A.47}$$

where the numerical parameter k controls the order of the scheme. Unbounded terms corresponding to central differencing (CD), second order (linear) upwind differencing (LUDS), and QUICK schemes arise by setting k = 1, -1, and 0.5, respectively. To provide a monotonic scheme in terms of Equation (A.47), a slope limiter ψ (r_f) is introduced:

$$\phi_f = \phi_C + \frac{1}{4}[(1+k)\psi(r_f)(\phi_D - \phi_C) + (1+k)\psi(1/r_f)(\phi_C - \phi_U)] \tag{A.48}$$

where

$$r_f = \frac{\tilde{\phi}_C}{1-\tilde{\phi}_C} \tag{A.49}$$

$\tilde{\phi}_C$ is as defined in Equation 7.4-15.

In FLUENT, for the QUICK scheme (k = 0.5), four different kinds of limiters have been implemented:

- UMIST or SMART:

$$\psi(r) = \max[0, \min(2r\ ,\ 0.75 + 0.25r\ ,\ 2)] \tag{A.50}$$

- MUSCL:

$$\psi(r) = \max\left[0, \min\left(2r\ ,\ \frac{1+r}{2}\ ,\ 2\right)\right] \tag{A.51}$$

- compressible MINMOD:

$$\psi(r) = \max[0, \min(1\ ,5r)] \tag{A.52}$$

- SUPERBEE:

$$\psi(r) = \max[0, \min(2r,1), \min(r,2)] \tag{A.53}$$

These limiters provide monotonic behavior of the variables in regions of steep gradients, and can be characterized by their different convergence properties: the steeper the limiter, the more difficult it is to converge. UMIST or SMART (the default) has optimal characteristics in terms of convergence and boundedness, while SUPERBEE (which is very good at resolving discontinuities) is the most difficult to converge. FLUENT also allows you to use the unbounded form of QUICK without limiters ($\psi(r) = 1$).

Linear Pressure Interpolation: For supersonic compressible flows in which shocks can occur, FLUENT provides a linear pressure interpolation option. The standard pressure interpolation at cell faces is a physical interpolation, which works well for nearly all flows, but which may fail to satisfy conservation of total temperature in compressible flows with shocks. Note that linear pressure interpolation cannot be used with porous-media flows or flows with strong body forces.

Higher-Order Density Interpolation: Four interpolation schemes are available for the calculation of density: upwind (default), linear, second-order-upwind, and QUICK. The default upwind scheme sets the density at the cell face to be the upstream cell-center value. This scheme provides stability for the discretization of the pressure-correction equation, and gives good results for most classes of flows. The linear density interpolation scheme uses a simple linear interpolation. For some incompressible flows (e.g., natural-convection flows or flows with large changes in density due to temperature or species concentration), better results can be obtained by using the linear density interpolation. In compressible flow with shocks, the default upwind scheme may tend to smooth the shocks; you should use the second-order-upwind or QUICK scheme for such flows. For compressible flows with shocks, using the QUICK scheme for all variables, including density, is highly recommended.

Viscosity-Weighted Velocity Interpolation: To calculate the differential viscous terms for the momentum equations and for the generation of turbulence, FLUENT provides an optional viscosity-weighted velocity interpolation scheme in addition to the default linear interpolation scheme. The viscosity-weighted method is based on the continuity of shear stress for control volumes. For the simple 1D case shown in Fig. A.24, the velocity at face c obtained with the viscosity-weighted interpolation will be

$$u_e = \frac{\mu_P u_P (\Delta x)_{e+} + \mu_E u_E (\Delta x)_{e-}}{\mu_P (\Delta x)_{e+} + \mu_E (\Delta x)_{e-}} \tag{A.54}$$

The viscosity-weighted interpolation option will give better results for turbulent kinetic energy inside shear layers without excessive generation of turbulence.

7.4.3 The Pressure-Velocity Coupling Algorithms: SIMPLE and SIMPLEC

The continuity and momentum equations, in three dimensions, provide four equations for solution of four unknowns: u_1, u_2, u_3, and p. Simultaneous solution of this (linearized) equation set would provide a solution in which all four unknowns satisfy each of the (linearized) mass and momentum equations. Because a simultaneous solution is computationally intensive, in FLUENT the equations are solved sequentially. In the sequential solution process, an equation describing the update of pressure is required, and is not explicitly available via the mass or momentum balances. The SIMPLE family of algorithms is based on using a relationship between velocity and pressure corrections in order to recast the continuity equation in terms of a pressure correction calculation.

Coefficient Form of Momentum Equation: the The discretized one-dimensional momentum equation developed in Section 7.4.1 above, can be written in a shortened notation as

$$A_P u_P = \sum_{NB} A_{NB} u_{NB} + (p_w - p_e)A + S \tag{A.55}$$

where Ap and A_{NB} are coefficients containing the convection and diffusion contributions in the momentum equation, Equation (A.39), and the subscript NB refers to neighbor points (e.g., *E, W* in 1D or *E, W, N, S* in 2D).

The SIMPLE Algorithm: The SIMPLE algorithm starts with substitution of a guessed pres sure field, p*, into the momentum equations (Equation (A.55)) which can then be solved to obtain a "guessed" velocity field, u*:

$$A_P u_P^* = \sum_{NB} A_{NB} u_{NB}^* + (p_w^* - p_e^*)A + S \tag{A.56}$$

Equation (A.55) is solved for the "guessed" velocity field (e.g. u_P^*). The actual velocity and pressure fields are related to the "guessed" values, u_P^* and p*, and

$$u_P = u_P^* + u_P^* \tag{A.57}$$

$$p_e = p_e^* + p_e^* \tag{A.58}$$

where u_P^* and p_e^* are the velocity correction and pressure correction, respectively. Substitution of Equations (A.57) and (A.58) into Equation (A.55), followed by subtraction of (A.56), yields a "momentum balance" in terms of the velocity and pressure corrections:

$$A_P u_P' = \sum_{NB} A_{NB} u_{NB}' + (p_w' - p_e')A \tag{A.59}$$

Equation (A.59) is used to relate the pressure and velocity corrections as

$$u'_P = \frac{1}{A_P}\left(p'_w - p'_e\right)A \tag{A.60}$$

where the term containing the neighbor influences $\left(\sum_{NB} A_{NB} u'_{NB}\right)$ is simply dropped for convenience (and will be zero at convergence since it involves only velocity corrections at the neighbor points) .

Equations similar to Equation (A.60) are used to cast the continuity equation in terms of an equation for the pressure correction. The basic mass balance

$$(\rho uA)_e - (\rho uA)_w = 0 \tag{A.61}$$

is first written in terms of the velocity u* + u':

$$(\rho A)_e \left(u^* + u'\right)_e - (\rho A)_w \left(u^* + u'\right)_w = 0 \tag{6.62}$$

Using equations like Equation (A.60), the continuity equation can be recast as an equation for the pressure correction:

$$\left(\rho A u^*\right)_e - \left(\rho A u^*\right)_w + (\rho A)_e \frac{1}{(A_P)_e}\left(p'_P - p'_E\right) - (\rho A)_w \frac{1}{(A_P)_w}\left(p'_W - p'_P\right) = 0 \tag{A.63}$$

Equation 7.4-32 can now be solved for a correction to the pressure field which is then used to compute the velocity correction via Equation (A.60). Finally, the velocity and pressure are updated via Equations (A.57) and (A.58).

The SIMPLEC Algorithm: The SIMPLEC algorithm is a variant on the standard SIMPLE algorithm described above. The derivation of SIMPLEC is the same as that for SIMPLE from Equations (A.55) – (A.59). From that point on, the SIMPLEC derivation proceeds as follows.

Equation (A.59) is used to relate the velocity and pressure corrections, after subtraction of a new term, $\left(\sum_{NB} A_{NB} u'_{NB}\right)$, from both the left and right sides:

$$\left(A_P - \sum_{NB} A_{NB}\right) u'_P = \sum_{NB} A_{NB}\left(u'_{NB} - u'_P\right) + \left(p'_w - p'_e\right)A \tag{A.64}$$

Next, the term involving the difference $\left(u'_{NB} - u'_P\right)$ is dropped, under the argument that this term is small and will vanish at convergence when the corrections are zero. The resulting relationship between pressure and velocity correction becomes

$$u_P' = \frac{1}{A_P - \sum_{NB} A_{NB}} \left(p_w' - p_e'\right) A \tag{A.65}$$

Equation (A.65) can be contrasted to the correction relationship used in SIMPLE (Equation (A.60)) by noting that here the neighbor term which is dropped involves a difference term $\left(\sum_{NB} A_{NB} \left(u_{NB}' - u_P'\right)\right)$ which is small compared to the neighbor term $\left(\sum_{NB} A_{NB}\right)$ dropped in SIMPLE.

Equations similar to Equation (A.65) are used to cast the continuity equation in terms of an equation for the pressure correction. The mass balance equation (in 1D Cartesian form) is first written in terms of the velocity $u^* + u'$:

$$(\rho A)_e \left(u^* + u'\right)_e - (\rho A)_w \left(u^* + u'\right)_w = 0 \tag{A.66}$$

Using equations similar to Equation (A.65), this continuity equation can be recast in terms of pressure correction as

$$\begin{aligned} \left(\rho A u^*\right)_e - \left(\rho A u^*\right)_w + (\rho A)_e \frac{1}{\left(A_P - \sum_{NB} A_{NB}\right)_e} \left(p_p' - p_E'\right) - \\ (\rho A)_w \frac{1}{\left(A_P - \sum_{NB} A_{NB}\right)_w} \left(p_W' - p_P'\right) = 0 \end{aligned} \tag{A.67}$$

Equation (A.67) can now be solved for a correction to the pressure field which is then used to compute the velocity correction via Equation (A.65). Finally, using Equations (A.57) and (A.58), the velocity and pressure corrections thus obtained are used to update the current velocity and pressure fields.

7.4.4 The Iterative Solution Procedure

The SIMPLE and SIMPLEC algorithms described above relate the velocity and pressure fields which satisfy the linearized momentum and continuity equations at a point. Because FLUENT does not solve the equations at all points simultaneously, and because the equations are coupled and non-linear, an iterative solution procedure is required with iterations continuing until all equations are satisfied at all points.

Each iteration of FLUENT's solution procedure consists of the following steps:

1. The u_1, u_2, and u_3 momentum equations are solved in turn using the guessed pressure field, p*.

2. The pressure correction equation (mass balance) is then solved to obtain the necessary corrections to the pressure field. Corresponding adjustments to the velocity components are also made.

3. For turbulent flows, the k and ε equations (or Reynolds stress transport equations) are solved using the updated velocity field to obtain the distribution of the effective viscosity and/or Reynolds stresses.

4. Any auxiliary equations (e.g. enthalpy, species conservation, and/or radiation) are solved using the previously updated values of other variables.

5. Fluid properties are updated

6. When interphase coupling is to be included, the source terms in the appropriate continuous phase equations may be updated via a dispersed phase trajectory calculation.

These steps can be continued until the error in each conservation equation within each volume and hence over the global domain has decreased to a required value.

7.4.5 Iterative Full-Field Solution of the Equations

On those computer system supporting the required matrix libraries, FLUENT optionally uses a full-field iterative solver called GMRES (Generalized Minimum Residual Method) to solve the system of equations. This full-field solver can vield significant speed-up of convergence compared to the Line Gauss-Seidel technique described below.

7.4.6 Line-by-Line Solution of the Equations

The algebraic equation to be solved by FLUENT for any variable at point P may be written as:

$$A_P \phi_P = \sum_{NB} A_{NB} \phi_{NB} + S_\phi \qquad \text{(A.68)}$$

where the subscript NB denotes neighbor values, the coefficients A_p and A_{NB} contain convection and diffusion coefficients, and S_ϕ is the source of ϕ in the control volume surrounding point P. For each unknown, ϕ, an equation of this form must be solved at all points within the domain. This solution process may be accomplished via a "line-by-line" solver, in which the equations along a single "line" of cells (e.g. a line of I = constant) are solved simultaneously. The line-by-line solver gives rise to a tri-diagonal matrix which is solved via Gaussian elimination to update the values of ϕ along the line considered. This procedure, also referred to as Line Gauss-Seidel (LGS), is repeated for all lines in the domain so that ϕ is updated at all points P. FLUENT provides flexibility in its line-by-line solution procedure, giving the user control over the directions) of the lines to be considered and over the number of times each line is visited in order to update a given variable within each global iteration loop.

Multigrid and 1D Block Correction to Accelerate Line-By-Line Solver: While the LGS solver is good at reducing local errors, it is relatively poor at reducing errors which require collective change of many cell the values (long-wavelength errors). Therefore the speed of solution of the LGS solver deteriorates with increasing grid size. Also for large aspect-ratio cells in combination with gradient boundary conditions, as may occur in highly stretched grids, convergence may be poor. FLUENT provides two devices to speed up the LGS procedure:

- One-dimensional block correction
- Multigrid (MG) acceleration.

Both methods accelerate the convergence of the equations by deriving global corrections that drive the solution toward global conservation. One-dimensional block correction is also useful in combination with multigrid acceleration, when cells are highly stretched or otherwise strongly anisotropic coefficients are to be expected. Each of these methods is described in the following sections.

1D Block Correction vs. Multigrid: One-dimensional block corrections reduce long-wavelength errors in the direction in which they are applied, but may introduce large short-wavelength errors. Therefore, application of block correction is followed by application of LGS to reduce the short-wavelength errors. Sufficient sweeps must be specified to this purpose, otherwise the effect of block correction may be adverse. If very steep gradients exist in the final solution, ID block correction may increase the solution effort for this reason. These disadvantages are to a large extent avoided in multigrid (MG) acceleration.

7.4.7 Multigrid Acceleration of the Line-by-Line Solver

The line-by-line solution approach is accelerated in FLUENT using an Additive-Correction Multigrid procedure. This procedure computes corrections to the current solution field within successively coarser blocks of control volumes. The corrections obtained on these multiple coarse-grid levels are used to refine the fine grid solution and to thereby accelerate convergence.

The Additive Correction Multigrid Scheme: Additive Correction is a technique which seeks to apply a correction, ϕ', to the current solution field, ϕ^*, such that the resulting corrected solution, $\phi^* + \phi'$, obeys a global conservation of ϕ within some subregion considered. In FLUENT, the subregions considered are constructed via grouping together of neighboring control volumes. The equations to be solved on each multigrid level are constructed via summation of the equations on the original fine grid level. This summation, over the fine grid cells used to construct the coarse grid element, can be written as:

$$\sum_i \sum_j \sum_k \left[A_{ijk}^P \phi_{ijk} = A_{ijk}^E \phi_{i+1jk} + A_{ijk}^W \phi_{i-1jk} + A_{ijk}^N \phi_{ij+1k} + A_{ijk}^S \phi_{ij-1k} + A_{ijk}^U \phi_{ijk+1} + A_{ijk}^D \phi_{ijk-1} + b_{ijk} \right] \quad \text{(A.69)}$$

where the coefficients A^E A^W,A^N , A^S, A^U, and A^D are the neighbor coefficients (A_{NB}) of the point P at cell *ijk* of the fine grid.

Next, the unknowns, ϕ_{ijk} , are assumed to consist of the current solution value in each cell, ϕ_{ijk}^* , and a correction, ϕ_{IJK}' on the *IJK*th block of the coarse grid level:

$$\phi_{ijk} = \phi_{ijk}^* + \phi_{IJK}' \quad \text{(A.70)}$$

Substitution of Equation (A.70) into (A.69) yields an equation to be solved for the correction field, ϕ_{IJK}' , on the coarse grid level. This correction equation relates the correction in the *IJK*th block of the coarse grid to the corrections in the neighbor blocks on the coarse grid. The set of equations derived via similar summations on each coarse grid block are then solved iteratively, using an alternating direction Line-Gauss-Seidel solution method. The set of corrections thus obtained are then added to the current fine grid solution as in Equation (A.70). The resulting corrected solution then satisfies global balances on the coarse grid level. Satisfaction of local conservation on the fine grid level then proceeds as usual, using the line solver to update ϕ_{ijk}^* .

Control of Grid Levels During the Multigrid Solution Process: The multigid procedure invokes calculations on the next coarser grid level when the error reduction rate on the current level is insufficient, as defined by the parameter β:

$$R_i \succ \beta R_{i-1} \quad \text{(A.71)}$$

Here R_i is the absolute sum of residuals computed on the current grid level after the *i*th sweep of the line solver on this level. Equation (A.71) states that if the residual (error) present in the iterative solution after *i* sweeps is greater than some fraction, β, of the residual present after the (*i*-1)th sweep, the next coarser grid level should be visited. Modifications to β control the frequency with which higher grid levels are visited.

Provided that the residual reduction rate is sufficiently rapid, FLUENT will converge the correction equations on the current grid level and apply the resulting corrections to the solution field on the next finer grid level. The correction equations on the current grid level are considered sufficiently converged when the error in the correction solution reduces to some fraction, a, of the original error on this grid level:

$$R_i \prec \alpha R_o \quad \text{(A.72)}$$

Here, R_i is the residual on the current grid level after the ith iteration on this level, and R_0 is the residual which was initially obtained on this grid level at the current global iteration. Equation (A.72) is also used to terminate calculations on the lowest (finest) grid level during the multigrid procedure. Thus, FLUENT will continue sweeping the line solver on each grid level (including the finest grid level) until the criteria of Equation (A.72) is obeyed (or until a maximum number of sweeps has been completed, in the case that the criteria of Equation (A.72) is never achieved.)

Adding 1D Block Correction with Multigrid: As noted above, the convergence of the coarse grid correction equations may be accelerated by computing corrections on an even coarser grid and/or by applying 1D block correction to the current grid level. 1D block correction can be understood as a simple version of the Additive Correction Multigrid technique, with the coarser grid level consisting of a one-dimensional grid created by summation over all cells in two of the three grid directions on the finer grid. 1D block correction is of particular benefit in problems with large cell aspect ratios and in problems with large abrupt changes in material properties.

7.4.8 1D Block Correction

FLUENT optionally applies a 1D block correction to the continuous phase transport equations in order to accelerate convergence of the line-by-line solution process described above. In the block correction procedure used by FLU ENT, the transport equations for a variable 0 are summed in each plane of constant 1, J, or K, and the resulting set of "one-dimensional" equations are solved for a correction to on each plane. The details of this process are described below.

Consider the discretized equation for ϕ_{ijk} at point P in 3D:

$$A_{ijk}^{P}\,\phi_{ijk} + A_{ijk}^{E}\,\phi_{i+1jk} + A_{ijk}^{W}\,\phi_{i-1jk} + A_{ijk}^{N}\,\phi_{ij+1k} + A_{ijk}^{S}\,\phi_{ij-1k} + A_{ijk}^{U}\,\phi_{ijk+1} + A_{ijk}^{D}\,\phi_{ijk-1} = b_{ijk} \qquad \text{(A.73)}$$

where the superscripts *E, W, N, S, U,* and D represent the east, west, north, south, up, and down neighbors of the point P. For the case of 3D to 1D block correction in the I direction, the equations are summed in each I plane:

$$\sum_j \sum_k \left(A_{ijk}^{P}\,\phi_{ijk} + A_{ijk}^{N}\,\phi_{ij+1k} + A_{ijk}^{S}\,\phi_{ij-1k} + A_{ijk}^{U}\,\phi_{ijk+1} + A_{ijk}^{D}\,\phi_{ijk-1}\right) + \sum_j \sum_k A_{ijk}^{E}\,\phi_{i+1jk} + \sum_j \sum_k A_{ijk}^{W}\,\phi_{i-1jk} = \sum_j \sum_k b_{ijk} \qquad \text{(A.74)}$$

If $\tilde{\phi}_{ijk}$ is the current best estimate of the solution, the improved solution will be given $\phi_{ijk} = \tilde{\phi}_{ijk} + \delta_I$. Here δ_I is the correction over the plane. Substituting this into the above equation yields

$$\sum_j \sum_k \left(A_{ijk}^P + A_{ijk}^N + A_{ijk}^S + A_{ijk}^U + A_{ijk}^D\right)\delta_I + \sum_j \sum_k A_{ijk}^E \, \delta_{I+1} + \sum_j \sum_k A_{ijk}^W \, \delta_{I-1} = \bar{b}_I \qquad \text{(A.75)}$$

where:

$$\bar{b}_I \equiv \sum_j \sum_k \left(b_{ijk} - A_{ijk}^P \tilde{\phi}_{ijk} - A_{ijk}^E \tilde{\phi}_{i+1\,jk} - A_{ijk}^W \tilde{\phi}_{i-1\,jk} - A_{ijk}^N \tilde{\phi}_{ij+1k} - A_{ijk}^S \tilde{\phi}_{ij-1k} - A_{ijk}^U \tilde{\phi}_{ijk+1} - A_{ijk}^D \tilde{\phi}_{ijk-1}\right) \qquad \text{(A.76)}$$

Defining a set of coefficients for these 1D equations, the correction equation can be written as

$$\bar{A}_I^P \, \delta_I + \bar{A}_I^E \, \delta_{I+1} + \bar{A}_I^W \, \delta_{I-1} = \bar{b}_I \qquad \text{(A.77)}$$

where:

$$\bar{A}_I^P \equiv \sum_j \sum_k \left(A_{ijk}^P + A_{ijk}^N f^N + A_{ijk}^S f^S + A_{ijk}^U f^U + A_{ijk}^D f^D\right) \qquad \text{(A.78)}$$

$$\bar{A}_I^E \equiv \sum_j \sum_k A_{ijk}^E \qquad \text{(A.79)}$$

$$\bar{A}_I^W \equiv \sum_j \sum_k A_{ijk}^W \qquad \text{(A.80)}$$

The factors f^N, f^S, f^U, and f^D in Equation (A.77) are used to remove the influence of neighbors in the J or K directions in the I direction block correction equation. This is accomplished by setting $f^N = 1$ if N is a computational cell and 0 otherwise, with similar treatments for f^S, f^U, and f^D.

The correction equations, Equation (A.77), for the corrections δ_I, at each I plane are solved using the Thomas tri-diagonal matrix algorithm, and then the unknowns are corrected using $\phi_{ijk} = \tilde{\phi}_{ijk} + \delta_I$. Similar equations are derived and solved for the corrections in the J and K directions.

7.5 Speeding Convergence

Introduction: Convergence can be hindered by a number of factors. Large numbers of computational cells, overly conservative underrelaxation factors, and complex flow physics are often the main causes. In this section, some of the numerical controls and modeling techniques that can be exercised to enhance convergence are examined.

7.5.1 Initial Guesses and Step-by-Step Solution Processes

Introduction: Two of the simplest techniques to get your calculation off to a good start are covered in this section. These include starting with guessed values for some of the variables at some or all locations within the domain, and techniques for solving difficult problems in stages.

Patching Initial Guesses: Supplying an initial guess for important flow variables, using the PATCH command, is an excellent way to begin the solution of a problem. In the absence of an initial guess, all of the variables are assumed to have a value of 0 throughout the domain, with the exception of temperature, (which has the default value of the freezing point for water, 273 K) and the turbulence parameters k and c (which are set to averages of the inlet values). Use of the PATCH option is illustrated below, where the entire domain (except protected boundaries) is covered with the patched values for temperature (TE) and u velocity (UV) by using the defaults on the minimum and maximum I and J indices.

Some of the most common examples where patching can be helpful are listed below:

- An initial guess for the fluid temperature should always be made in problems involving heat transfer and/or when the gas law is used.
- An initial guess of the velocity field is particularly useful when a large number of computational cells is used in the problem setup.
- In natural convection problems, it is helpful to patch both the temperature and velocities at the start of the problem.
- In problems with reacting flows, you can choose to solve the reacting flow right from the start or use a step-by-step method as described in the next section. If you decide to use the first option, it is a good idea to patch mass fractions for the reactants in the region where the reaction is most likely to occur. In combustion problems, where a threshold temperature is required to sustain a reaction, it is a good idea to patch in this temperature at the start.

Patching the Heat Capacity When Patching Temperature: When you supply an initial guess for the fluid temperature, FLUENT will update the enthalpy using the current stored value for the mixture heat capacity c_p. When the heat capacity is composition dependent, FLUENT's current stored value for c_p, may be considerably different from that expected in the converged solution. In some instances, this may lead to poor initialization of enthalpy, resulting in a sudden change of temperature, away from your patched values, when the solution process updates the stored value of c_p. You can work around this start-up issue by first patching c_p, and then patching

temperature. This is not required, however, as the converged solution will be independent of your patched initial guess.

Step-by-Step Techniques: One important technique for speeding convergence for complex problems is to tackle the problem one step at a time. When modeling a problem with heat transfer, you can begin with the calculation of the isothermal flow. When modeling a reacting flow, you can begin by computing a partially converged solution to the non-reacting flow, possibly including the species mixing. When modeling a dispersed phase, such as fuel evaporating from droplets, it is a good idea to solve the gas phase flow field first. Such solutions generally serve as a good starting point for the calculation of the more complex problems. This option is explained below.

FLUENT automatically solves each equation that is turned on in the problem setup via the Models panel or the DEFINE-MODELS menu. If you specify that the flow is turbulent, equations for conservation of turbulence quantities are turned on. If you specify that FLUENT should calculate temperature, the enthalpy equation is activated. Convergence can be speeded by focusing the computational effort on the equations of primary importance. The SELECT-VARIABLES table allows you to turn individual equations on or off temporarily.

A typical example of using the SELECT-VARIABLES command is in the computation of a flow with heat transfer. Initially, you would define the full problem scope, including the thermal boundary conditions and temperature-dependent flow properties. Following the problem setup, you would use the SELECT-VARIABLES command to turn off the enthalpy equation. You could then compute an isothermal flow field, using a patched value for the temperature of the fluid. When the isothermal flow was reasonably well converged, you would turn the enthalpy equation back on. You could, in fact, turn off the momentum and continuity equations while the enthalpy field was being computed. When the enthalpy field began to converge well, you would turn the momentum and continuity equations back on so that the flow pattern could adjust to the new temperature field. The temperature would couple back into the flow solution via its impact on fluid properties such as density and viscosity. The temperature field would have no effect on the flow field if the fluid properties (e.g., density, viscosity) did not vary with temperature.

Turning Reactions On and Off: To solve a species mixing problem prior to solving a reacting flow, you should set up the problem including all of the reaction information, and save the complete case file. To turn off the reaction so that only the species mixing problem can be solved, you can open the Define Species panel and decrease the number of Reactions to 0.

Once the species mixing problem has partially converged, you can return back and restore the correct number of reactions as originally specified. You can then resume the calculation starting from the partially converged data.

As noted above, for combustion problems you may want to patch a hot temperature in the vicinity of the anticipated reactions before you restart the calculation.

Starting from a Previous Solution: In the above examples, it was shown how you can solve a complicated problem in steps. In doing so, you can use the partially converged data from the first step, where some of the equations or models are not included, as a starting point for a later step in which these equations or models are included. This is a general technique which can be used in other ways. Suppose, for example, that you want to compare the flow through a channel with and without an internal obstruction. You can solve the problem first without the obstruction and obtain a converged solution. You can then modify your case file so as to include the obstruction, and read in the data from the first calculation as a starting point for the second.

7.5.2 Underrelaxation

Introduction: Because of the nonlinearity of the equation set being solved by FLUENT, it s not generally possible to obtain a solution by fully substituting the "improved" values for each variable which have been generated by the approximate solution of the finite difference equation. Convergence can be achieved, however, by underrelaxation which reduces the change in each variable produced during each iteration. In a simple form, the new value of the variable Φ_P at node P depends upon the old value, $\Phi_{P,old}$, the computed change in Φ_P, $\Delta\Phi_P$, and the underrelaxation factor, a, as follows:

$$\phi_P = \phi_{P,old} + \alpha\Delta\phi_P \tag{A.81}$$

In FLUENT, the default underrelaxation parameters for all variables except the velocities are set to low values in order to ensure convergence in the largest possible number of cases. Unfortunately, this may not give rise to the fastest rate of convergence, and an improvement can often be obtained by a judicious increase in one or more of these parameters.

Increasing the Underrelaxation Parameters: As mentioned earlier, FLUENT currently incorporates two different velocity-pressure coupling algorithms: SIMPLE and SIMPLEC, both of which have been modified to handle the complexities of nonorthogonal body-fitted coordinates. The optimal choice of underrelaxation factors is dependent not only on whether SIMPLE or SIMPLEC is used, but also on the type of flow being modeled and properties of the mesh. Underrelaxation factors for the transport equations are set in the range of 0 to 1. The smaller the factor, the heavier is the degree of underrelaxation and the greater is the degree of control exercised over the change permitted from one iteration to the next. While small underrelaxation factors damp out nonlinearities, they also serve to inhibit the rate of convergence for more straightforward problems.

The default underrelaxation factors in FLUENT are set rather conservatively. In other words, the low default values ensure stability for virtually all problems, but in many cases lead to slow convergence. Provided that the coupling between the transport equations is reasonable, property variations are not very large, and the mesh is not very distorted, larger values of the underrelaxation factors will lead to faster convergence. Table A.2 below summarizes suggested underrelaxation factors for problems that are reasonably benign and for time-dependent flows where the advancement of the solution from one time step to another already provides a reasonably good guess.

Note that the only difference between the SIMPLE and SIMPLEC settings is the underrelaxation factor for the pressure correction equation. When SIMPLEC is used, generally no underrelaxation is required for the pressure correction equation (i.e., the factor should be set at 1.0). An exception to this may be required for highly compressible flows where the effect of large density variations on stability can be controlled by decreasing the underrelaxation factor for the pressure correction equation.

The residuals should decrease monotonically or near monotonically after an initial startup phase where some residual increase or oscillations may be observed (typically 10-20 iterations). When the problem being solved is particularly "bard", however, one or more of the residuals will not decrease and corrective measures are required. These "hard" problems probably have one or more of the following properties:

- mesh distortion
- large body forces (e.g., due to buoyancy, rotation)
- multiphase phenomena (e.g., large particle loading for the Lagrangian model, Eulerian multiphase model)
- large property variations (e.g., in combustion or phase change problems with highly temperature- and composition-dependent properties, non-Newtonian flows) highly compressible flows

The corrective measures usually revolve around reduction of the underrelaxation factors. Reduction should be done in increments of 0.05 to 0.1 and applied to the equations for which the residuals are increasing. If the offending residuals are for the pressure and momentum equations, the reduction should be applied to the velocities. Increasing the number of sweeps may also be worthwhile. For turbulent flow problems, combustion problems, and problems with variable properties, the underrelaxation factors for enthalpy, species, and viscosity can be reduced as well.

Occasionally, you may make changes in the underrelaxation factors and resume your calculation, only to find that the residuals begin to increase. This often results from increasing the underrelaxation factors too much. A cautious approach is to save a Data File before making any changes to the underrelaxation factors, and to give the solution time to adjust to the new parameters. Typically, an increase in the underrelaxation factors brings about a slight increase in the residuals, but these increases usually disappear as the solution progresses. If the residuals jump by a few orders of magnitude, you should consider halting the calculation and returning to the last good Data File saved.

7.5.3 Solution Methods for the Discretized Equations

FLUENT uses iterative techniques to obtain an approximate solution to the set of discretized equations. Iterative methods of solution require much less effort than a direct (exact) solution, but attention has to be paid to solution accuracy at each iterative stage. Controlling solution accuracy requires some basic understanding of equation solution procedures available in FLUENT.

The Line-by-Line Solver (LGS): One technique used by FLUENT is the line-by-line solution tech nique, known as Line-Gauss-Seidel (LGS). In LGS the equations are solved simultaneously for small groups of cells, one at a time. The groups consist of lines of cells, where a line is either a complete row or a complete column of cells. The direction of the line is called the sweep direction. During the update of the solution on a line the solution on neighboring lines is treated as correct and kept constant. The direction in which the solution process proceeds through the domain (line-by-line in 2D, or plane-by-plane in 3D) is called the marching direction. A solver sweep is a complete traversal of the domain. A number of sweeps may be required for sufficient solution accuracy.

Multigrid and 1D Block Correction to **Accelerate the Line-By-Line Solver:** Generally LGS is good at reducing local errors, but poor at reducing errors which require collective change of many cell values (long-wavelength errors). Therefore the speed of solution of LGS deteriorates with increasing grid size. Also for large-aspect-ratio cells in combination with gradient boundary conditions, as may occur in highly stretched grids, convergence may be poor. FLUENT provides two devices to speed up the LGS procedure:

- One-dimensional block correction.
- Multigrid (MG) acceleration.

Of these, MG acceleration is recommended for pressure in almost any case and is active, by default, on the pressure and enthalpy equations.

GMRES: A Full-Field Iterative Solver: On selected computer hardware, FLUENT also provides access to a full-field iterative solver, GMRES. This alternative to the line-by-line solver is provided on those computers which provide access to GMRES math libraries.

7.5.4 Controlling the Sweeps of the Line-by-Line (LGS) Solver

Introduction: Sometimes a problem shows extremely slow convergence, with the residuals for one or more equations remaining nearly constant over a large number of iterations. In addition to modifications in the underrelaxation parameters, two other types of modifications in the solver parameters are available which can help:

- The sweep direction, which controls the way in which cells are grouped together to be solved
- The number of sweeps on each equation, which controls the extent to which the solution of any single equation is refined during each iteration

In this section, the nature of these solution controls is explained in more detail, along with guidelines on how and when to make changes to them.

Solver Sweep Direction: If an exact solution were performed on a computational domain with N cells, an $N \times N$ matrix would need to be solved. Rather than solve a problem via this "direct method," FLUENT uses an iterative solution technique, solving the equations simultaneously for small groups of cells, one group at a time. The groups contain either a

complete row or a, complete column of cells, starting at one boundary and ending at the other. The solver sweep direction is the direction in which these groups of cells are formed, i.e., columns represent one direction while rows represent another. To further illustrate the meaning of the solver sweep direction, consider the computational grid shown in Fig. A.25.

Figure A.25 illustrates a solver sweep in the J-direction (direction 2). Sweep Direction of J means that the equations are solved simultaneously for a single column of cells (or a sweep of cells in the J-direction). The solver then marches forward in the positive Indirection to solve the next column of cells.

Choosing the Best Sweep Direction: Generally speaking, the sweep direction should be in a direction that is normal to the primary direction of flow. In this manner, the effects of the boundary conditions are propagated along the sweep direction, and this information can then be propagated forward along the direction of flow. Thus the choice of sweep direction 2 (or J) works well when flow is primarily in the I-direction, as indicated in Fig. A.25. When flow is primarily in the J-direction, you should consider Sweep Direction of I, as shown in Fig. A.26.

Alternating Sweep Direction: FLUENT uses an alternating sweep direction, by default, sweeping lines in the I direction and then sweeping lines in the J direction (in 2D).

The alternating-direction solver begins by using the first sweep direction to update the current dependent variable at each point. It then repeats the calculation using the alternate direction as the sweep direction. The process is illustrated in Fig. A.27. This technique is particularly useful for problems in which there is no single dominant flow direction, e.g., flows with jets or particles injected into a crossflow.

If the option is used in 3D, the solver operates as in the following example. Suppose you choose MARCHING DIRECTION 3 (March Direction of K). The alternating-direction solver then updates the dependent variables by using:

1. sweep direction I (1), marching direction 3 (K) (first)
2. sweep direction 2 (J), marching direction 3 (K) (second)

In other words, the marching direction is always the same, and the sweep direction alternates (beginning with the smaller directional index).

Sweep and March Directions in 3D Problems: In 3D problems, you can choose both a sweep direction and a marching direction. The sweep direction is as defined above, and the marching direction is that along which the sweep solution propagates. The rule of thumb once again is to march in the flow direction and sweep in the direction across which boundary conditions are imposed. For example, SWEEP DIRECTION 3 (Sweep Direction of K) should be selected when boundary conditions in the K-direction are of particular importance to the solution. MARCHING DIRECTION I (March Direction of 1) should be chosen for flows which are primarily in the I-direction, and so forth.

Multiple Sweeps on Equations: In addition to choosing the solver sweep direction, you can control the accuracy with which each equation is solved during each iteration. This is accomplished by increasing the NUMBER OF SWEEPS or Number of Sweeps of an equation, and it is particularly useful for equations that are having difficulty converging. When you choose multiple sweeps for a variable, you are requesting that the equation be solved by marching across the domain a multiple number of times. In Fig. A.28, this process is illustrated for the pressure equation, where 5 sweeps are performed by default.

With each march across the domain, the variables at the "downstream" nodes get updated, thereby improving the accuracy that can be obtained during each iteration. In other words, the updated information obtained when a column (or row) of cells is solved gets propagated throughout the domain more efficiently with each additional sweep of an equation.

Choosing the Optimum Number of Sweeps: Some guidelines are available which can help you choose the best number of sweeps for the various equations which are relevant to your problem. In problems with heat transfer, especially those with conjugate heat transfer, you should increase the number of sweeps on the enthalpy up to 20 or so. If you are having difficulty getting the pressure to converge, it is recommended that you increase the sweeps on pressure to 20 as well. Occasionally, you may find that one (or more) of the species equations has difficulty converging in some reacting flow problems. In most cases, increasing the sweeps on the problematic species equation to 5 or 10 is enough to make a difference. In some 3D flows, one velocity component may have more difficulty converging than the other two. In such cases, increasing the sweeps on the equation for that component to 5 or 10 is again adequate. Since one consequence of increasing the number of sweeps on an equation is that each iteration takes more time, you should request multiple sweeps for only those equations that are having difficulty converging.

By default, 1 sweep is performed for each equation except the pressure-correction equation, for which 5 are performed. Note that these settings are not used when the equations in question are being solved using multigrid, as the multigrid procedure exercises its own control over the sweeping procedure.

7.5.5 Block Correction

FLUENT provides an optional block correction procedure for solution of the governing equations in the LGS-BLOCK-CORRECTIONS (and BLOCK-CORRECTIONS-MG) tables. When you are not using the multigrid option, you can add block correction on the enthalpy and species equations using the LGS-BLOCK-CORRECTIONS command.

If you are using multigrid, you can add block correction on any transport equation using the BLOCK-CORRECTIONS-MG command.

The block correction option accelerates the convergence of the equations by deriving global corrections that drive the solution toward global conservation. Block correction of the enthalpy equation is especially recommended for the solution of coupled convection/conduction problems "conjugate heat transfer" and in any problem involving regions with highly different

thermal conductivities. The block correction technique speeds up convergence by applying a quasi-one-dimensional correction to the current solution field in order to satisfy global conservation, with the correction vanishing as the local balance is achieved throughout the domain.

1D Block Correction vs. Multigrid: One-dimensional block corrections reduce long-wavelength errors in the direction in which they are applied, but may introduce large short-wavelength errors. Therefore, application of block correction is followed by application of LGS to reduce the latter errors. Sufficient sweeps must be specified to this purpose, otherwise the effect of block correction may be adverse. If very steep gradients exist in the final solution, 1D block correction may increase the solution effort for this reason. These disadvantages are to a large extent avoided in multigrid (MG) acceleration.

One-dimensional block correction is also useful in combination with multigrid acceleration, when cells are highly stretched or otherwise strongly anisotropic coefficients are to be expected. In such cases, you can activate 1D block correction with the BLOCK-CORRECTIONS-MG command.

7.5.6 Multigrid Acceleration of the Line Solver

FLUENT uses a multigrid scheme to accelerate the convergence of the standard line solver, using additive correction to compute corrections on a series of coarse grid levels. The use of this multigrid scheme can greatly reduce the number of iterations and the CPU time required to obtain a converged solution, particularly when your FLUENT model contains a large number of control volumes and/or control volumes which are of large aspect ratio. This section describes the mathematical basis of this multigrid approach and provides details on the user inputs and controls over this important solver feature.

The Line-by-Line Solver: The standard line-by-line solution technique used in FLUENT provides a robust and memory-efficient approach to the solution of the finite difference equations in FLUENT. The essence of the line-by-line solver is to update the field for a given unknown ϕ by solving simultaneous sets of equations for ϕ over a subset of elements which lie on lines of constant I, J, or K. This approach avoids simultaneous solution of equations at all points in the domain, along with the large memory requirements associated with such direct matrix calculations. In the line-by-line approach, the matrix to be solved is a simple tri-diagonal matrix which can be solved via efficient Gaussian elimination. This line-by-line approach is also referred to as the Line-Gauss-Seidel (LGS) method.

The Need for Multigrid Acceleration: The LGS method, in which unknown values on neighboring lines are left explicit during the solution process, reduces local errors with relative ease. That is, the effect of the solution on one line is communicated to adjacent lines relatively quickly. However, the line-by-line solver is less effective at reducing "long-wavelength" errors-errors which exist over a large number of control volumes. Thus, global corrections to the solution across a large number of control volumes occur slowly, over many iterations, when the line-by-line solver is used. This implies that performance of the line solver will deteriorate as the number of control volumes along any coordinate direction increases. Multigrid provides a

remedy for this weakness in the line solver by deriving "global" corrections which are based on a control volume balance over a large number of cells. Figure A.29 shows the convergence history of a moderate size (36,000 nodes) 3D turbulent flow problem with and without multigrid.

The convergence or error reduction rate of the line-by-line solver will also deteriorate when the finite difference coefficients in the equations to be solved are anisotropic. Anisotropic coefficients occur when large cell aspect ratios exist in the finite difference grid and when rapidly varying or anisotropic transport properties occur in the domain. One instance of anisotropic transport properties occurs in the energy equation when your problem includes conjugate heat transfer between regions of very different conductivity. Multigrid can accelerate the convergence of such problems by enforcing a global balance over larger regions of the grid, in effect "smoothing" the anisotropy that exists on the local scale. Figure A.30 illustrates the effect of multigrid on the solution history of a conduction heat transfer calculation in a composite medium, where coefficient anisotropy slows the convergence of the line solver.

Choosing When to Use Multigrid: In most cases, multigrid (MG) should be applied to the pressure-correction (continuity) equation and will reduce the number of iterations required to converge it. Multigrid is of particular help for convergence of the continuity equation because the mass balance depends on reduction of long-wavelength errors. In addition, multigrid should also be applied to scalar equations (like enthalpy), especially when these equations are loosely coupled to the flow solution. In such cases, given sufficiently high underrelaxation, convergence of the scalar equations will primarily depend on global error reduction, and will be limited by the linear equation solver procedure. Again, multigrid should provide significant speedup when this is the case.

Applying multigrid to momentum or "source-dominated" scalar equations, on the other hand, provides little if any benefit. (Source dominated scalars include the turbulence parameters and enthalpy or species in reacting flows.) Such equations tend to be dominated by local conditions, and the line-by-line solver will do well at reduction of these local errors. In fact, convergence may be hindered by application of multigrid to such equations as the global corrections may introduce significant local errors that are difficult to remove.

7.6 Solution Options for Large Problems

By default, FLUENT automatically updates internally stored information about your problem whenever you make certain changes to the problem definition. For example, when you make changes in the Models panel and click Apply, or when you quit from the SETUP-1 text menu, FLUENT will check and update the geometry and property information that is used internally by the solver. (Note that this information is not saved to a file at this time- you must always remember to save the problem definition to a case file yourself.)

Since FLUENT's check and update of the geometry and properties includes verification of the grid, this process can be very timeconsuming for very large problems (i.e., problems with a very large number of cells). For such problems, you may want to enable the Prompt Before Geometry Calc. option in the Numerical Options panel.

When this option is enabled, FLUENT will prompt you before it updates the geometry and property information. Rather than performing this update several times during your problem setup, you can postpone the update until you have completed the setup. Simply answer NO in the text interface (or click on No in the Question dialog box) when FLUENT asks if you want to calculate the geometric parameters and properties. When you are ready to perform the update, you can either answer YES (or click on Yes) the next time you are prompted, or request the update yourself by selecting the Update Geometry menu item in the Solve pull-down menu.

Table A.1 Values of θ in common discritization schemes

Discretization Scheme	θ
Second-order Central Difference	1
Second-order Upwind	0
QUICK	$\frac{3}{4}$
Third-order Upwind	$\frac{2}{3}$

Table A.2 underrelaxation factors for SIMPLE and SIMPLEC

Variable	SIMPLE	SIMPLEC
u, v, w	0.7	0.7
Swirl (w)	0.8	0.8
Pressure Correction	0.3	1.0
k	0.7	0.7
ϵ	0.7	0.7
Enthalpy	1.0	1.0
Temperature	1.0	1.0
Reynolds Stresses	0.5	0.5
Species	1.0	1.0
Viscosity	0.7	0.7
Body Forces	1.0	1.0

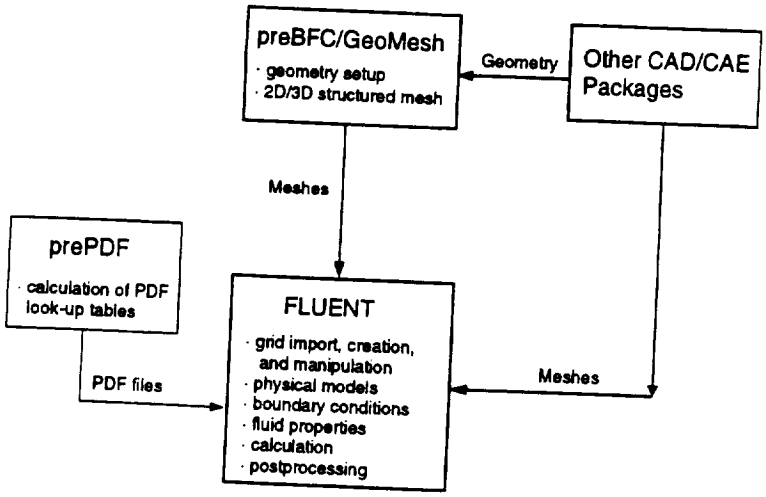

Fig. A.1 Basic program structure.

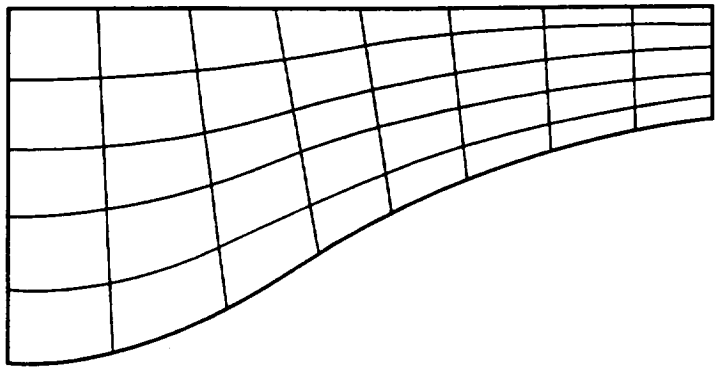

(a) Body-Fitted Coordinates

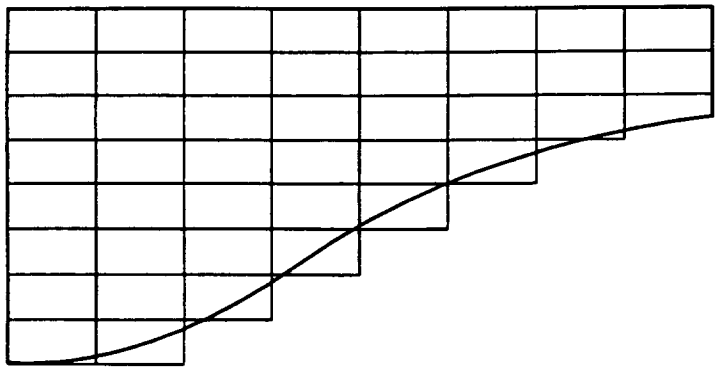

(b) Cartesian Coordinates

Fig. A.2 Geometry representation in body-fitted coordinates vs. Cartesian coordinates.

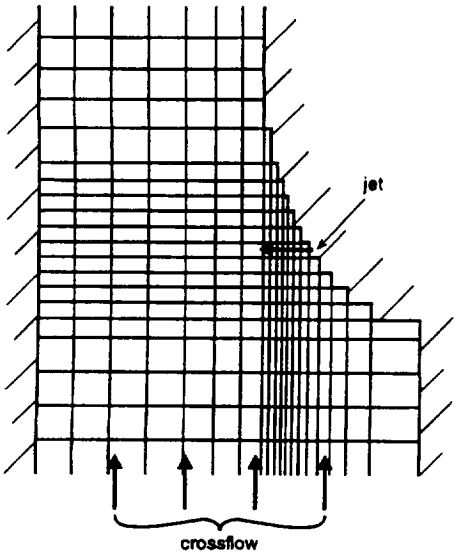

(a) Approximate Geometry in Cartesian Coordinates Has a Very Small Impact on the Flow Prediction

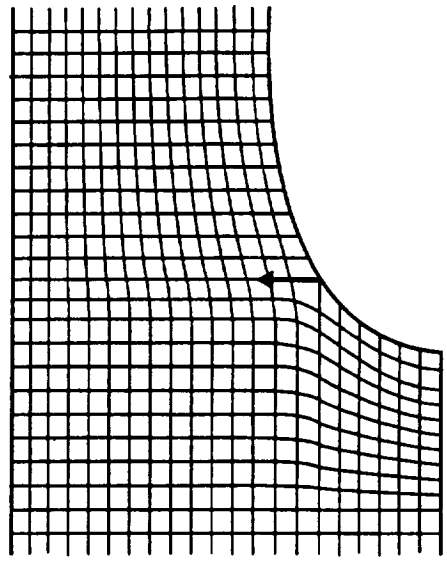

(b) Body-Fitted Coordinates Can also be Used, but Require More Computer Resources

Fig. A.3 Satisfactory approximation of the geometry and flow physical coordinates.

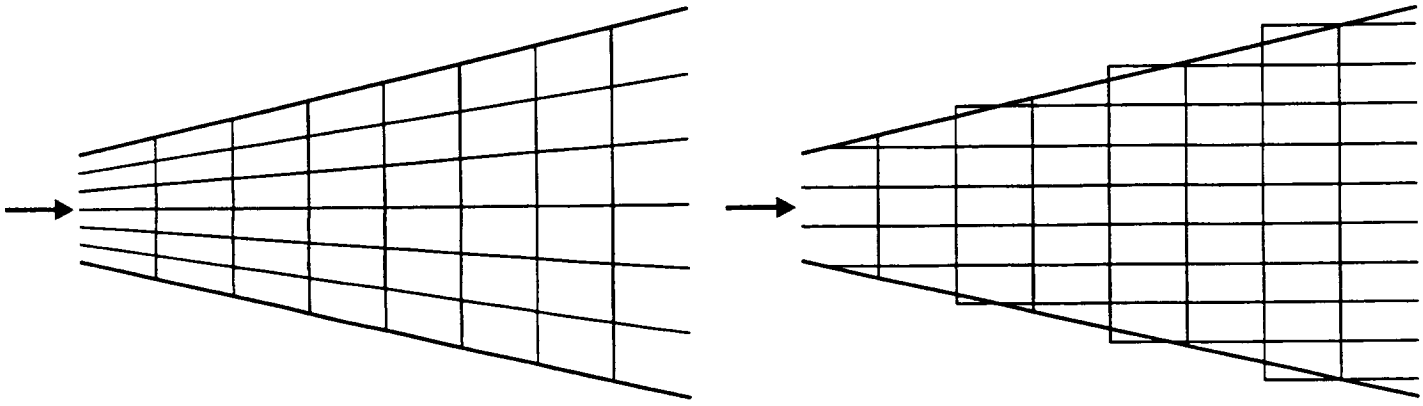

(a) Body-Fitted Coordinates Provide a More Accurate Description of the Wall Shear Stress

(b) Cartesian Coordinates Predict the Wall Shear Stress Inaccurately

Fig. A.4 Unsatisfactory approximation of the flow physics in Cartesian coordinates.

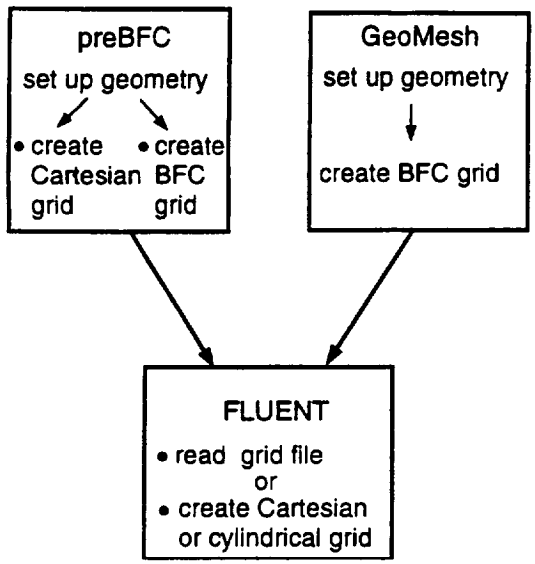

Fig. A.5 Grid generation alternatives.

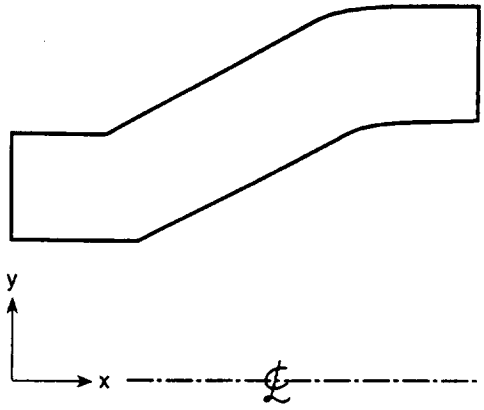

Fig. A.6 Setup of axisymmetric geometries with the x-axis as the centerline.

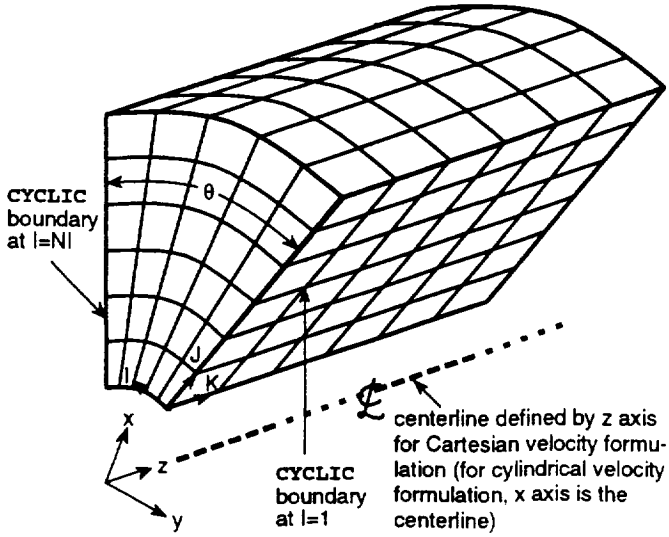

Fig. A.7 Geometry and grid construction constraints in problems using rotationally-cyclic boundaries.

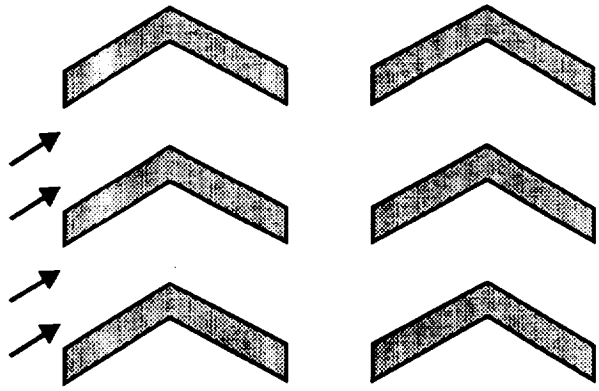

(a) Physical Domain

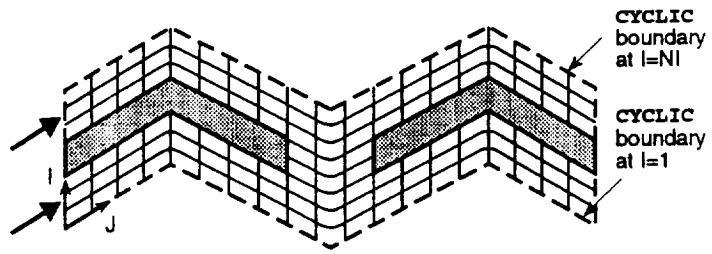

(b) Modeled Domain

Fig. A.8 Geometry and grid construction constraints in problems using translationally-cyclic boundaries.

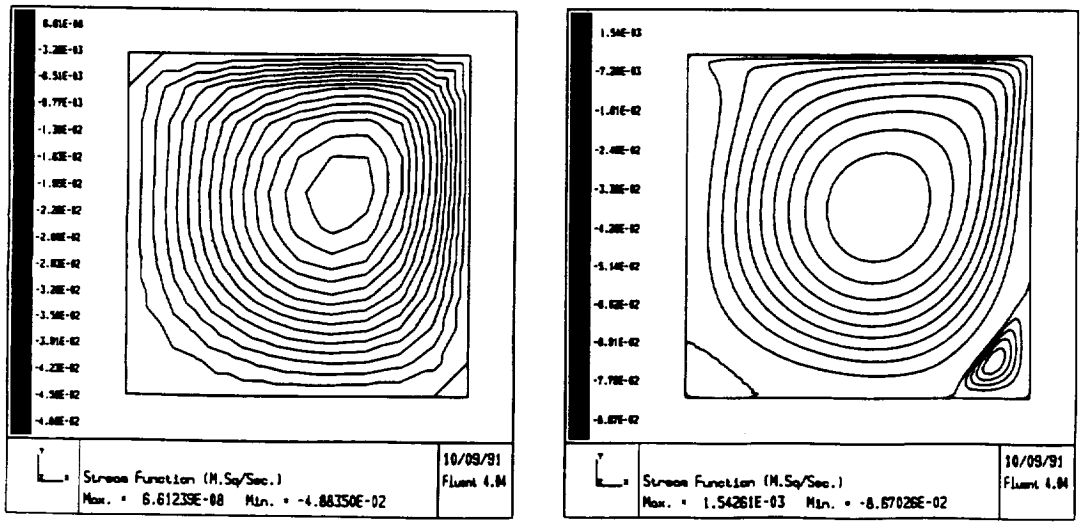

(a) Coarse Grid Solution

(b) Fine Grid Solution

Fig. A.9 Impact of the computational grid on the resolution of flow details in a simple driven cavity.

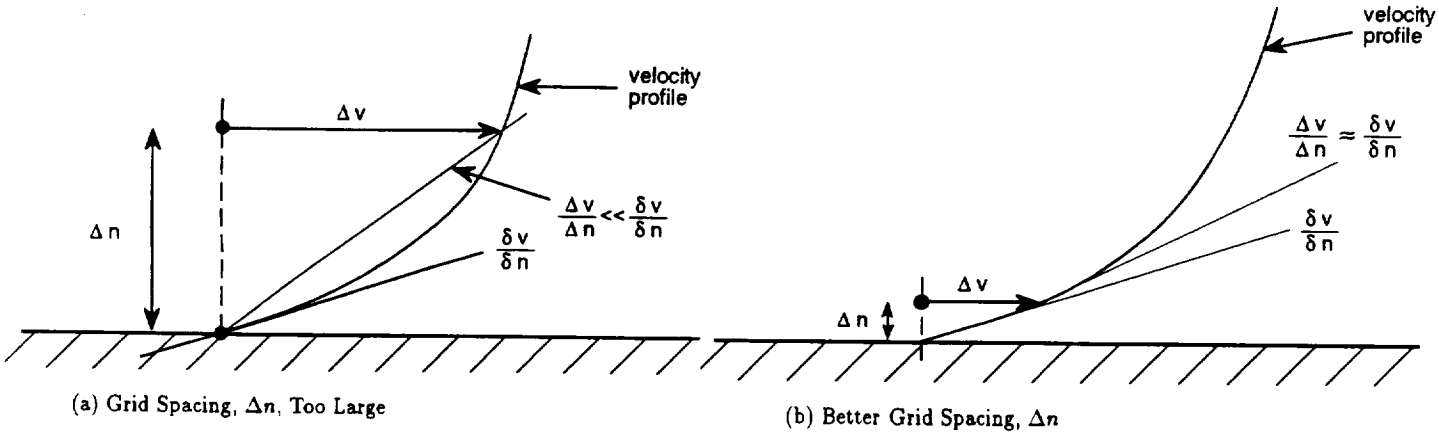

Fig. A.10 Impact of the near-wall grid spacing on the shear stress calculation in laminar flow.

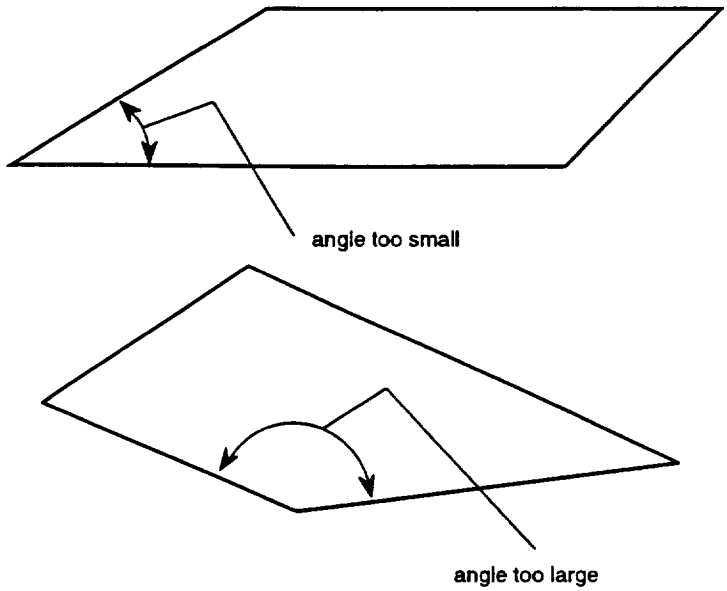

Fig. A.11 Undesirable skew in body-fitted grid cells.

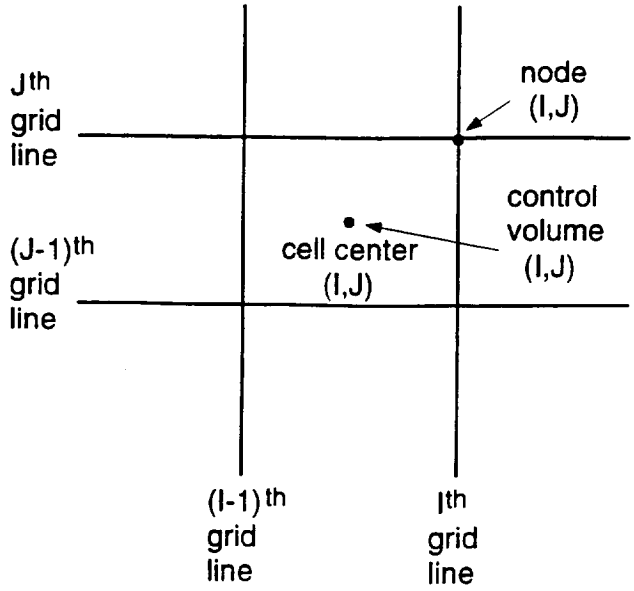

Fig. A.12 Grid lines, nodes, and control volumes in FLUENT.

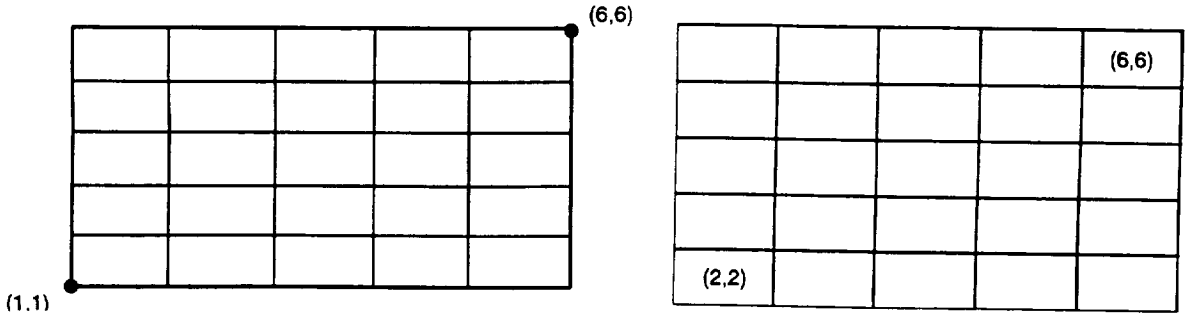

(a) Grid Lines and Node Numbering

(b) Cell Numbering

Fig. A.13 Grid numbering vs. cell numbering in FLUENT.

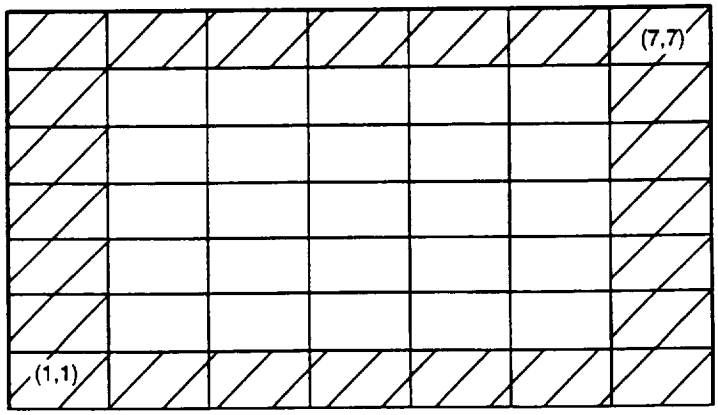

Fig. A.14 Fictitious perimeter cells added by FLUENT.

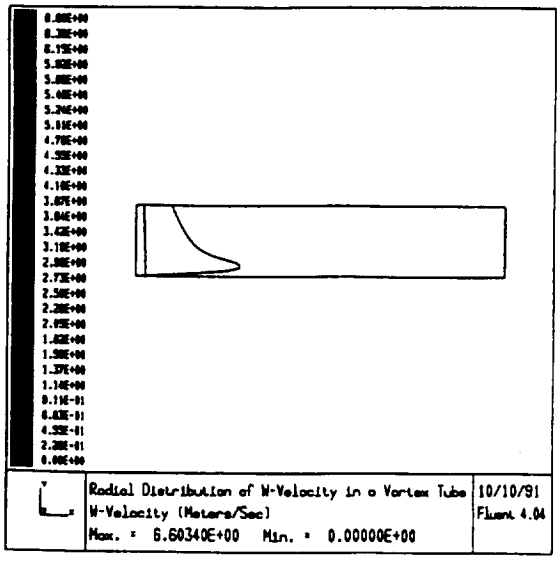

Fig. A.15 Free vortex formation in a swirling flow.

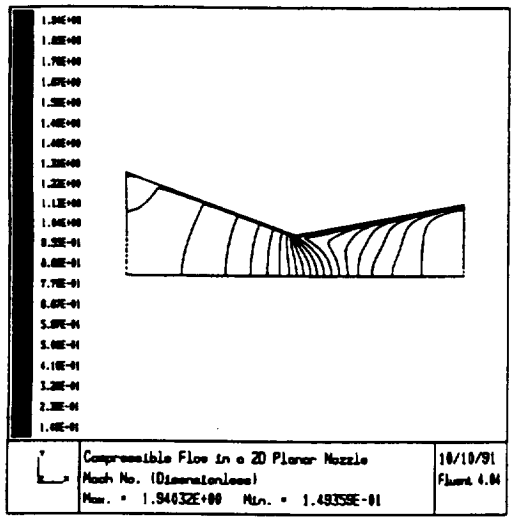

(a) Transonic Flow in a Converging-Diverging Nozzle

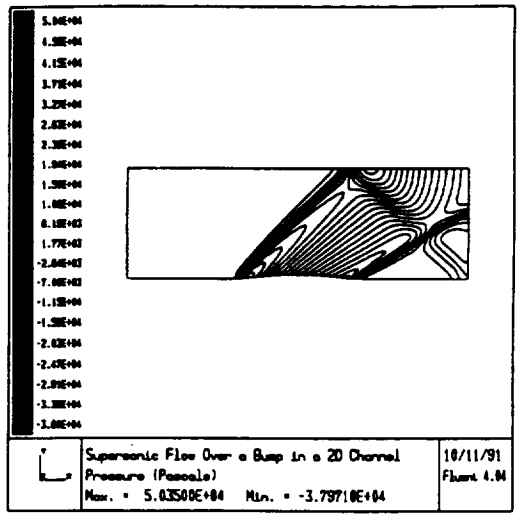

(b) Supersonic Flow Over a Bump in a 2D Channel

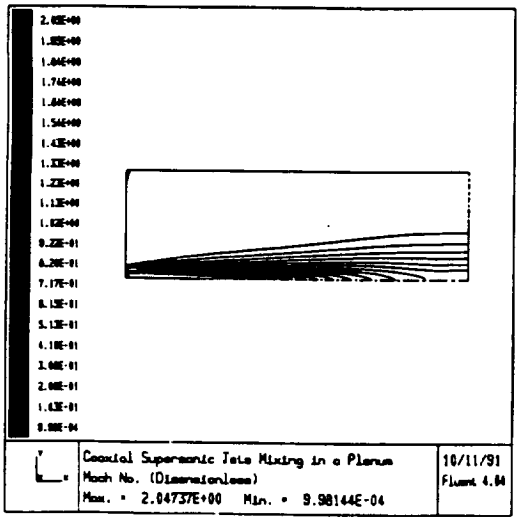

(c) Supersonic Jet Mixing in an Ambient Plenum

Fig. A.16 Typical compressible flow applications modeled by FLUENMT.

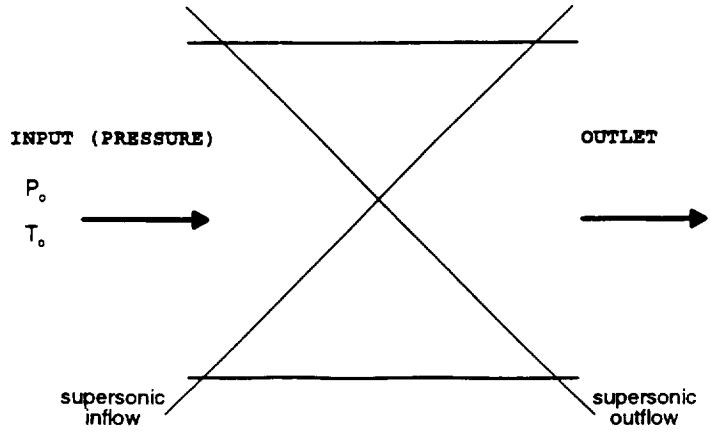

Fig. A.17 Ill-posed boundary conditions for supersonic inflow.

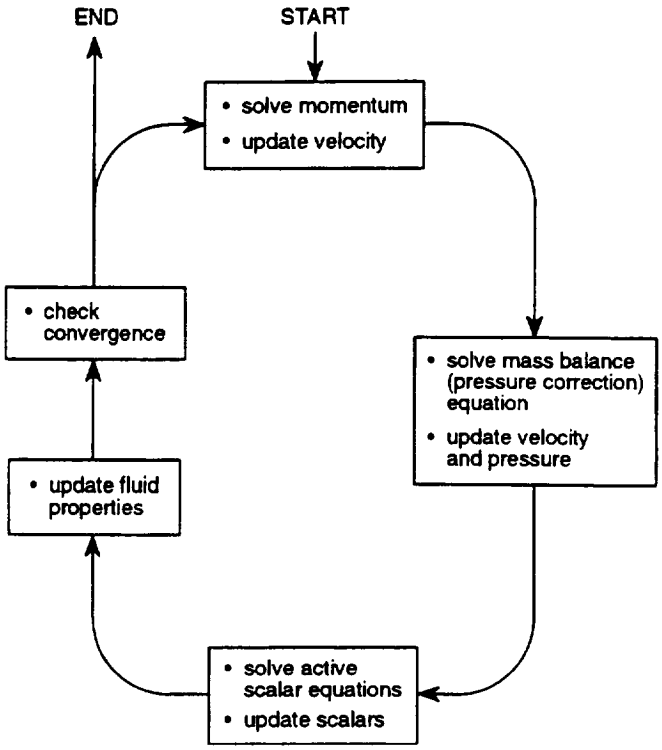

Fig. A.18 Overview of the solution process.

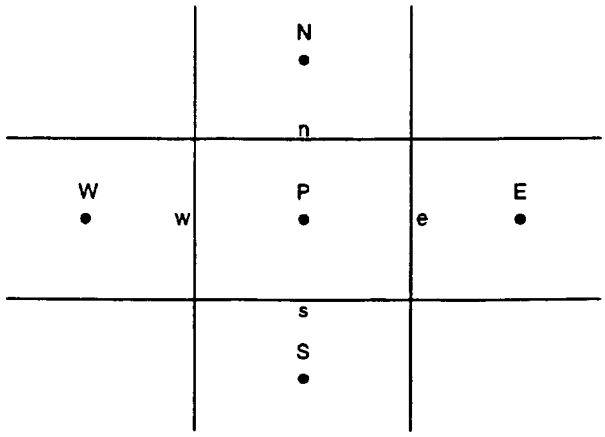

Fig. A.19 Typical computational cell surrounding node P.

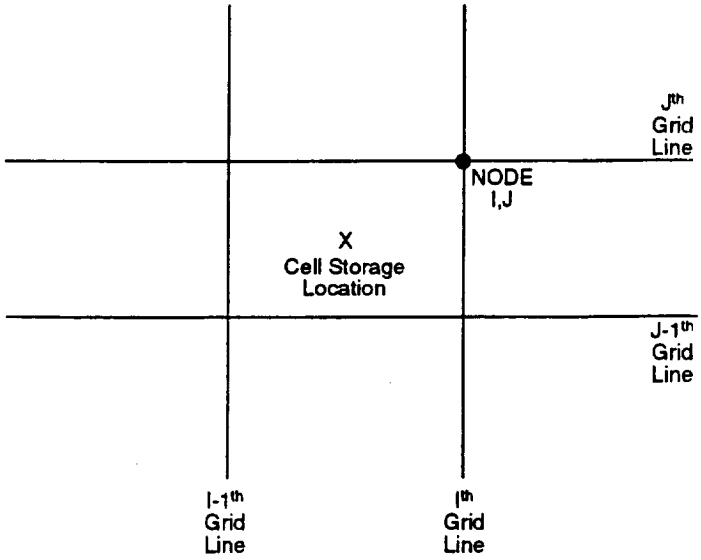

Fig. A.20 Non-staggered control volume storage scheme.

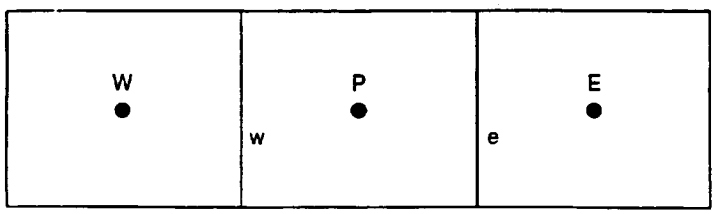

Fig. A.21 One dimensional control volume nomenclature used to illustrate volume integration.

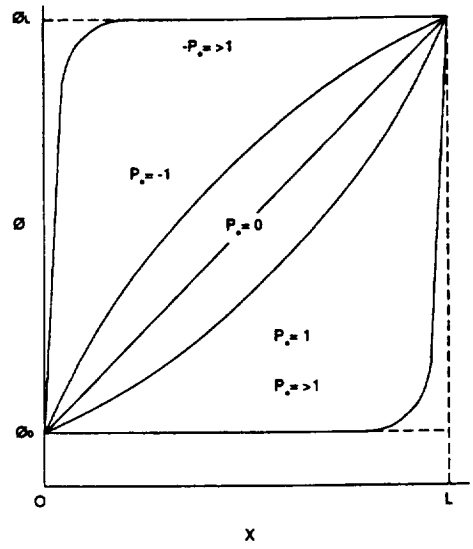

Fig. A.22 Variation of a variable ϕ between x=0 and x=L.

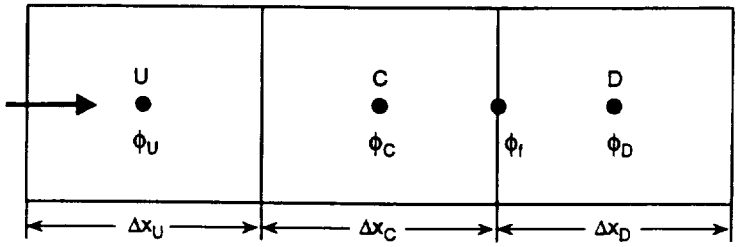

Fig. A.23 Central, downwind, and upwind cell nomenclature employed in the higher order interpolation schemes.

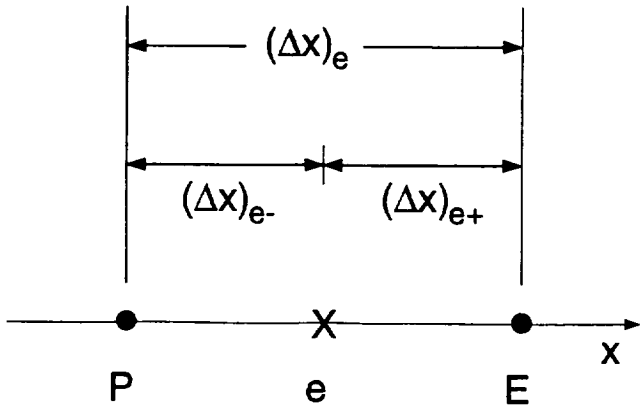

Fig. A.24 Points and distances for viscous-weighted velocity interpolation.

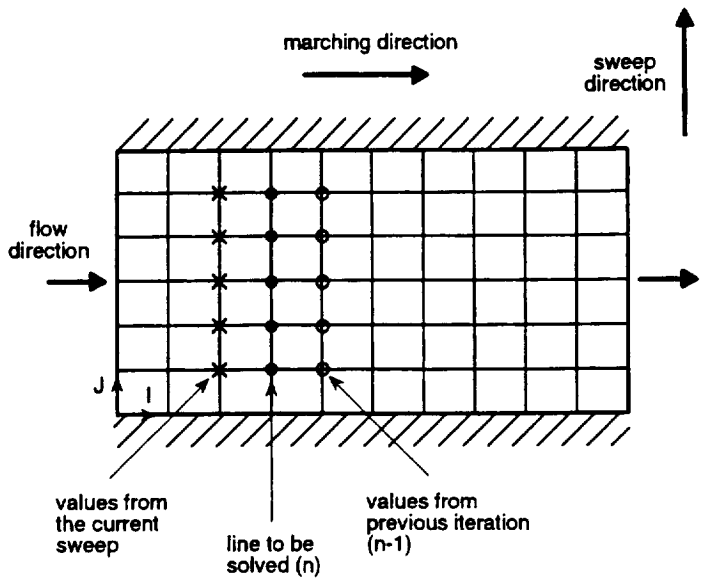

Fig. A.25 Illustration of sweep direction 2 (J).

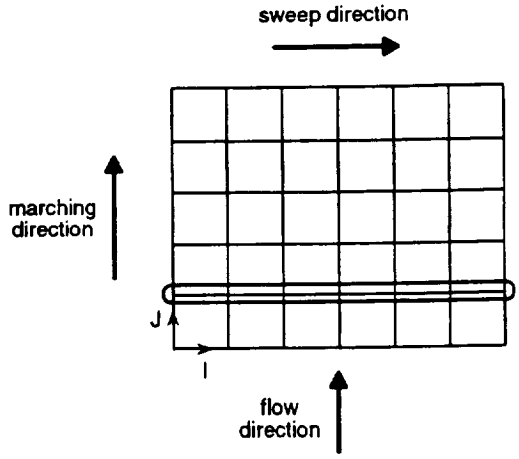

Fig. A.26 Illustration of sweep direction 1 (I).

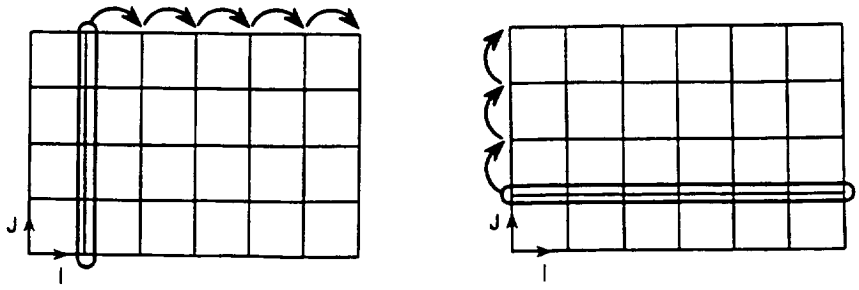

Fig. A.27 Alternating direction sweeps.

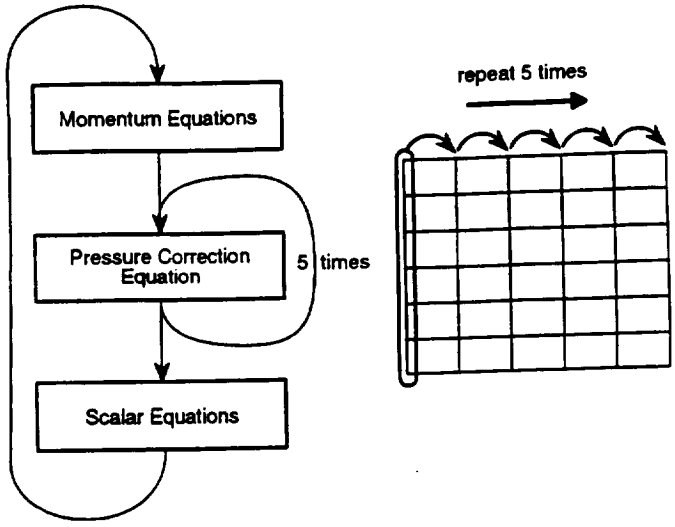

Fig. A.28 multiple sweeps for the pressure equation.

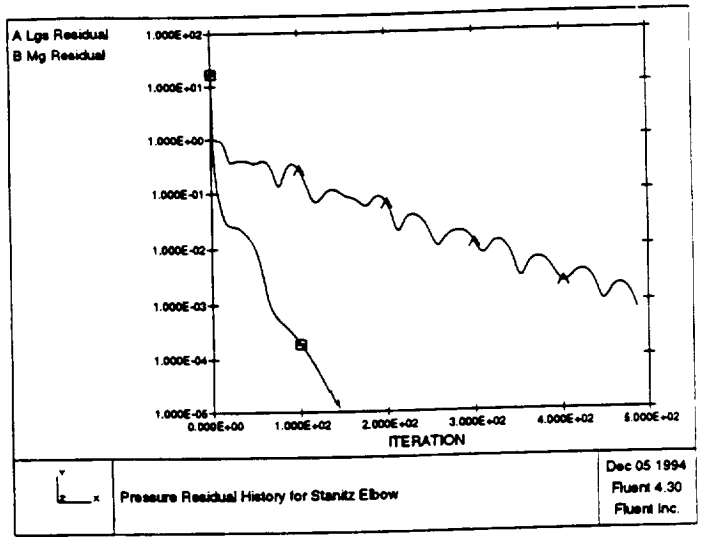

Fig. A.29 Pressure-correction equation residual vs. iteration for flow in a 3D elbow bend.

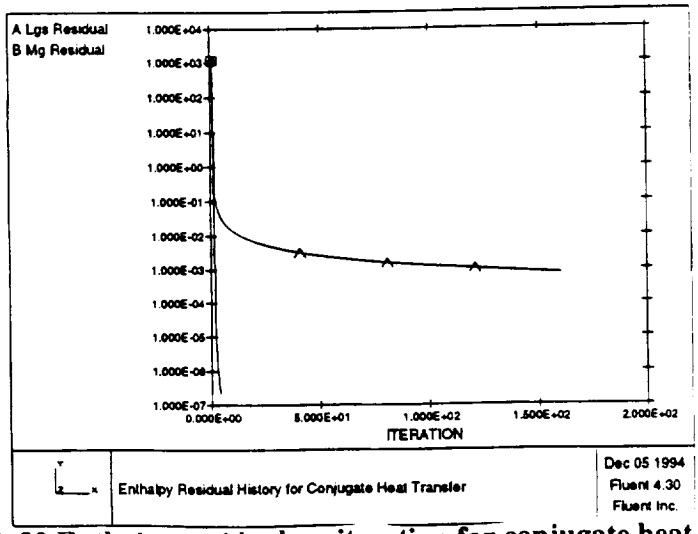

Fig. A.30 Enthalpy residual vs. iteration for conjugate heat transfer on a composite medium.